University of Zurich[UZH]

Trends in Snow Water Equivalent (SWE) and its Spatial Variation across the Wägital, Switzerland: A Long-Term Analysis from 1943 to 2023

GEO 511 Master's Thesis

Author
Fiona Luisa Sigrist
16-118-697

Supervised by
Dr. Ilja van Meerveld

Faculty representative
Prof. Dr. Jan Seibert

23.09.2024
Department of Geography, University of Zurich

University of Zurich

Department of Geography

Master Thesis

Trends in Snow Water Equivalent (SWE) and its Spatial Variation across the Wägital, Switzerland:

A Long-Term Analysis from 1943 to 2023

Author:

Fiona Sigrist

Lincolnweg 13c

8840 Einsiedeln

16-118-697

Supervisor:

Dr. Ilja van Meerveld

Faculty Member:

Prof. Dr. Jan Seibert

23. September 2024

Acknowledgements

The completion of this master thesis would not have been possible without the support and help of several people.

First and foremost, I would like to express my sincere gratitude to Dr. Ilja van Meerveld and Prof. Dr. Jan Seibert for their guidance throughout the entire process. Your open doors and all your answers to my questions were really appreciated. I am deeply grateful for the knowledge and experience you shared with me, as well as for your constructive feedback. I would also like to extend my thanks to Marc Vis, whose assistance in troubleshooting my model and brainstorming for improvements was greatly appreciated.

A special thanks go to Meteodat GmbH, especially Dr. Mario Rohrer, Daniela Lorenzi, and Dr. Manfred Schwarb, for granting me the opportunity to work with this interesting data set. Accompanying you during the measurement period in 2024 gave me a true appreciation for the effort and energy required to collect and maintain this data set. I also gained insights into both the digitalization and cleaning processes associated with historical datasets. Thank you for allowing me to join you and for patiently answering all my questions.

I am also deeply appreciative of Katja Rupf and Dominik Bär who generously gave their free time to review my thesis and provide me with invaluable feedback.

Further, I would like to thank my employer, Steidle Consulting GmbH, especially Max Steidle, who has supported my decision to pursue a master's degree from the very beginning. I am extremely thankful for the flexibility you provided, your willingness to accommodate my academic pursuits and your interest in my studies. My job served as a welcome contrast when I needed a break from R-coding.

A heartfelt thanks goes to Christian Trinkler for his mental support and his time spent giving me helpful feedback on various topics regarding the thesis. Your positivity and observing your strong work ethic were a great source of motivation, helping me stay focused and energized throughout the process.

I also wish to acknowledge my fellow master's students, with whom I spent many days, particularly during the hot summer months, in the master's study room. It was a big motivation to have you around and to exchange concerns as well as advances of our thesis.

Lastly, I want to thank my family and friends, who are always by my side and have supported me throughout the years, particularly during the challenging process of completing this thesis.

Abstract

Snow serves as a crucial temporal water storage, impacting downstream water management, agriculture, and hydroelectric power generation. In the pre-alpine Wägital in Switzerland, one of the longest-standing global monitoring programs of snow water equivalent (SWE) exists, with April 1st SWE data spanning from 1943 to 2023. To overcome the limitations of relying solely on April 1st SWE measurements, a degree-day model was employed to reconstruct daily SWE and identify the annual maximum SWE (maxSWE). This thesis analyzes spatial variations in maxSWE with respect to elevation, aspect, and slope, as well as long-term trends and changes in meteorological parameters, SWE, and snow cover days. The model results reveal that April 1st measurements often fail to capture peak SWE, highlighting the importance of using maxSWE for more accurate trend analysis. Spatially, SWE increases with elevation, is lowest on south-facing slopes, highest on wet-facing locations, and decreases with steeper terrain. Temporally, a general decline in maxSWE is observed across the catchment and the study period. Positive trends dominate from the 1940s to the 1980s, followed by stronger negative trends from the 1980s onward. The start year of the trend analysis significantly influences the strength of these negative trends. Similar patterns are noted for annual snow cover days. Additionally, the distribution of maxSWE across different meteorological categories indicates that "cold and wet" years produce the most snow, while "warm and dry" years result in the least, with higher elevations exhibiting greater variability in maxSWE, particularly in "cold and wet" conditions. These findings suggest that both temperature and precipitation are critical in determining SWE, while other factors, such as wind patterns and local topography, also influence snow accumulation. While uncertainties in input data and modeling limitations exist, this study underscores the value of long-term data sets like the Wägital monitoring program for understanding past trends and anticipating future challenges related to climate change.

Table of Contents

List of Figures

List of Tables

List of Abbreviations

CFMAX	Degree-day Factor
CFR	Refreezing Coefficient
CWH	Water Holding Capacity
DEM	Digital Elevation Model
E	East
HMA	High Mountain Asia
IQR	Interquartile range
m a.s.l.	meters above sea level
maxSWE	maximal snow water equivalent
MK	Mann-Kendall test
N	North
NE	North-east
NW	North-west
S	South
SFCF	Snowfall Correction Factor
SE	South-east
SLF	Swiss Federal Institute of Snow and Avalanche Research
SSE	sum of squared errors
SSW	South-south-west
SW	South-west
SWE	Snow Water Equivalent
TT	Threshold Temperature
W	West

1 Introduction

The snowy white alpine mountain ranges are not only scenic, but the snowpack is also a critical component of water storage in winter. Snowmelt provides water for downstream areas, including water for urban and agricultural use (Lopez et al., 2020; Marty et al., 2023; Viviroli et al., 2007a). Snow is also the foundation for winter sports and tourism (Marty et al., 2023). Additionally, snow can present natural hazards, such as avalanches and floods when it melts (Marty et al., 2023), which can lead to disruptions in transportation and impact livestock, wildlife, and infrastructure (Berghuijs et al., 2016; Croce et al., 2018).

Snow plays a crucial role in the climate system, with its high surface reflectance (albedo) affecting the surface energy balance(Wiscombe & Warren, 1980). The snow-albedo feedback mechanism, where initial warming reduces snow cover, lowers the albedo, and increases absorbed solar energy, further increases the air temperature. Additionally, snow's thermal insulating properties and the large energy requirement for melting ice (latent heat) affect the energy balance (Armstrong & Brown, 2008).

From a hydro-meteorological perspective, snow is just temporally frozen precipitation. Measuring snow water equivalent (SWE) provides insights into the amount of water stored in the snowpack as frozen precipitation. This information is crucial for predicting seasonal discharge, making short-range forecasts of the discharge, and assessing water quality aspects (Rohrer et al., 1994). The significance of snow as temporary water storage has been acknowledged in the literature since at least 1939 (Bader et al., 1939). The collection of SWE data by institutions such as the Swiss Federal Institute of Snow and Avalanche Research (SLF) helps to create snow-climatological data products, perform trend analyses, and develop numerical models that further enhance the understanding of snow's role in the climate system (WSL, 2024). Furthermore, various hydroelectric companies rely on SWE data to anticipate meltwater contribution to reservoirs and hydroelectric power stations (Rohrer et al., 1994).

SWE can be measured every week (e.g. Stähli & Gustafsson, 2006), every month (e.g., several SLF stations (Marty et al., 2023)), or once per year. If SWE is only measured once per year, it is typically measured on or around April 1st. Measuring SWE on the same day of the year and at the same sites allows one to compare the relative differences in snow storage for different years and thus obtain a measure of water availability. Observational data on snow, especially SWE, and other meteorological data, like precipitation and temperature, are also essential for understanding historical and ongoing climate change (CH2018, 2018) because snow cover reacts quickly to climate change and has a significant impact on the atmosphere(Armstrong & Brown, 2008).

SWE needs to be measured at many points because snow accumulation and melt rates are influenced by elevation and aspect, as these factors affect air temperature and solar radiation inputs to the snowpack. SWE can vary significantly across different areas, primarily due to wind-driven snow drifting during

and after snowfall events, which is further influenced by topography and vegetation cover. For instance, much deeper snow accumulation is often observed on the leeward side of ridges. Additionally, there are feedback effects where deeper snow cover can enhance water availability for vegetation, promoting growth. In forested areas, this increased growth can lead to greater snow capture, as trees trap more snow carried by the wind (Beven, 2012).

Historical observational data sets are the foundation for future climate change projections and scenarios. Additionally, the variability within the present climate offers insight into contemporary climate related risks (CH2018, 2018). In Switzerland (and elsewhere), several changes in snow characteristics have been observed since the 1960s. The proportion of precipitation that falls as snow is linked to air temperature and has notably diminished as a consequence of global warming. In Switzerland, this change is especially evident at lower and middle elevations (FOEN, 2021). Furthermore, since 1961, snowfall days below 500 m above sea level (m a.s.l.) have decreased by approximately 40 %, and the water stored in snow, respectively the SWE, during spring below 1000 m a.s.l. has declined by up to 75 % (Marty et al., 2017). The zero-degree isotherm has risen significantly since the late 19th century (Scherrer et al., 2021). Additionally, the FOEN (2018) has stated that the zero-degree isotherm in future winters will be higher because of climate change, which means that less precipitation will be stored in the snowpack and snow will melt earlier in the year. Impacts of climate change on the water cycle that are already apparent are changes in annual river streamflow (Nijssen et al., 2001), alterations in flow duration curves (Arora & Boer, 2001), shifts of flood peak magnitude and timing of it (Hirabayashi et al., 2013), and changes in magnitude of low-flow periods (Stahl et al., 2010). Further changes in regional hydrology are to be expected.

Several studies investigating SWE data used April 1st SWE as a proxy for the maximum SWE (maxSWE) because SWE on April 1st is typically the day with the highest observed SWE during the winter season (Cayan, 1996; Changnon et al., 1991). Research has scrutinized the reliability of April 1st SWE measurements. For instance, Bohr & Aguado (2001) found that April 1st SWE tends to underestimate the maximum SWE (maxSWE) by about 6 cm (12 %) in the Rocky Mountains. Similar studies in the Rio Grande, Great Basin, and Colorado River Basin have shown inconsistent trends in April 1st SWE, possibly due to trend detectability issues or physical mechanisms that buffer the snowpack against temperature changes (Harpold et al., 2012).

Accurate monitoring and modeling of snow improves the ability to assess Earth system conditions, trends and future forecasts while serving the global interests regarding water supply and weather forecasting (Girotto et al., 2020). The environmental complexity and limited number of long-term in-situ observations are challenging the simulation and observation of fine-scale spatial and temporal seasonal snow-cover patterns (Peters-Lidard et al., 2018).

For snowmelt, there are two main types of models: temperature index models and energy balance models (Girotto et al., 2020). Temperature index models, also called degree-day models, use empirical relationships between local air temperature and snowmelt to estimate the snow decline (Ohmura, 2001). Energy balance snow models are designed to simulate all energy exchanges within a snowpack, calculating snowmelt based on the net internal energy determined by these energy fluxes (Girotto et al., 2020). The appropriate modeling choice should depend on how well a process should be represented and what the intended application is.

For this thesis, a unique dataset of April 1st SWE measurements from 1943-2023 from the Wägital in Switzerland was analyzed. A long-term dataset like that can offer valuable insights into historical variation in snowpack and trends in the region. The importance of historically available data sets cannot be overstated, as they provide a baseline for detecting and analyzing long-term climate trends (CH2018, 2018). This available dataset from the Wägital is particularly valuable because it spans multiple decades, allowing for a comprehensive analysis of how snow patterns have evolved in response to climatic shifts and variability. However, April 1st measurements may not give good information on the maximum snowpack and lead, for example, to a potential underestimation of maximum SWE (Bohr & Aguado, 2001). This is especially problematic if there is variability in snowmelt timing due to climate change (Harpold et al., 2012). It is therefore important to critically assess the data set and to capture the full picture of snow accumulation and melt dynamics before determining trends in SWE in the Wägital.

1.1 Aim and Research Questions

The overall goal of this thesis is to advance the research on the spatial and temporal variability in SWE while also providing valuable insights for decision-making in water resource management, ecological conservation, and climate adaptation strategies in alpine regions. The main goal of this research is to develop a degree-day model to simulate SWE using only two input datasets, precipitation and temperature, and to use the model simulations to determine the maximum SWE for each year. In addition to the creation of the model, the thesis includes comprehensive data and statistical analyses, as well as trend analysis based on the simulated SWE data. The following research questions are investigated in this thesis:

(i) How well does April 1st SWE represent the maxSWE in the Wägital?

(ii) What is the spatial variability in maxSWE across the Wägital? i.e., what is the relation between maxSWE and elevation, aspect, and slope?

(iii) What is the trend in maxSWE and the number of snow cover days?
   a. How does the trend for maxSWE differ by elevation, aspect, and slope?
   b. How do the length and starting point of the observation period affect the identified trends in maxSWE and number of snow cover days?

(iv) How does the SWE differ for warm years and cold years, and for wet years and dry years?

The observed April 1st SWE values were expected to reflect the maxSWE in the Wägital. However, due to interannual variability, these measurements may not always capture the absolute peak. It is anticipated that significant spatial variability regarding SWE exists within the Wägital. Specifically, higher elevations are expected to have a higher SWE than lower elevations. In terms of aspect, south-facing measurement stations, which receive more sunlight, are expected to have less snow than north-facing stations, while east-facing stations, often on the leeward side, are predicted to accumulate more SWE than west-facing ones. Additionally, steeper terrain is likely to have lower SWE due to the influence of gravity, in contrast to flatter terrain, which is expected to retain more snow.

When examining trends over time, the overall trend in maxSWE in the Wägital is expected to be negative, reflecting the broader impacts of climate change (cf. (FOEN, 2021)). This negative trend is anticipated to be more pronounced at lower elevations compared to higher ones. As for aspect, the trends in maxSWE are expected to be most negative in the northern aspect and least negative in the southern aspect. Concerning slope, flatter terrains are expected to show a stronger negative trend in SWE than steeper terrains. Similar to the trend patterns in maxSWE, a decrease in snow cover days over time is expected.

Regarding meteorological year categories, it is hypothesized that cold and wet years will yield the highest SWE levels, followed by warm and wet years. Conversely, warm and dry years are expected to produce the lowest SWE levels. This analysis will help to further understand the interplay between climate variability and SWE dynamics in the Wägital.

2 State of the Art

This chapter will provide an introduction to the key parameter examined in this thesis, the SWE. Additionally, it will review current and past research on SWE measurements and trend analyses, both in Switzerland and internationally, to identify existing knowledge gaps. By understanding these gaps, the context of this thesis will be established, highlighting how its objectives aim to contribute to the already existing research.

2.1 Snow water equivalent (SWE)

The snow water equivalent (SWE), measured in millimetres of water equivalent (mm w.e.), kilograms per square meter (kg/m2), or liters per square meter (l/m^2), indicates the depth of water that would result if the snow were to melt completely. This metric applies to a unit surface area of the snow sample and represents the snow cover across a specific region or confined area of snow (Fierz et al., 2009).

Cover-snow depth, bulk snow density, and snow water equivalent are the three basic properties used to describe snow. These three properties are interconnected with each other because bulk density multiplied by snow depth determines the SWE (Marty et al., 2023).

$$\boldsymbol{SWE = relative\ snow\ density \times snow\ depth}$$

SWE is a key component of the water budget of a catchment because it is an important resource for hydroelectricity production but is also a potential flood risk when a high snowpack melts rapidly in spring (Brown et al., 2019). Water resource management in snow-dominated regions depends on the clear distinction between snow accumulation and snowmelt seasons. This separation allows for the prediction of annual river flows based on the amount of maximum snow accumulation (Musselman et al., 2021). The date April 1st is often used to distinguish between the winter snow accumulation and spring melt seasons. It also serves as an approximation for the maximum annual SWE (Pagano et al., 2004).

However, examining the measurements of SWE across Switzerland by Pielmeier et al. (2024) (Figure 1) for selected winters it reveals that the maxSWE does not always occur on April 1st. This observation highlights potential issues with the accuracy and representativeness of using April 1st SWE measurements as maxSWE and also the accuracy of using April 1st for long-term trend analyses and snowpack dynamics. This discrepancy raises important questions about the reliability of this date as a proxy for capturing peak SWE and suggests a need for more nuanced approaches in trend analysis and snowpack assessment.

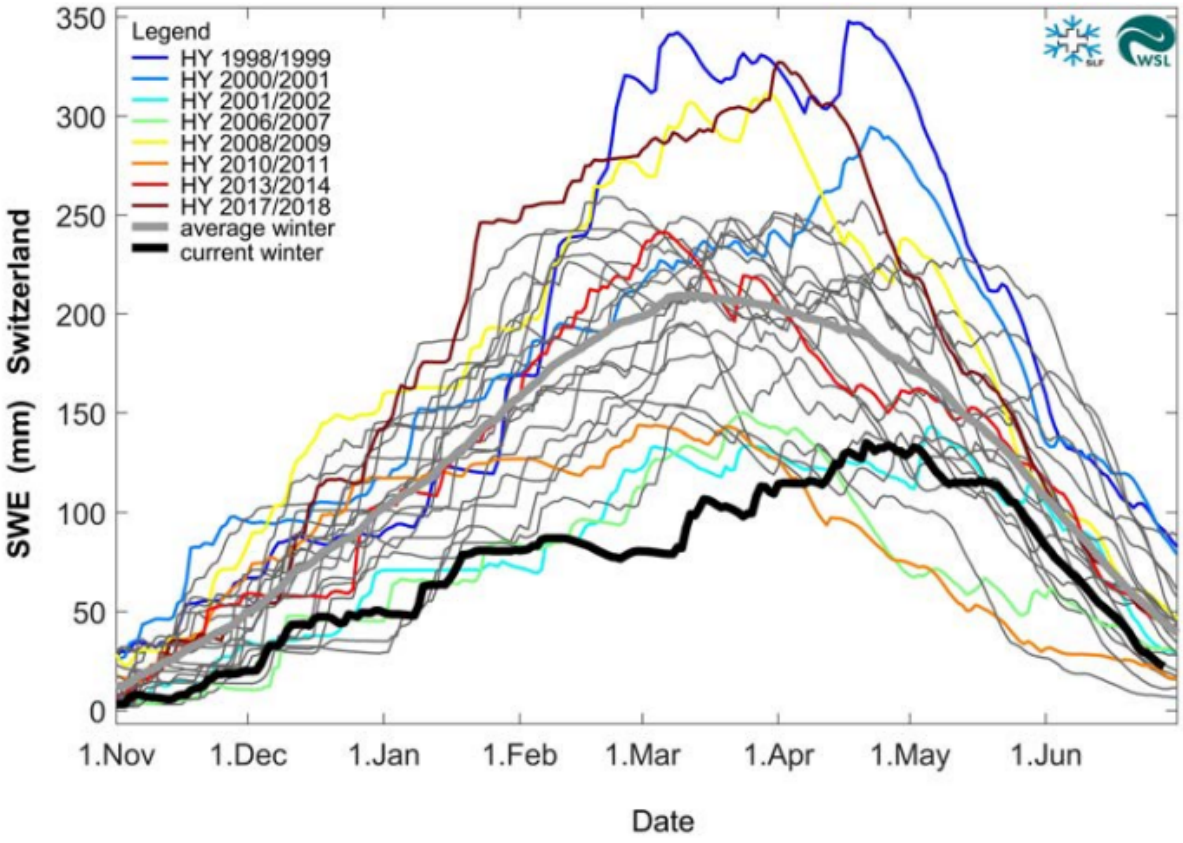

Figure 1: Comparison of SWE across Switzerland in selected winters. The black line representing the current winter meaning winter 2022/2023 and the grey line representing the average SWE for the period 1999-2023 (Pielmeier et al., 2024).

2.2 Spatial Variation in SWE

At a Swiss national scale, the mean SWE shows significant spatial variation. In low-altitude regions, such as the Swiss Plateau, only a few millimeters of SWE are recorded. In contrast, the Alpine regions exhibit far higher SWE values, typically ranging between 100 mm and 300 mm, with the highest values observed in the Bernese Alps and the Gotthard region, reaching up to 600 mm. Regarding days with measurable snowfall, on the Swiss plateau, snowfall occurs on approximately 10 to 30 days between September and May. In most Alpine regions, the number increases, ranging from 30 to 120 days. In southern Switzerland, in the Rhone Valley and the Lake Geneva region, the mean number of days with snowfall is less than ten days, marking the lowest in Switzerland (CH2018, 2018).

At the catchment scale, the variability of snow accumulation and snowmelt is influenced by topography, whereas elevation and aspects are the dominant factors (Anderton et al., 2004; Pomeroy et al., 1998). The high variability of SWE at smaller scales presents challenges in establishing clear relationships between SWE and topographic controls like elevation and aspect (Jost et al., 2007). Jost et al. (2007) showed that elevation, slope aspect, and vegetation contributed 80 % to 90 % of the spatial distribution of snow cover and identified areas where elevation most strongly affected snow cover in British

Columbia, Canada. In the Swiss Alps, Grünewald et al. (2014) observed that snow depth increases with increasing elevation up to a certain altitude, after which it decreases at the highest elevations. Lower snow accumulations in forests are primarily due to the interception of snow by the canopy (Faria et al., 2002; Winkler et al., 2005). Similarly, Zhong et al. (2021) examined snow cover distribution in the Chinese Altai Mountains and found that elevation and latitude are the primary factors influencing snow depth and SWE. Snow depths and SWE generally increase with elevation, reaching maximum values at specific altitude ranges, but show varying patterns depending on the region, with some areas experiencing decreases at higher elevations. SWE generally increased with slope angle in the regions of alpine Koktokay and piedmont sloping plain but showed the opposite trend in the alpine Kanas-Hemu, where the effects of wind, gravity, and forest sheltering led to higher SWE on gentler slopes.

The spatial variability of SWE is driven by a number of different processes. In Alpine areas, snow accumulation is influenced by the preferential deposition of snow in microscale topographic depressions or on the leeward side of ridges. In forests, the spatial variability of snow accumulation is related to preferential deposition around fallen tree trunks, as well as the spatial variability of snow interception and discharge from the forest canopy. Additionally, the spatial variability of melt energy is related to the local advection of energy across patchy snowpacks and the spatial variability of radiative forcing and air temperature (Clark et al., 2011).

2.3 SWE Monitorings in Switzerland

Switzerland currently has four distinct SWE monitoring programs which are still in operation today. Each of these programs was initiated with different specific focuses, reflecting diverse research objectives and regional needs (Marty et al., 2023).

a) Glaciers: SWE measurements at the end of winter on about a dozen of Swiss glaciers
b) Nation-wide: In-situ SWE measurements at two dozen stations, which are mainly used for daily snow and avalanche monitoring.
c) Alpthal: In-situ SWE measurements at multiple sites for the long-term investigation of forest-snow interactions.
d) Wägital: Catchment-based SWE measurements on April 1st, originally used for water resource monitoring for hydro-power.

End-of-winter snow depth measurements on glaciers in Switzerland (a) have been available since 1914. However, only the observations on the Claridenfirn are complete and consistent. Additionally, the end-of-winter SWE measurements have only been available since 1957. The measurements are typically taking place in May, at the end of the accumulation period, with the goal of determining the winter's SWE.

The SLF carries out nationwide SWE measurements at SLF stations (b). The number of stations where the SWE is measured twice a month has increased from 10 stations in the 1940s to around 45 stations. Because of the growing demand for SWE measurements in the early 2000s as verification for flood forecasting models, a decline in measurement stations could be halted. Some of the long-term measurement series had to be abandoned due to challenges such as the lack of available observers or insufficient funding. At least 22 series exist with a measurement period of at least 50 years (Marty et al., 2023).

In the Alpthal (c), manual SWE measurements are made at 15 locations which are located within different elevations, slope exposures and vegetation types. The longest available measurement series consists of SWE and snow depth measurements at one location since 1969 (Stähli & Gustafsson, 2006).

The Wägital monitoring program (d) started on April 1st 1943. Within the Wägital catchment, SWE measurements were accomplished at 13 locations. Nowadays, SWE is measured at 11 locations, and additionally, snow depth is measured at 26 locations. With the measured data, a function is fitted every year by interpolating the snow densities for each 100 m elevation zone and main exposures. Together with the respective snow depth measurements, the snow mass is estimated for the elevation zone and exposure. The SWE for the entire catchment can be calculated by integrating the snow mass values over altitude and exposition zones. To also look at possible elevation-dependent differences, the catchment has also been separated into two elevation bands, a lower band from 900 to 1'500 m a.s.l. with 24.68 km^2 and an upper band from 1'500 to 2'300 m a.s.l. which covers 13.49 km^2 (Noetzli and Rohrer, 2014). The Wägital measurement series also serves as the data source for this thesis. Further details about the monitoring program will be discussed in Chapter 4.1.

Several studies (e.g. Schmucki et al., 2014; Stähli et al., 2021; Stähli & Gustafsson, 2006) have been conducted using data from one of the discussed individual monitoring programs. Marty et al. (2023) conducted the first joint analysis of these measurements despite the different temporal resolutions. To compare the different monitoring programs, Marty et al. (2023) used the DeltaSnow model (Winkler et al., 2021) to derive daily SWE values since 1957. This model only requires daily snow depth as data input, which was available for all but four stations and the Wägital catchment. The temporal evolution of daily SWE values in the Wägital was therefore not derived by the study. For the other measurement stations, possible long-term changes were derived using the Mann-Kendall test (MK) and Theil-Sen slope estimator. The long-term trends of all SWE indicators showed no clear elevation dependence. At almost 80 % of the stations, the date of disappearance of SWE showed a decreasing trend, suggesting that the snow cover disappears earlier in the year. More than 40 % of the stations showed a significant decreasing trend for maxSWE; the trends in April 1st SWE were similar to the maxSWE trends but with only 20 % significance. However, the analysis confirmed that the April 1st SWE is not a good indicator for trend analysis because the variability between the individual years is much higher than for maxSWE.

They found little evidence of a long-term trend in SWE indicators until the late 1980s; however, since then, the trends emerge towards decreasing.

Noetzli & Rohrer (2014) analyzed the trends for the April 1st SWE data in the Wägital. At first glance, it is challenging to recognize a clear trend in Figure 2. Phases of high SWE alternate with periods with little SWE, where the spring snow cover contributed only minimally to the runoff from the Wägital area. Notably, some phases exhibit substantial variability; for instance, between the exceptionally snowy years of 1970 and 1975, there were a few average years and the minimum year of 1972. Snowy years have also occurred in more recent times, as presented by the years 1999, 2000, and 2009. In their statistical evaluation, Noetzli & Rohrer (2014) revealed only a weak negative trend in the lower altitudes and no trends in the higher altitudes.

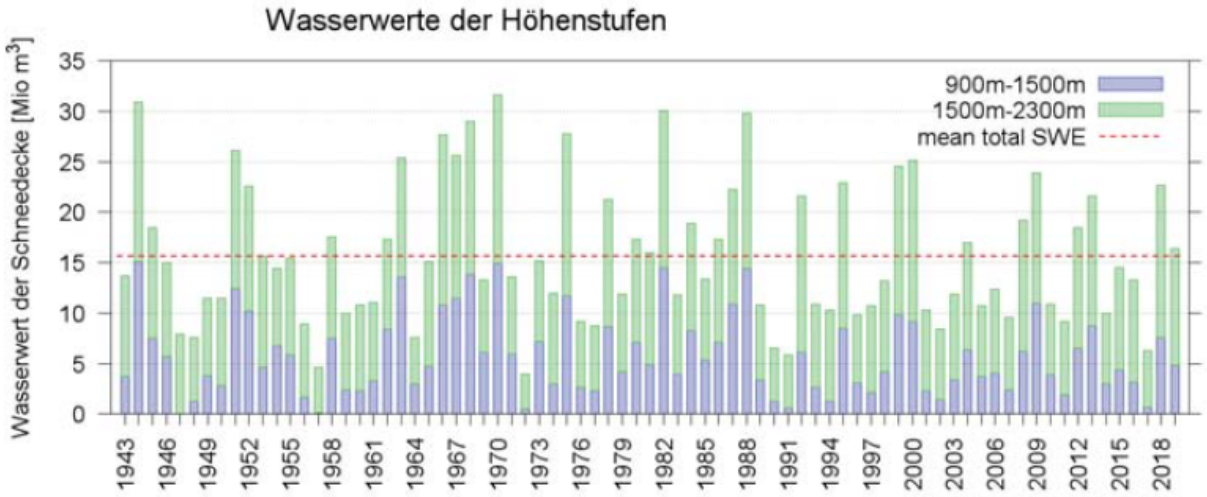

Figure 2: Volume of water stored in the snow cover in the Wägital on April 1st split in two elevation bands. X-axis representing the years and y-axis representing the SWE [Mio m³], the red line represents the long-term mean SWE for both elevation bands together (Noetzli et al., 2019).

In order to show trends in the April 1st data, a Gaussian low-pass filter was applied. The results showed only indistinct trends, especially at higher altitudes. At lower altitudes (900-1500 m a.s.l.), three very sharp downward shifts were observed. The first two shifts occurred in the early 1950s and late 1960s, followed by a recovery of snow and water reserves, returning to levels observed before the respective decline. The third downward shift occurred toward the end of the 1980s, followed by only a partial recovery in the measured snow values.

2.4 International SWE Monitorings and Trend Analyses

Across large parts of **Canada,** a manual biweekly gravimetric snow survey has been conducted since the mid-1950s. The measurements begin each year once the snowpack is well established and continue until the main melt period has started. Additionally, daily SWE observations are collected at 72 automated snow pillow sites (Brown et al., 2019). An analysis of trends in SWE was carried out by Brown

et al. (2019), focusing on three key dates, February 1st, March 1st, and April 1st, from 1967 to 2016. The analysis was conducted using grid cells (0.1° x 0.1° latitude-longitude). The non-parametric Kendall's rank correlation was employed to assess trends. The results revealed remarkable spatial variability, but only a small percentage of grid points showed statistically significant trends. Among those that did, the significant trends predominantly indicated a decrease in SWE. For the April 1st measurements, the average SWE decreased by 5.7 mm over the observation period. The largest negative trends were observed at lower latitudes, while a tendency to mainly positive trends could be found in the Arctic circle.

The study by Musselman et al. (2021) analyzed historical daily snowmelt patterns using automated SWE measurements from 1'065 remote telemetry stations across the mountainous regions of **western North America**. For each station and year (1982 to 2016), they computed the cumulative annual daily melt, the date of maximum SWE, as well as the April 1st SWE. A trend analysis of these parameters with data records ≥ 30 years was conducted using a MK and the Theil-Sen slope estimator. For the full period of record, the average date of maximum SWE computed on all stations was found to be within one day of April 1st, however, with a geographical variability. The snowpack peaks around early April occurred in the Sierra Nevada and intercontinental regions, peaks in early March occurred in the US Pacific Northwest and Southwest, mid- to late-April maximums in interior Alaska, and near early May in cold continental regions. The melt and snowpack trends indicate that while stations with significant melt increases have recorded mostly in November and March, melt is increasing in all cold season months from October to March. The study revealed that when using April 1st as the date of maximal SWE, snowmelt has already started during the accumulation period in 34 – 42 % of the stations. This blurs the seasonal distinction between accumulation and melt phases. Additionally, the study found that the decline in the reported April 1st SWE is more strongly influenced by a decrease in precipitation than by temperature changes.

To assess trends in SWE across **High Mountain Asia** (HMA) from 1987 to 2009, Smith & Bookhagen (2018) used passive microwave data from the special sensor microwave imager (SSMI) spatially averaged from raw swath data across ten catchments. The trend was tested by using a MK test followed by the performance of a linear regression. The results reveal that annual trends in SWE are generally negative; however, there are distinct seasons and elevations that show heterogeneities. Across all catchments, a strong, nonlinear elevation-SWE relationship could be observed. The magnitude of the relation is distinct and unique for each catchment.

The recent international studies discussed above extend back as early as 1957, whereas the available SWE data from the Wägital dates back to 1943. Only the SLF measurement station at the Weissfluhjoch in Davos, Switzerland, offers a longer record of SWE than the Wägital dataset. The Wägital dataset includes 14 years of SWE measurements that have not been covered by previous research outside of Europe. Analyzing these earlier years will provide valuable insights into previously unexamined periods

and contribute additional knowledge about the historical evolution of SWE, enhancing the understanding of long-term trends and changes.

With this foundational background information about important key definitions and prior studies on SWE trend analysis in Switzerland and internationally, the focus now shifts to the study site where the data for this thesis was sampled.

3 Study Site – Wägital

The Wägital is a north-facing catchment in the central Swiss pre-Alps, south of Lake Zurich (coordinates: 2'712'675 / 1'216'471). Its main stream, the Wägitaler Aa, flows out of the Wägitalersee and leads eventually into the Lake Zurich. The Wägital extends in Siebnen on 445 m a.s.l., passing through Vorderthal and Innerthal, where the Wägitalersee is situated and reaches up to the surrounding mountain ranges that define the catchment's boundaries (Figure 3). The highest peak in the catchment is the Mutteristock, which rises to 2'294 m a.s.l.

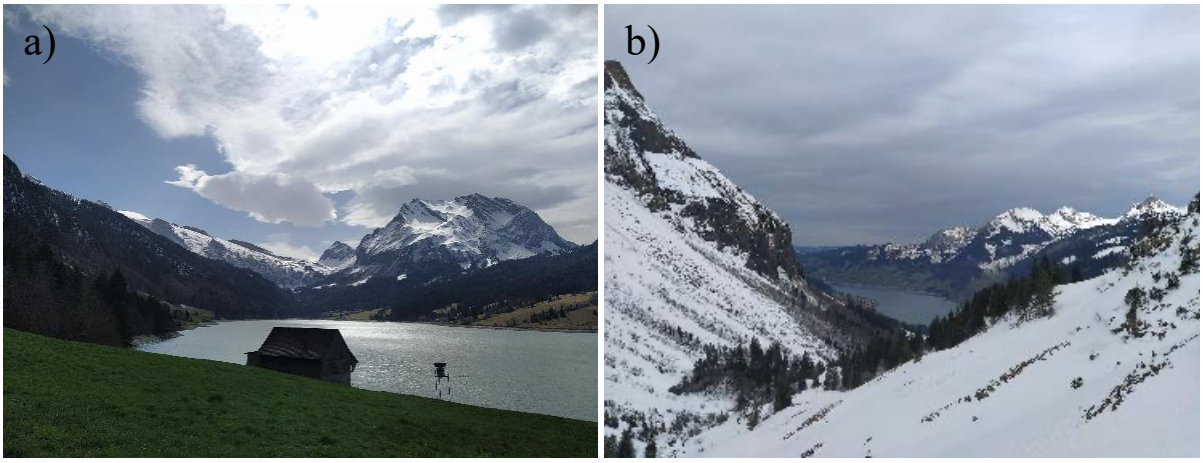

Figure 3: Picture a) shows the Wägital in direction South, and picture b) in direction North. Both pictures were taken on 26.03.2024 during the yearly SWE monitoring (Fiona Sigrist, 2024)

Geologically (Figure 4), the Wägital is situated within a significant tectonic structure that extends in a southwest to northeast direction, forming a shear zone within the Drusberg nappe, which is part of the Helvetic radiolarite. This zone lies between the Rederten element to the east and the eastern edge of the Drusberg element. The Wägitalersee is located in an area characterized by the extensive Wägital Flysch. Additionally, the region is marked by extensive karst landscapes (Schrattenkalk Formation). Significant karst springs in the Wägital include the Fläschloch and Hundsloch springs. The rain and meltwater infiltrating through karst fissures flow rapidly through the underground systems. Due to the lack of reaction time, the water from karst springs is poorly filtered (Hantke & Kuriger, 2003).

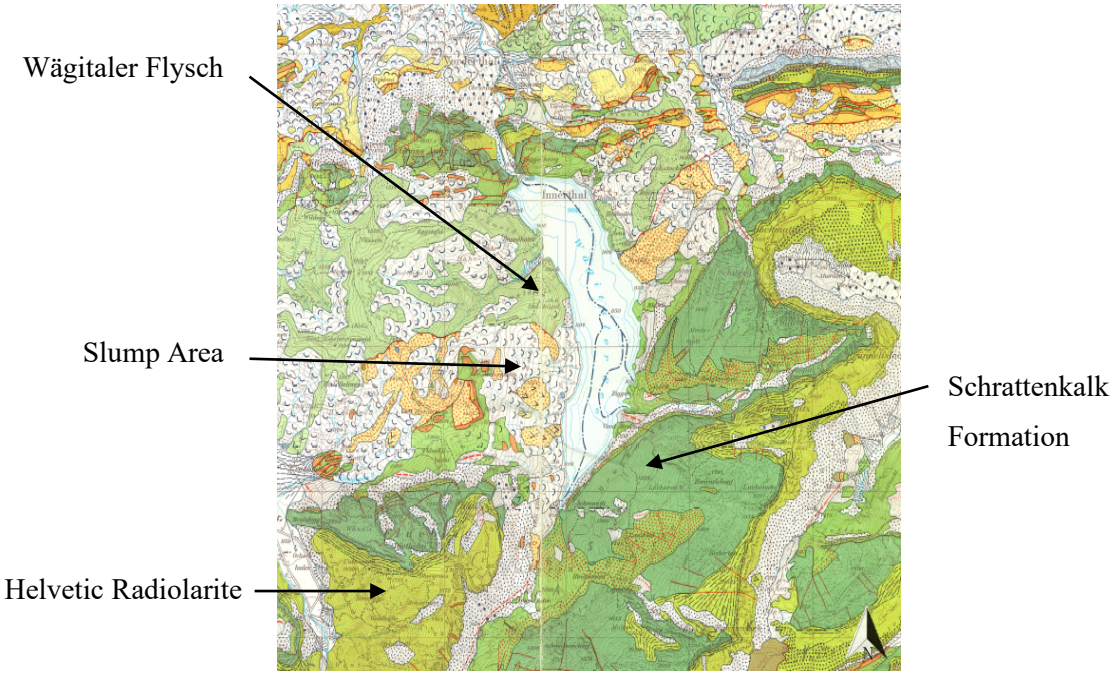

Figure 4: Excerpt of geological map showing the Innerthal area of the Wägital including the Wägitalersee (Hantke, 1967), edited. In the east the Wägital is dominated by the Schrattenkalk formation, to the west the Wägitaler Flysch is predominant additionally, the west is also characterized by several slump areas.

For this thesis the focus lies on the Innerthal, the part of the catchment that reaches from the artificial Wägitalersee up to the surrounding mountain peaks above 2000 m a.s.l. This part of the catchment has an average slope of 22°. Almost one-third (32 %) of the catchment is covered by forest, whereas 27 % is characterized by coniferous forest, 4 % by mixed woodland, and 1 % by scrubs. Another 34 % of the catchment is distinguished by grass and herbaceous vegetation. Rock and loose rock make up 19% of the total land area, and the lake and some additional wetlands cover 14 % (HADES, 2023). With 181 inhabitants (as of 31.01.2023), the municipality of Innerthal is not heavily populated (Gemeinde Innerthal, 2024).

Meteodat GmbH operates a snow measurement network in the Wägital catchment with the purpose of assessing the SWE of the catchment on April 1st. The snow measurements are nowadays performed at 37 locations for snow depth, and within those locations at 11 locations, snow density is additionally measured (Figure 5). These snow measurements already started in 1943 when interest arose by the hydropower authority of how much water would melt in wintertime, reach the lake, and furthermore, how it influences the hydropower supply (stated by Dr. Ilja van Meerveld, Prof. Dr. Jan Seibert, and Meteodat GmbH). The power authority started to measure the SWE at 13 locations, with the number of measurement points increasing over the years to a maximum of 45 operational locations.

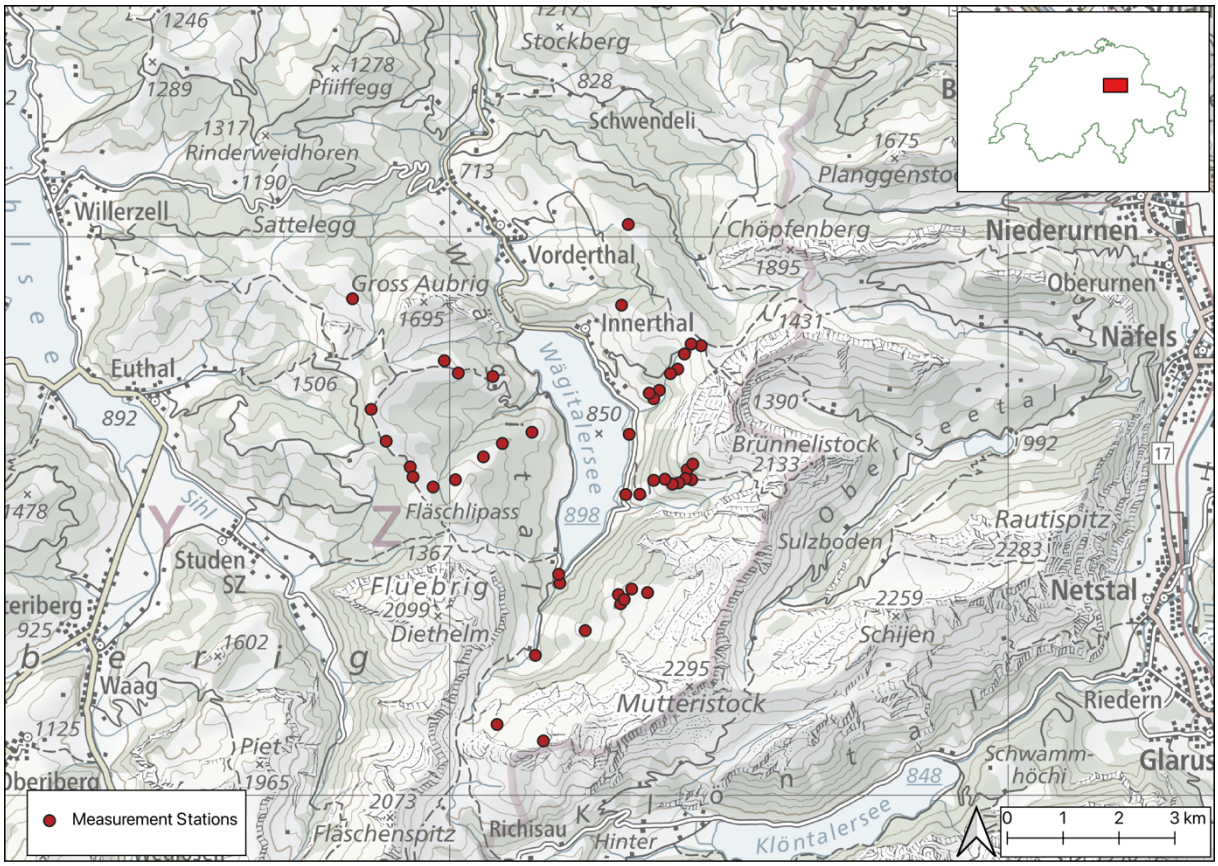

Figure 5: Map of all 45 locations of the measurement stations in the Wägital.

4 Methodology

This chapter describes the methodological framework for this thesis. The approach includes the collection of SWE and meteorological data, the implementation of a degree-day modeling approach for snowmelt estimation and the calibration of the model to ensure accuracy. In addition, this chapter describes the systematic grouping of the measurement stations, which provides insight into the organization and analysis of the data to support the research objectives.

4.1 SWE and Meteorological Data Collection

The SWE measurements in the Wägital were originally (1943 – 1984) carried out by Hans Siegenthaler from the Laboratory of Hydraulics, Hydrology and Glaciology (Versuchsanstalt für Wasserbau, Hydrologie und Glaziologie (VAW)). From 1985, the Geographical Institute of the ETH Zurich (GIETHZ) continued the measurements. Meteodat GmbH has been responsible for the measurements since the spring of 1998 and provided the current data set used for this thesis, including the April 1st SWE data, elevation, aspect, and coordinates for each measurement station. A list of all stations and their exact locations can be found in Appendix A1.

The SWE is measured by weighting snow cores. For the monitoring program in the Wägital, an aluminum cylinder called the ETH-tube, is used (Figure 6a). This tube has a cross-sectional area of 70 cm^2 and a height of 60 cm. The SWE is assessed by weighing multiple snow cores taken perpendicular to the ground surface along the total snow depth. When necessary, a snow pit is dug to ensure that the total depth is accounted for (Figure 6b). The snow cores are weighed using a calibrated spring balance, and the individual weights are summed to calculate the total SWE of the snowpack (Egli et al., 2009). The measurements are repeated until the ground surface is reached, ensuring the final sum of SWE values reflects the entire snowpack's water equivalent (Marty et al., 2023). Since neither the ground nor the snow cover surface is perfectly level, it is essential that SWE measurements are always related to the corresponding snow depth. That is why, in the end, SWE for a measurement station or an area is calculated by multiplying the bulk snow density by the measured snow depth and averaged as appropriate (Marty et al., 2023).

In the Wägital, the annual SWE measurements are conducted at 11 locations. Additionally, snow depth is measured at various locations. A maximum of 34 locations existed; nowadays, snow depth is measured at 24 locations. Some funding reasons in the 1990s caused the annulment of some stations. When possible, snow depth is measured using an avalanche probe, capable of reaching depths up to 240 cm. A longer probe, also used by the military, is required for deeper snowpacks.

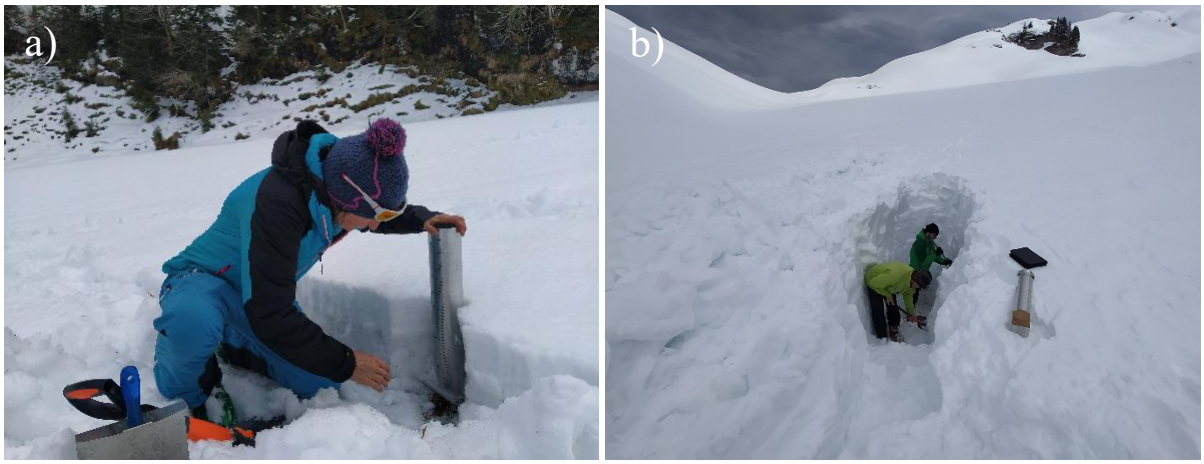

Figure 6: Pictures of the manual SWE measurement with ETH-tube during the monitoring 2024. a) at station Aberenalp and b) at station Oberalp Boden where a snowpit had to be dug (Fiona Sigrist, 2024).

This technique with the ETH-tube is a point-wise in-situ measurement, allowing for the investigation of various snow characteristics like wetness, hardness, layering, and specific surface area. However, this manual technique is labor-intensive and destructive, limiting its efficiency. Additionally, it offers low temporal and spatial resolution and cannot be applied in areas with potential avalanche risk (Botteron et al., 2013).

Snow measurements in the Wägital are typically scheduled around April 1st. However, whether the measurements can be conducted depends on weather conditions and avalanche risk. Due to the extensive measurement network, multiple days are often required to complete all the measurements. Despite this, the data collected over several days is collectively considered as measurements taken on April 1st.

Snow data has been collected without interruption since 1943. It was previously used to produce inflow forecasts for the pumped storage power plant the Wägitalersee, which was one of the largest artificial lakes in the world in its first years of operation. The snow data was used in particular to estimate the hydroelectric potential of this catchment area. Nowadays, the data is only collected for scientific purposes (Noetzli and Rohrer, 2014). Based on the measured snow densities and considering the exposure, functions are developed which represent the elevation dependence of the snow density. These functions vary from year to year and depend strongly on the course of the respective winter. The functions are then used to interpolate the SWE values for those measurement stations where only the snow depth was measured (stated by Meteodat GmbH).

Daily precipitation and temperature data are required for the degree-day model, which will be discussed in Chapter 4.2. Precipitation has been recorded daily since 1925 at the guardhouse (“Wärterhaus”) in Innerthal, as well as at Rempen, the compensating reservoir of the Wägitalersee and in Siebnen where the Wägital opens into the Linth valley. The three rain gauges are currently operated by the Federal

Office of Meteorology and Climatology (MeteoSwiss). The digitized precipitation data from these stations prior to 1987 had not been checked for correctness. After cleaning the data and verifying with Meteodat GmbH, it was decided to use the daily precipitation records from the guardhouse as the input data for the degree-day model because this rain gauge was situated in the Innerthal and was expected to represent best the precipitation patterns of the surrounding area, where the measurement stations were located. Daily temperature data has been recorded since 1956 at the same three stations as the precipitation. However, temperature data was only available until 1991, and the data has not yet been verified for accuracy. A comparison between the existing temperature data from the Innerthal guardhouse and data from the Einsiedeln weather station, where continuous temperature measurements have been recorded since 1931, revealed a strong correlation of 0.966 between the datasets. The Einsiedeln meteorological station is located 12 km to the west of Innerthal at an elevation of 911 m a.s.l. Due to these similarities of the two locations, it was decided to interpolate the Einsiedeln data with the Wätigal temperature data to fill the gaps in the daily temperature records for the Innerthal.

The precipitation data was also provided by Meteodat GmbH, while the temperature data from Einsiedeln was downloaded from MeteoSwiss. In this thesis, whenever years are mentioned, they refer to hydrological years, which run from October 1st to September 30th. For example, the year 1943 refers to the hydrological year spanning from October 1, 1942, to September 30, 1943.

With the observational SWE data, along with daily precipitation and temperature records, all data required for the next step—developing a degree-day model—was available. The detailed construction and methodology of the model will be examined in the following chapter.

4.2 Degree-day Modeling Approach

One of the purposes of snow modeling is to forecast and estimate the snowmelt input into a streamflow. Forecasts of streamflow are necessary for issuing flood warnings and for making decisions about water regulation. The model should not only produce daily snowmelt discharge series but also produce an estimate of the water stored in the snowpack. The estimate of the water stored in the snowpack can be compared with field measurements, which allows for an update on the estimated water storage (Kokkonen et al., 2006).

As outlined in the Introduction, snow models generally fall into two categories: temperature index models and energy balance models (Girotto et al., 2020). For representing snowpack processes, the temperature index method also called the degree-day modeling approach, has become the most widely used modeling approach in rainfall-runoff modeling. The reasons for that are that it has a comparatively simple structure and follows a straightforward approach (Lopez et al., 2020). The degree-day models are based on the assumption that the temporal variability of incoming solar radiation is well represented by the variations in air temperature (Ohmura, 2001; Sicart et al., 2008). These kinds of models easily meet

data requirements and computational demands. This allows them to offer a satisfactory balance between simplicity and performance, making them effective in various contexts and applications, even when data availability is limited (Hock, 2003).

As foundation for the degree-day model constructed for this thesis, the snow routine of the HBV (Hydrologiska Byråns Vattenbalansavdelning) model was used. The HBV model is a conceptual bucket-type and semi-distributed rainfall-runoff model used for various applications (Bergström, 1976). The snow routine of the HBV model relies on widely adopted and thoroughly tested conceptualizations of key snow processes, which are essential for rainfall-runoff modeling. Specifically, it addresses the partitioning of precipitation into snow and rain phase and the dynamics of snow accumulation, including subsequent melting and refreezing cycles of the snowpack (Figure 7). To simulate the evolution of the snowpack, the HBV model uses a simple approach based on the degree-day method (Lopez et al., 2020). It is assumed that snowmelt rate is directly proportional to the temperature above the freezing point over time, with a constant factor known as the degree-day factor (Collins, 1934; Martinec, 1960). The snow routine requires precipitation and temperature data as input. Using five calibration parameters, the model outputs snowpack and snowmelt results, with the latter corresponding to the SWE (Lopez et al., 2020). The snow routine of the HBV model contains five calibration parameters, which will be discussed in detail below.

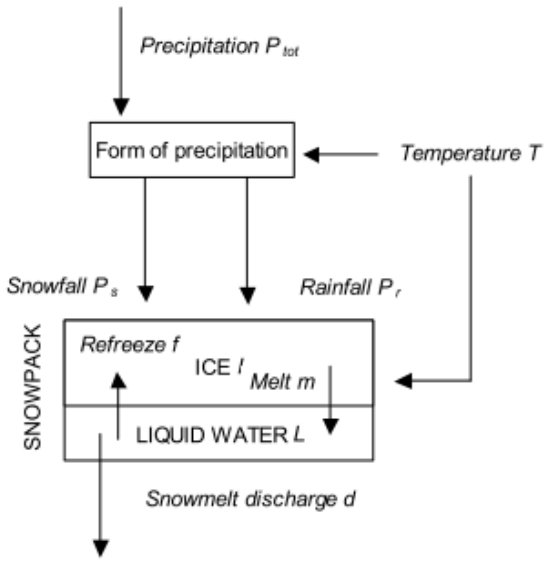

Figure 7: Schematic conceptualization of snow processes (Kokkonen et al., 2006)

For the degree-day model constructed for this thesis, the **degree-day factor CFMAX** is utilized. Unlike models with a fixed degree-day factor (Valéry et al., 2014), CFMAX can vary since it is sampled from a defined range, in this case from 1-10 with increments of 0.1. This allows to account for spatial variations like slope, aspect or vegetation cover (He et al., 2014).

Many models use the freezing point (0°C) as the threshold temperature where precipitation falls as snow instead of rain (Walter et al., 2005), but some include a calibrated parameter to account for spatial variations (Viviroli et al., 2007b). In the model developed for this thesis, the **threshold temperature TT** is sampled from a range of -1.5 to 2.5°C in increments of 0.1°C. This flexibility allows the model to adjust the TT based on calibration, enhancing its accuracy across different spatial contexts. A single threshold temperature per day may not fully capture snow accumulation and snowmelt when temperatures are near 0°C, as the transition between rain and snow is not always abrupt in reality. Rain and snow can occur simultaneously, leading to a more gradual transition (Dai, 2008; Magnusson et al., 2014; Sims & Liu, 2015)

Additionally, the model includes a **snowfall correction factor SFCF,** which represents the combined effect of snowfall undercatch and interception of snowfall by vegetation (Lopez et al., 2020). This parameter is sampled from a range from 0.4 to 2, also in increments of 0.1. SFCF accounts for discrepancies in snowfall measurements.

The following parameters extend beyond the simple degree-day model. They are, however, part of the HBV snow routine and add a degree of detail (Lopez et al., 2020).

Some models disregard refreezing as it is often negligible compared to snowmelt (Magnusson et al., 2015). The constructed model includes refreezing, controlled by the constant **refreezing coefficient CFR** set to 0.05. When temperatures fall below the threshold temperature, a portion of the liquid water refreezes, adding more details to the snowpack dynamics (Lopez et al., 2020).

Furthermore, the water holding capacity CWH (set to 0.1) is incorporated into the model. The CWH determines the certain volume of melted water remaining in the snowpack. It is given as a fraction of the corresponding SWE of the snowpack (Lopez et al., 2020).

The goal of the constructed model for this thesis is to identify the optimal parameter combination for TT, CFMAX, and SFCF that minimizes the objective function in each measurement station. The parameter range and values (Table 1) were defined based on Seibert & Vis (2012) and slightly adjusted during the modeling process to improve performance. With the chosen parameter ranges, a total of 63’427 parameter combinations were possible.

Table 1: Model parameter ranges used for optimization for degree-day model.

Parameter	Description	Unit	Range / Value
TT	Threshold temperature	°C	[-1.5 to 2.5 by 0.1]
CFMAX	degree-day factor	mm t^{-1} $°C^{-1}$	[1 to 10, by 0.1]
SFCF	snowfall correction factor	-	[0.4 to 2 by 0.1]
SP	initial snowpack	mm	0
CFR	refreezing coefficient	-	0.05
CWH	water holding capacity	-	0.1

4.2.1 Model Calibration

The calibration of the model is the process where the parameters get adjusted until the simulated SWE closely matches the observed SWE. This process relies on an objective function to quantify the difference between observed and simulated SWE (Solomatine & Wagener, 2011).

To calibrate the model, parameter values were randomly sampled from their respective distribution using a Monte Carlo approach. Specifically, 10'000 random parameter sets were selected from a potential pool of 63'437 combinations. Each parameter set was then used to run the degree-day model, generating daily SWE data. From these model outputs, the SWE values corresponding to April 1st of each year were extracted. These simulated SWE values were then compared with the observed April 1st SWE data. The performance of each parameter set was assessed by calculating the sum of squared errors (SSE), which serves as the objective function. The SSE quantifies the discrepancy between the simulated and observed SWE values and is calculated as follows:

$$SSE = \sum_{i=1}^{n} (x_i - \hat{x})^2$$

Where n is the number of samples (years with observed April 1st data), x_i is the observed SWE value and $\hat{x}$ is the predicted value.

The parameter set which minimized the SSE was selected as the optimal set. To achieve this, the parameter sets were sorted by their SSE values, and the set with the lowest SSE was chosen.

Following this initial run with 10'000 parameter sets across all measurement stations, further optimization of the model was conducted. By analyzing the dotty plots of the best-performing parameter values, the parameter ranges were adjusted, as detailed in Table 1. Additionally, a lapse rate was incorporated for both temperature and precipitation data, accounting for the variation in these variables with elevation. Specifically, a temperature lapse rate of -0.6°C per 100 meters of elevation gain and a precipitation lapse rate of 10 % per 100 meters of elevation gain were implemented. These adjustments lead to more accurate simulations of SWE.

However, results from modeling are inevitably subject to some uncertainty because models can only approximate real-world conditions in a simplified form and do not represent the physical world. Sources of uncertainty include model selection and structure, scaling and correction of model results, input data, initial conditions, model parameters, data for calibration and validation, natural variability, process understanding, and unforeseeable events which tip the balance of a system. To mitigate these uncertainties, combining different model approaches could yield in more reliable and robust conclusions (FOEN, 2018).

4.3 Grouping of Measurement Stations

To have a look at smaller spatial resolutions and how the trends of SWE vary regarding different external factors the measurement stations were put into groups regarding the different topics: elevation, aspect and slope.

4.3.1 Elevation

The measurement stations are located at elevations ranging from 905 to 1’800 m a.s.l. and are distributed throughout the catchment area. To examine whether trends vary across different elevation ranges, the catchment and the measurement stations were divided into distinct elevation bands.

In order to ensure the comparability of the data output with other studies, the delimitation of the elevation bands corresponds to the proposed methodology by Noetzli and Rohrer (2014). They divided the catchment into two bands: a lower band spanning from 900 to 1’500 m a.s.l. and an upper band ranging from 1’500 to 2’300 m a.s.l.

As a result, 38 stations are situated in the lower band (Group: elevation 900-1500 m a.s.l.), and seven stations are located within the upper band (Group: elevation 1500-1800 m a.s.l.). This distribution should facilitate a comprehensive analysis of the spatial variability of the SWE with respect to elevation across the catchment.

4.3.2 Aspect

In the data set provided by Meteodat GmbH, aspects were assigned to each measurement station. According to a discussion with the company, the aspects were assigned subjectively by Hans Siegenthaler, who categorized the stations into eight different aspect groups (N, NE, E, SE, SSW, SW, W, NW). To limit the number of groups somewhat for this thesis, the aspect groups were reduced to the four primary directions: N, E, S, and W. These orientations were determined by measuring the angular orientation from each station on the map (swisstopo, 2024a). As a result, the stations were distributed as follows: ten stations were assigned to the N aspect (Group: aspect N), seven stations were in the aspect E (Group: aspect E), five stations to the S oriented group (Group: aspect S), and 23 stations to the W oriented group (Group: aspect W). This simplified classification facilitates a more manageable analysis of the influence of aspects on the data.

4.3.3 Slope

The slope for each station was derived from the DHM25 (swisstopo, 2024b), a digital elevation model (DEM) of Switzerland. It is represented as a raster in the scale 1:25’000, and it provides elevation data for Switzerland, excluding vegetation and buildings. The slope angles at the measurement stations range from 4.7 to 24.5°. To analyze the variation of SWE with respect to the steepness of the individual locations, the measurement stations were categorized into four groups. There are eleven stations between 0-9.99° (Group: Slope 0-10°), 19 stations have a slope between 10-14.99° (Group: Slope 10-15°), eight

stations with a slope between 15-19.99° (Group: Slope 15-20°) and finally seven stations with slope between 20-25° (Group: Slope 20-25°). This grouping allows for a more detailed analysis of the relationship between slope steepness and SWE distribution across the stations.

A list of all characteristics per measurement station can be found in Appendix A1.

4.3.4 Meteorological Year Categories

Considering different meteorological inputs, it can be valuable to examine how SWE responds to varying climate conditions. To capture the impact of these differing climatic conditions on the SWE, each year in the dataset was categorized into one of four distinct meteorological categories:

- Cold and dry
- Cold and wet
- Warm and dry
- Warm and wet

These categories were determined by comparing annual average temperature and yearly precipitation data to their median values from the total observation period. A year was categorized as "cold" if its annual average temperature was below the median and "warm" if it was above the median. Similarly, a year was classified as "dry" if its annual precipitation was below the median and "wet" if it was above the median.

To further explore the variation in maxSWE, the analysis was conducted within the two different elevation zones discussed in Chapter 4.3.1. For each meteorological year category and elevation band, the maxSWE values were then aggregated to find the median maxSWE per year across all stations within each elevation band. This approach allows to capture both the temporal (yearly) and spatial (elevation-based) variations in SWE, providing a comprehensive view of how SWE responds to different climatic conditions.

4.4 Statistical Analyses

All statistical analyses, trend assessments, and visualizations were conducted using the R version 4.3.2 (R Core Team, 2023). To evaluate the relationship of maxSWE within the grouping factors (elevation, aspect, slope, and meteorological category), several statistical tests were employed, depending on the distribution of the data. First, the normality of maxSWE values within each group was tested using the Shapiro-Wilk normality test (Shapiro & Wilk, 1965). If the Shapiro-Wilk test indicated a non-normal distribution ($p < 0.05$), the Kruskal-Wallis test was utilized. This non-parametric test compares ranks among more than two groups and does not assume normality, making it suitable for comparisons across aspects, slopes, and meteorological year categories (Kruskal & Wallis, 1952). For post-hoc analysis, Dunn's test was applied (Dunn, 1964). However, in cases where the Kruskal-Wallis test was not significant ($p > 0.05$), no further post-hoc analysis was conducted. In the case of elevation groups, where the

Shapiro-Wilk test indicated normal distribution, a t-test was applied, as there were only two specific characteristics in the group. For all statistical analyses, a significance level of $\alpha = 0.05$ was adopted. Any p-values below this threshold were considered indicative of statistically significant differences between groups.

4.4.1 Trend Analyses

To analyze possible long-term changes, the non-parametric Mann-Kendall (MK) test was applied. This test is designed to detect the presence of a monotonic tendency in a time series of a variable, making it suitable for examining changes in maxSWE over time. It is a non-parametric method which does not assume any specific underlying data distribution and uses rank-based measures that remain unaffected by outliers. The MK test provides three key pieces of information. The Kendall Tau is the Kendall rank correlation coefficient, which measures the monotony and direction of the trend. The value of Kendall's Tau ranges from -1 to 1, with positive values indicating an increasing trend and negative values indicating a decreasing trend (Kendall, 1955; Mann, 1945). To assess the strength of a trend, a robust simple linear regression is performed using the Theil-Sen slope estimator. This method calculates the median of all slopes between pairs of points in the series, providing a reliable estimate of the trend's magnitude (Sen, 1968). The third information the MK test provides is the statistical significance of the trend. The trend is considered statistically significant if the p-value is less than 0.05, meaning that the hypothesis of no trend can be rejected with 95 % confidence (Kendall, 1955; Mann, 1945).

This trend analysis method was chosen for this thesis because studies discussed in Chapter 2, such as (Stähli et al., 2021) and (Marty et al., 2023), employed the same approach.

5 Results

This chapter presents the results of the model performance, followed by an analysis of the spatial distribution and the findings from the trend analysis. Finally, the impact of different meteorological categories is presented. Given the large number of measurement stations, it is difficult to present all details comprehensively. Therefore, in certain sections, specific stations or groups of interest were selected for closer examination. A complete list, including model performance values for the objective function, the best parameters, and any additional plots included in this study, are available in the Appendix.

5.1 Model Performance

The performance of the model is evaluated in three ways: first, through a visual comparison of observed versus simulated SWE on April 1st and throughout the entire time series, along with the results of the objective function. Second, a summary of the regression parameters and bias for each station is provided.

The following figures compare the simulated and observed SWE at the stations Mittl. Tannstofel (Figure 8) and Ziggen (Figure 9) for the period from 1943 to 2023. The top panels of the figures represent the SWE values recorded on April 1st of each year, while the bottom panel display the daily SWE values throughout the year compared to the observed April 1st SWE.

For the Mittl. Tannstofel, the visual comparison of April 1st values (Figure 8) reveals a general agreement between the simulated and observed values, indicating that the model captures the annual variability to a reasonable extent. However, there are some discrepancies where the model either overestimates or underestimates the SWE for certain years. These discrepancies may be due to several uncertainties and limitations, which will be discussed in Chapter 6.6.

The bottom panel for Mittl. Tannstofel captures successfully the seasonal accumulation and ablation of snow with the highest SWE values typically occurring in wintertime and early spring months. However, this daily comparison does not offer any clear conclusions about the model performance.

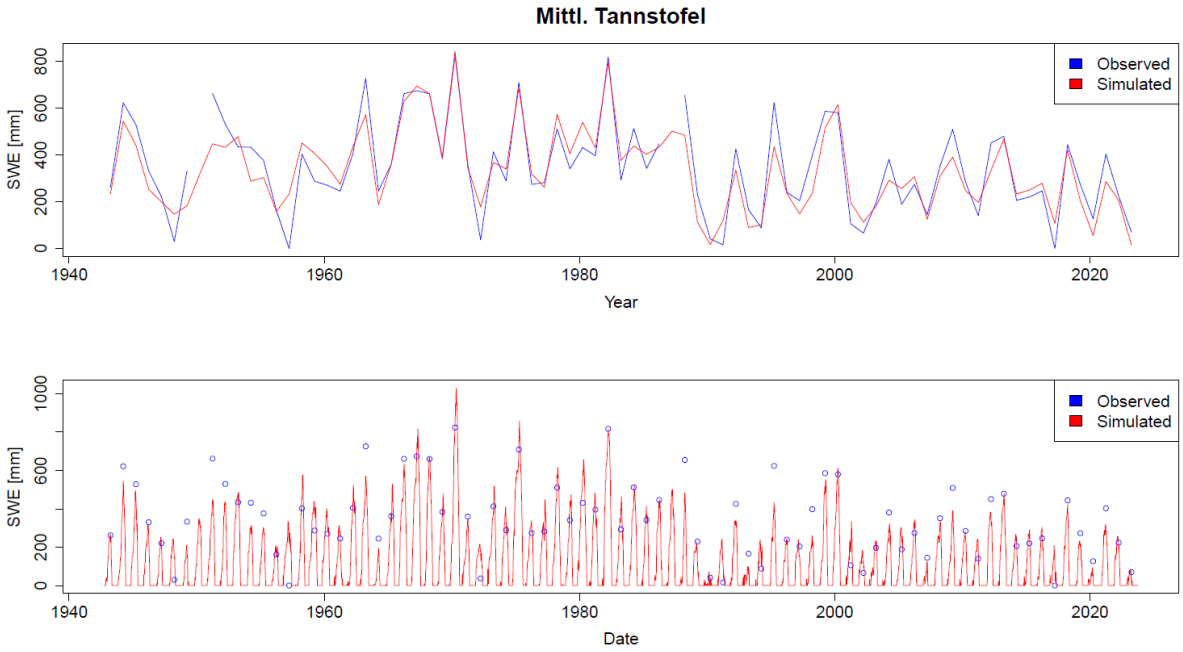

Figure 8: Simulated vs. Observed SWE for Mittl. Tannstofel. The top panel displays simulated (red) and observed (blue) SWE values on April 1st of each year, the bottom shows simulated daily SWE values (red) and the observed April 1st SWE (blue).

For the Ziggen station (Figure 4), the top panel presents notable differences between the observed and simulated values of April 1st. The simulated values are generally lower and show less variability compared to the observed values, indicating that the model generally underestimates the SWE on April 1st. The bottom panel demonstrates that while the model generally captures the trend of SWE accumulation and melt, it is difficult to evaluate the performance of the model just visually.

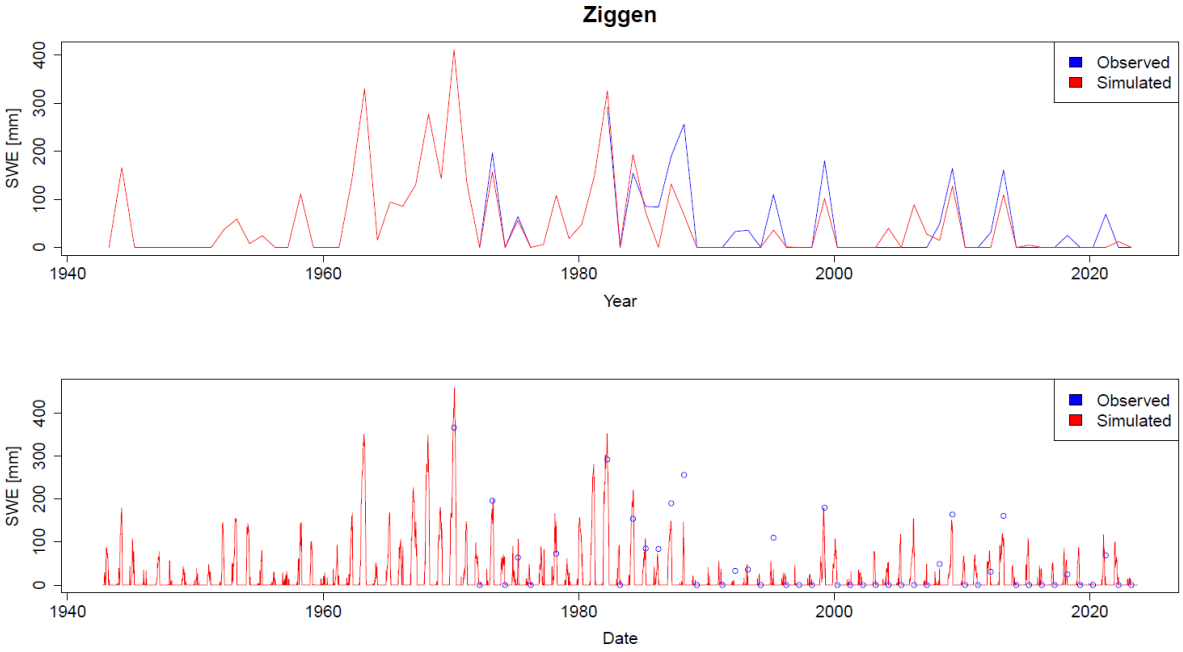

Figure 9: Simulated vs. Observed SWE for Ziggen. The top panel displays simulated (red) and observed (blue) SWE values on April 1st of each year, the bottom shows simulated daily SWE values (red) and the observed April 1st SWE (blue).

Overall, the visual comparison between the simulated and observed SWE indicates that the model can effectively capture the general trends and seasonal patterns of SWE, but it also reveals specific areas where the model underperforms.

Since visual comparisons alone do not completely explain the model performance, the objective function values are examined. For the station Mittl. Tannstofel the SSE is 555'588, while for Ziggen, it is 89'658. This suggests a better fit between the observed and simulated SWE values of station Ziggen compared to Mittl. Tannstofel, which contradicts the visual inspection. Across all 45 measurement stations, SSE values range from 76'302 to 1'717'548, which highlights that the model performance can vary significantly between the different stations. A complete list of all SSE and the corresponding parameter set to each station is provided in Appendix A2.

To gain a more comprehensive understanding of model performance, key regression metrics are also analyzed. These include the regression coefficients (a and b), the coefficient of determination (R^2), and the bias for each station (Figure 10).

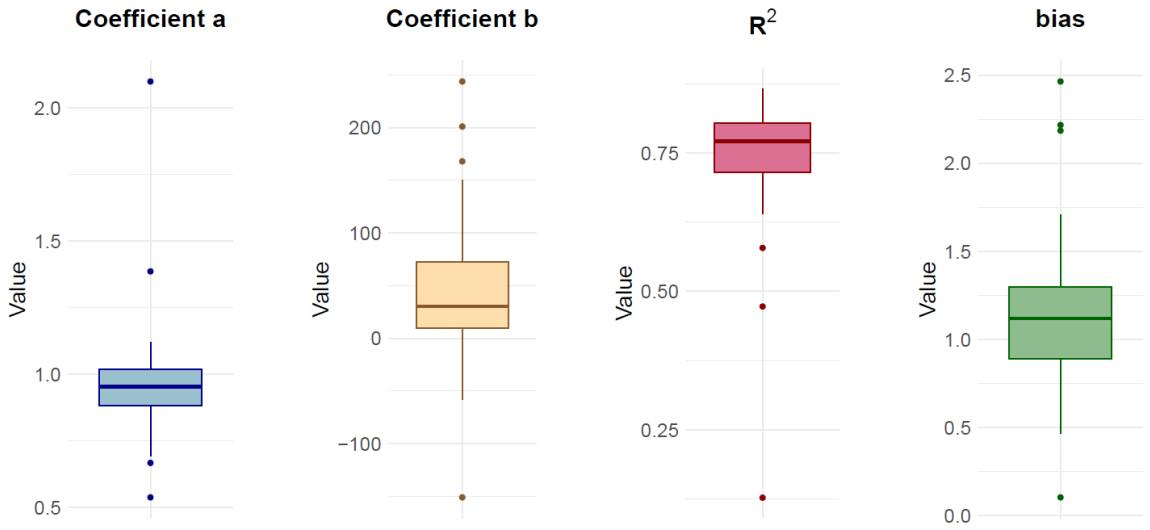

Figure 10: Boxplots of the regression values a, b, R^2, and bias for the degree-day model for each measurement station. The median values are represented by the horizontal line in each box, while the whiskers represent the data spread, including potential outliers.

Coefficient a represents the slope of the regression line when plotting observed values against the simulated values. A coefficient value of 1 indicates that the model's predictions are perfectly proportional to the observed values. As shown in Figure 10 the median value of coefficient a is close to 1, suggesting that, on average, the model's predictions are well-scaled with the observed values. However, the spread and presence of outliers indicate variability in model performance across the different stations, meaning that the model does not perform the same for each measurement station.

Coefficient b represents the intercept of the regression line, where the regression line crosses the y-axis. An intercept close to 0 is desirable, indicating that there is no systematic over- or underestimation by the model. The boxplot for coefficient b shows that the median value is near zero, with some outliers. This suggests that the model does not consistently underestimate or overestimates on average, but for certain stations, it significantly differs.

The **coefficient of determination R^2** measures the proportion of the variance in the observed data, which is explained by the model. Values closer to 1 indicate a better fit. The median R^2 value for the different stations is approximately 0.75, indicating a strong, though not perfect, fit between observed and predicted values. Some stations exhibit outliers with poorer fits.

The **bias** measures the systematic error in the model. A bias value of 1 indicates no systematic error, while values greater or less than 1 suggest systematic overestimation or underestimation, respectively. The boxplots for bias show a median of around 1, indicating minimal overall systematic error.

In summary, the model performs well overall. However, the variability and the presence of outliers suggest that there is room for improvement, particularly for certain stations.

5.1.1 Analysis of Degree-day Model Bias in relation to spatial characteristics

To investigate whether the outliers in model bias were connected to the specific spatial characteristics – elevation, aspect, and slope – a map was created to visualize the bias at each measurement station (Figure 11).

Upon examining the data, two stations with a bias of less than 0.5 were identified. Both stations belong to aspect W and are among the five stations located below 950 m a.s.l. However, no clear connection to the slope could be established. In contrast, four measurement stations exhibited a bias greater than 2. All of these stations are located within the lower elevation band (900-1500 m a.s.l.), although their elevations vary between 990 and 1360 m a.s.l. Two of these stations are also faced W, while the other two belong to aspect S, spanning across three different slope groups.

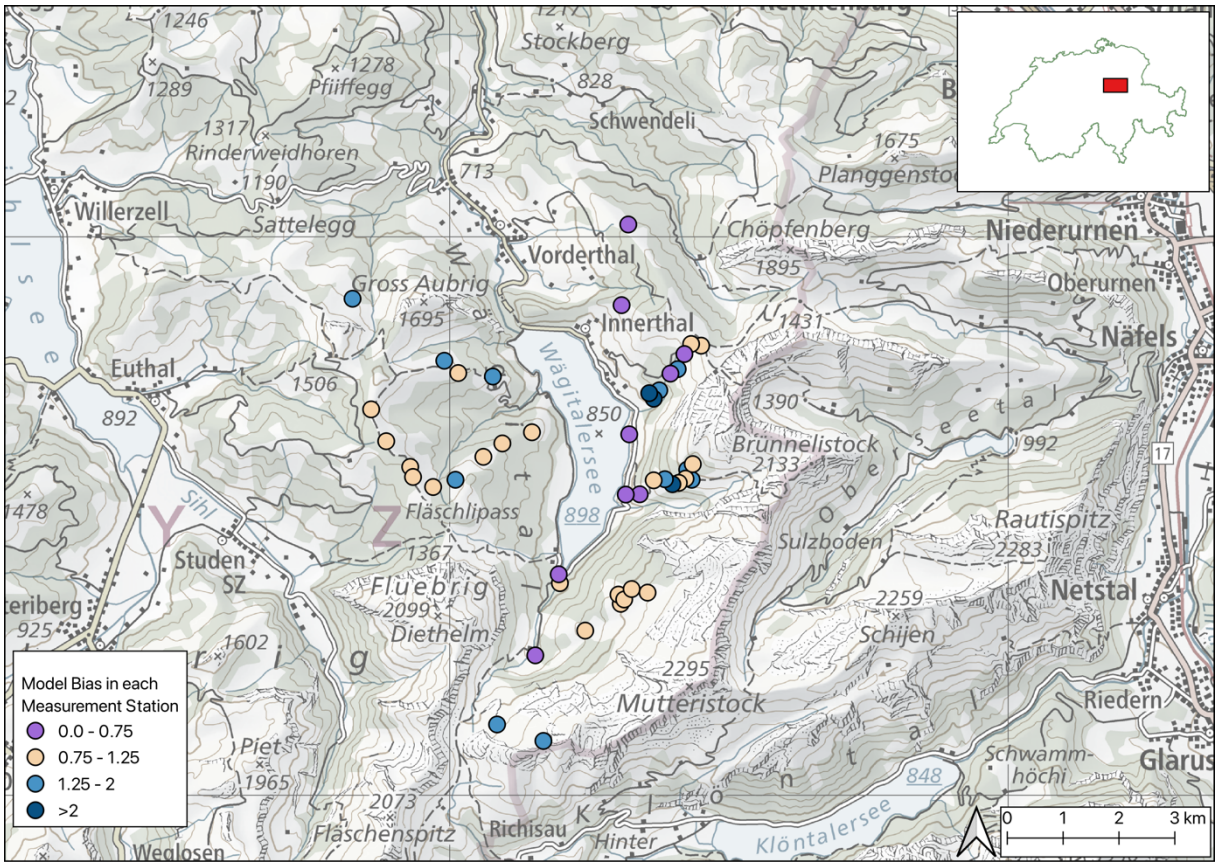

Figure 11: Map of the spatial distribution of model bias across measurement stations. Each station is represented by a color, where the color indicates the degree of bias. Purple represent bias below 0.75, the blue tones represent biases above 1.25, and beige markers indicate bias close to 1.

5.2 April 1st SWE vs. maxSWE

If the maxSWE consistently occurred always on April 1st each year, constructing the model would have been unnecessary, and trend analysis could have been performed directly using the observed data. However, other studies like Bohr & Aguado (2001) found that April 1st underestimates maxSWE. By using the degree-day model, the daily SWE throughout the entire time series could be calculated, which made it possible to identify the precise timing of maxSWE occurrence for each year and for each measurement station from 1943 to 2023.

The boxplots in Figure 12 illustrate the timing of maxSWE across the observation period and for all measurement stations. Each boxplot represents a specific year, and the spread within each boxplot reflects the variation in the dates when maxSWE occurred at each station in that year. The variability in timing among years suggests significant inter-annual differences between measurement stations. This analysis highlights the complex temporal pattern of maxSWE, which is station- and year-specific. However, it can be stated that maxSWE does not always occur on April 1st.

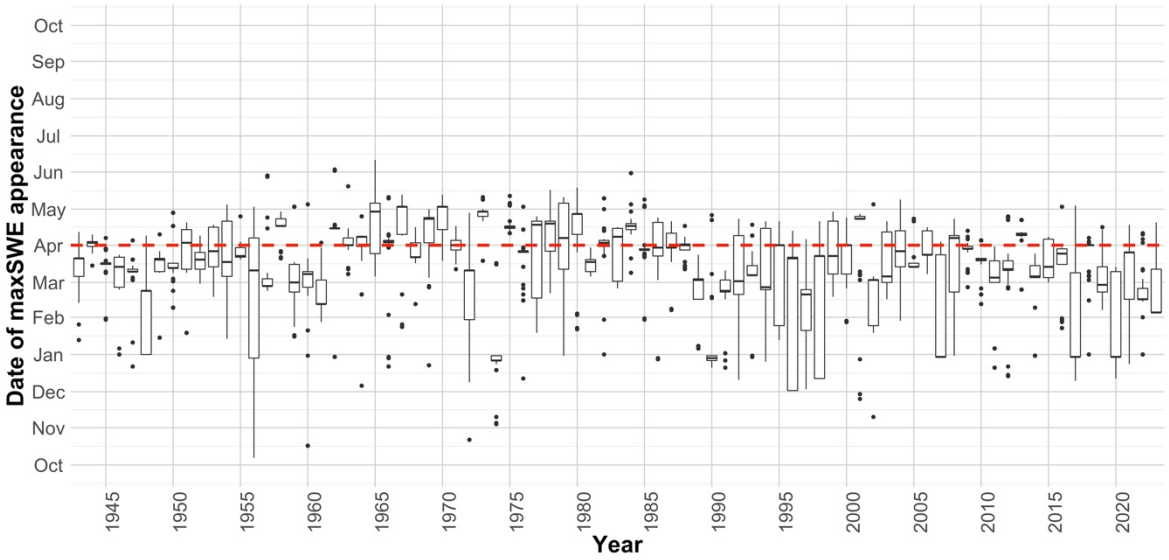

Figure 12: Box plots of the timing of maxSWE for each of the 45 stations for each year. Each box represents the interquartile range, the solid horizontal line the median, and the whiskers extend to the most extreme data points within 1.5 times the IQR from the first and third quartile. Data points outside this range are considered outliers and are shown as individual points. The dashed red line represents the April 1st date.

To better understand these patterns, the median date of maxSWE occurrence for each year was extracted. The corresponding plot (Figure 13) illustrates the median occurrence date of maxSWE, revealing the variability in timing throughout the years as well as the frequency of maxSWE occurrences on specific dates. Contrary to the assumption that maxSWE typically coincides with April 1st (indicated by the red dashed line), the findings reveal that maxSWE can occur at various times during the winter period. In the Wägital region, for example, maxSWE occurred before April 1st in approximately 60 % of observed years. Although there was a noticeable increase in the frequency of maxSWE occurrences on April 1st, many instances occurred both before and after this date.

In summary, while there is a higher likelihood of maxSWE occurring on April 1st, significant occurrences are distributed over a broader temporal range. These findings underscore the importance of modeling maxSWE to perform meaningful spatial and trend analyses, as maxSWE does not consistently align with April 1st.

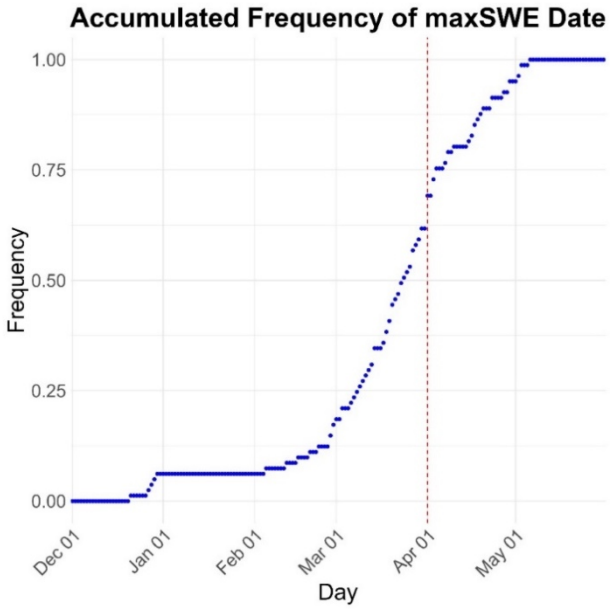

Figure 13: Cumulative frequency distribution of the data of maxSWE for all stations and all years, with April 1st indicated by the red dashed line.

5.3 Spatial Analyses of maxSWE

This chapter delves into the spatial analysis of maxSWE across the groups introduced in Chapter 4.3, focusing on how various geographic and topographic parameters influence the distribution and magnitude of maxSWE. The median maxSWE for each station was calculated and used to create the following boxplots.

5.3.1 Elevation

In Figure 14 the relationship between elevation and maxSWE is illustrated. The analysis includes 38 stations in the elevation band between 900-1500 m a.s.l. and seven stations in the 1500-1800 m a.s.l band. The boxplots provide a summary of the maxSWE distribution across the two elevation ranges.

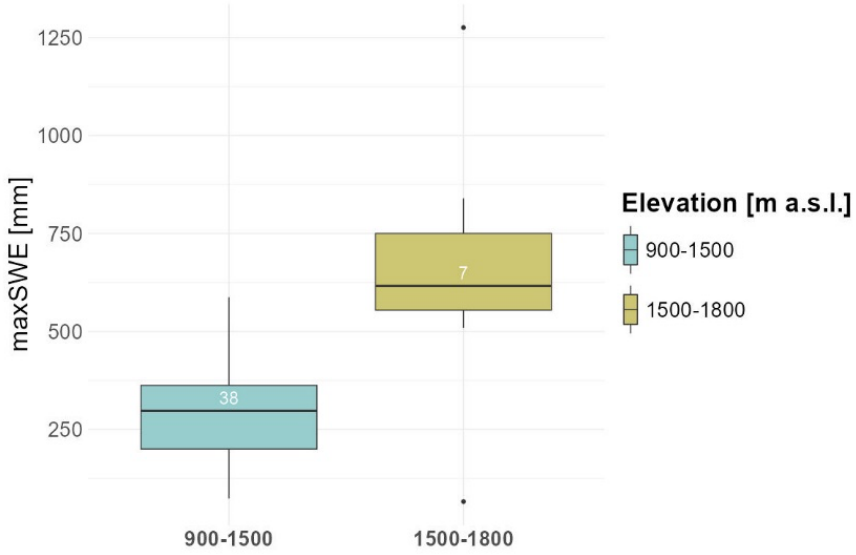

Figure 14: Boxplots of the maxSWE for the 1943-2023 period across the elevation bands, the number of stations in each elevation band is represented by the white numbers. Each box represents the interquartile range, the solid horizontal line the median, and the whiskers extend to the most extreme data points within 1.5 times the IQR from the first and third quartile. Data points outside this range are considered outliers and are shown as individual points.

The median of the lower elevation band (900-1500 m a.s.l.) is 302 mm SWE, and the inner quartile range (IQR), which measures the middle 50 % of the data, shows a moderate spread in maxSWE. In contrast, the higher elevation band (1500-1800 m a.s.l.) shows a median maxSWE of 616 mm SWE. The IQR is wider compared to the lower elevation band, suggesting a greater variability in maxSWE. Two outliers are present in the upper elevation band, representing a station with a significantly lower and a station with a significantly higher maxSWE, at the same time, these outliers also represent the highest and lowest maxSWE. Statistically, the results indicate a significant difference in maxSWE between the two elevation bands ($p = 0.03$). Overall, the data show that maxSWE increases with elevation.

5.3.2 Aspect

The following boxplot Figure 15 illustrates the distribution of maxSWE regarding the different aspects (see Chapter 4.3.2). There are seven measurement stations oriented into direction E, ten measurement stations look in direction N, five of the measurement stations are oriented to S, and 23 measurement stations have aspect W.

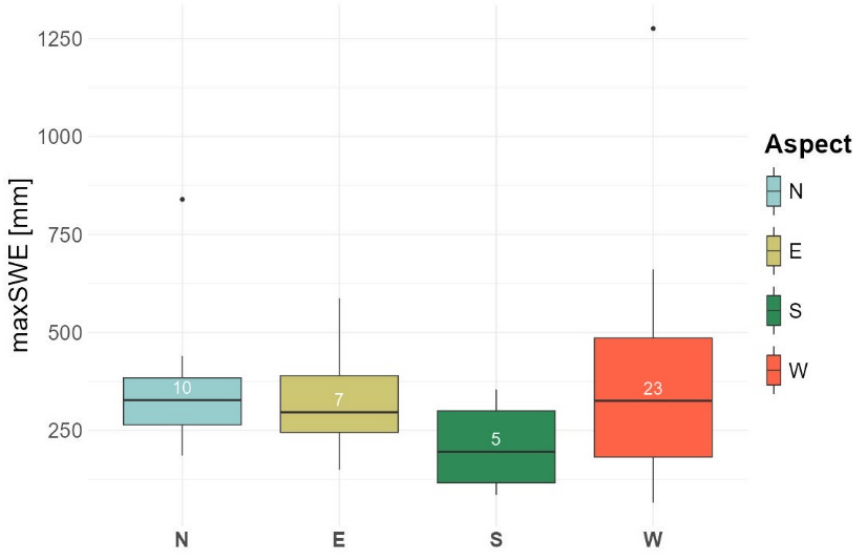

Figure 15: Boxplots of the maxSWE for the 1943-2023 period across the aspects, the number of stations in each aspect is represented by the white numbers. Each box represents the interquartile range, the solid horizontal line the median, and the whiskers extend to the most extreme data points within 1.5 times the IQR from the first and third quartile. Data points outside this range are considered outliers and are shown as individual points.

The highest median of maxSWE is found in aspect E with 365 mm, followed by aspect N with 337 mm. As the third follows aspect W with a maxSWE median of 319 mm, while the smallest maxSWE median is found in aspect S. The IQR is widest in aspect W and narrowest in aspect N. Two outliers are present, one in aspect N and one in aspect W, these outliers represent each a station with much higher maxSWE. Notably, the stations with both the highest and lowest maxSWE medians are in the Western aspect. However, assessing these results statistically, the results indicate no significant difference between the aspects ($p = 0.4$), suggesting that the variation in maxSWE is not statistically significant across the different aspects.

5.3.3 Slope

The boxplots in Figure 16 depict the relationship between slope and maxSWE in the Wägital. The measurement stations are divided as follows: 11 stations can be found in the flat terrain (0-10°), 19 stations are in the flat to medium terrain (10-15°), eight stations are in the medium to steep terrain (15-20°), and seven stations can be found in the steep terrain (20-25°).

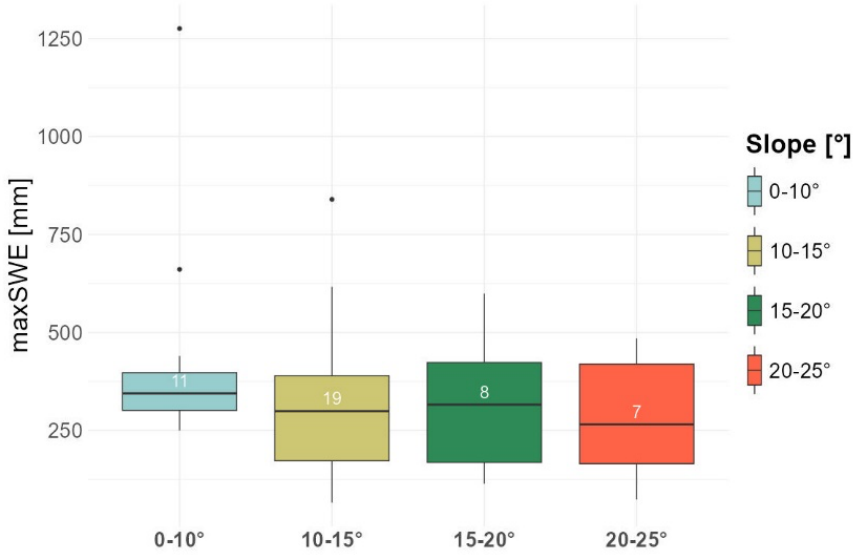

Figure 16: Boxplots of the maxSWE for the 1943-2023 period across the slopes, the number of stations in each slope section is represented by the white numbers. Each box represents the interquartile range, the solid horizontal line the median, and the whiskers extend to the most extreme data points within 1.5 times the IQR from the first and third quartile. Data points outside this range are considered outliers and are shown as individual points.

The highest measured median maxSWE regarding the slope was found in the flat terrain (0-10°) with 345 mm. The medians for the slope group 10-15° with 292 mm and group 10-15° with 297 mm indicate similar values. The steepest slope group (20-25°) has the lowest median maxSWE at 203 mm. The IQR has a very similar width for the three groups with slopes above 10°. In the flat terrain (0-10°), the IQR is narrower, suggesting a lower variability of maxSWE. Two outliers in the flat terrain group suggest stations with higher maxSWE. The station with the highest median maxSWE is located in the 0-10° slope group, while the station with the lowest maxSWE median is found in the 10-15° slope group. Statistically, the differences between the different slopes are not significant, with $p = 0.5$.

In addition, an attempt was made to combine the groups and compile the three above-discussed boxplots. The idea was to see how SWE interacted regarding elevation, aspect, and slope together, but because of data scarcity for some group elements, it delivers results with unsatisfactory significance, which renders the interpretation difficult. Nevertheless, a few general patterns emerged: in lower elevations, eastern aspects had the highest median maxSWE, followed by northern aspects, with southern aspects showing the lowest maxSWE. For elevation and slope, the pattern remained consistent, with maxSWE decreasing as the slope increased, regardless of the elevation band. No clear pattern could be determined for the relationship between slope and aspect. The corresponding plots for this combined analysis can be found in Appendix A4.

5.4 Trend Analyses

The trend analysis, outlined in Chapter 4.4.1, was performed first for each individual station across all years and then for the groups discussed in Chapter 4.3. To capture not only long-term changes from 1943 to 2023 but also trends within this period, heatmaps were employed to visualize trends.

5.4.1 Trends for Individual Stations

For each station, the maxSWE of each year was derived represented with the black dots in Figure 17 and Figure 18. These data points formed the basis for conducting the Theil-Sen trend analysis over the entire observation period from 1943 to 2023, with the trendline depicted in blue. The nonparametric MK-test was used to assess for the statistical significance of the trend ($p < 0.5$).

The station Oberalp Boden (Figure 17), situated at an altitude of 1800 m a.s.l., is the highest located station in the Wägital monitoring program. Located on a western aspect with a 5° slope, the station recorded its highest annual maxSWE of 2640 mm in 1975, while the lowest maxSWE of 643 mm occurred in 1997. The trend line at Oberalp Boden revealed a negative slope of 6.1 mm per year, with a p-value of 0.007, indicating a statistically significant decreasing trend.

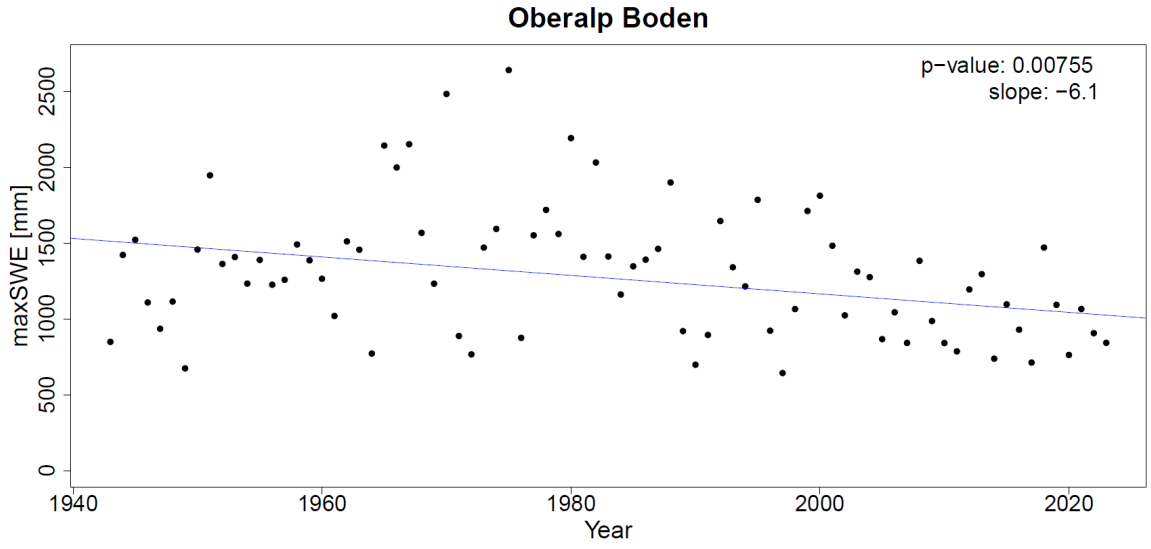

Figure 17: The simulated maximum SWE for the Oberalp Boden station (black dots) and linear trend line (blue line).

The station Seeende_1 (Figure 18) is situated at 930 m a.s.l. and is one of five stations across the monitoring program located below 1000 m a.s.l. The location is compared to Oberalp Boden at a steeper location with slope 18.6° and oriented to N. For this station, the highest annual maxSWE was recorded 764 mm in 1970, while the lowest maxSWE of 24 mm occurred in 2023. The trend line for Seeende_1 also displayed a negative slope of 1.7 mm per year, with a p-value of 0.014, signifying a statistically significant decreasing trend.

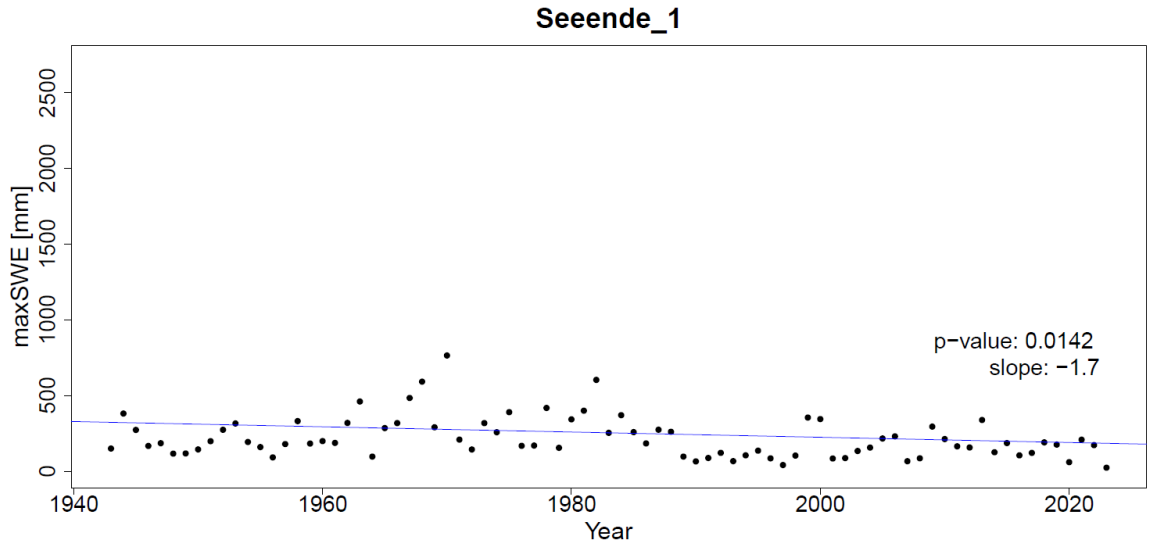

Figure 18: The simulated maximum SWE for the Seeende_1 station (black dots) and linear trend line (blue line).

The trend lines for all 45 stations revealed consistent negative and significant trends. The values of the slope ranging between -0.15 and -0.2. Due to the similarity in trends across stations, further individual details are not provided here. Instead, the focus shifts to how trends manifest within the designated groups. Slope values and p-values for each station are detailed in Appendix A5.

5.4.2 Trends in measurement groups across the total observational period

To understand broader trends, the stations were grouped according to the parameters discussed in Chapter 4.3. The median maxSWE for the stations in each group was calculated for each year, and these median values were used to derive the trend line for each group (blue line in the plots).

Two trend plots were generated to analyze the trends in maxSWE across the two different altitude ranges. The first plot (Figure 19a) represents the measurement stations between 900 and 1500 m a.s.l., while the second plot (Figure 19b) covers the stations between 1500 and 1800 m a.s.l.

For stations between 900-1500 m a.s.l., the slope of the Theil-Sen regression line is -2.9 mm per year, indicating a decreasing trend in the maxSWE. The p-value for the MK-test is 0.004, indicating that this negative trend is statistically significant and reflects a consistent decline in maxSWE over time.

The slope of the Theil-Sen regression line is -4.4 mm per year for the stations between 1500-1800 m a.s.l., which is steeper than that for the lower altitude range. The p-value (0.00598) accounts for the statistical significance of the slope, confirming the pronounced decreasing trend. The steeper negative trend suggests that stations at higher altitudes are experiencing a more rapid decline in maxSWE compared to lower altitude stations.

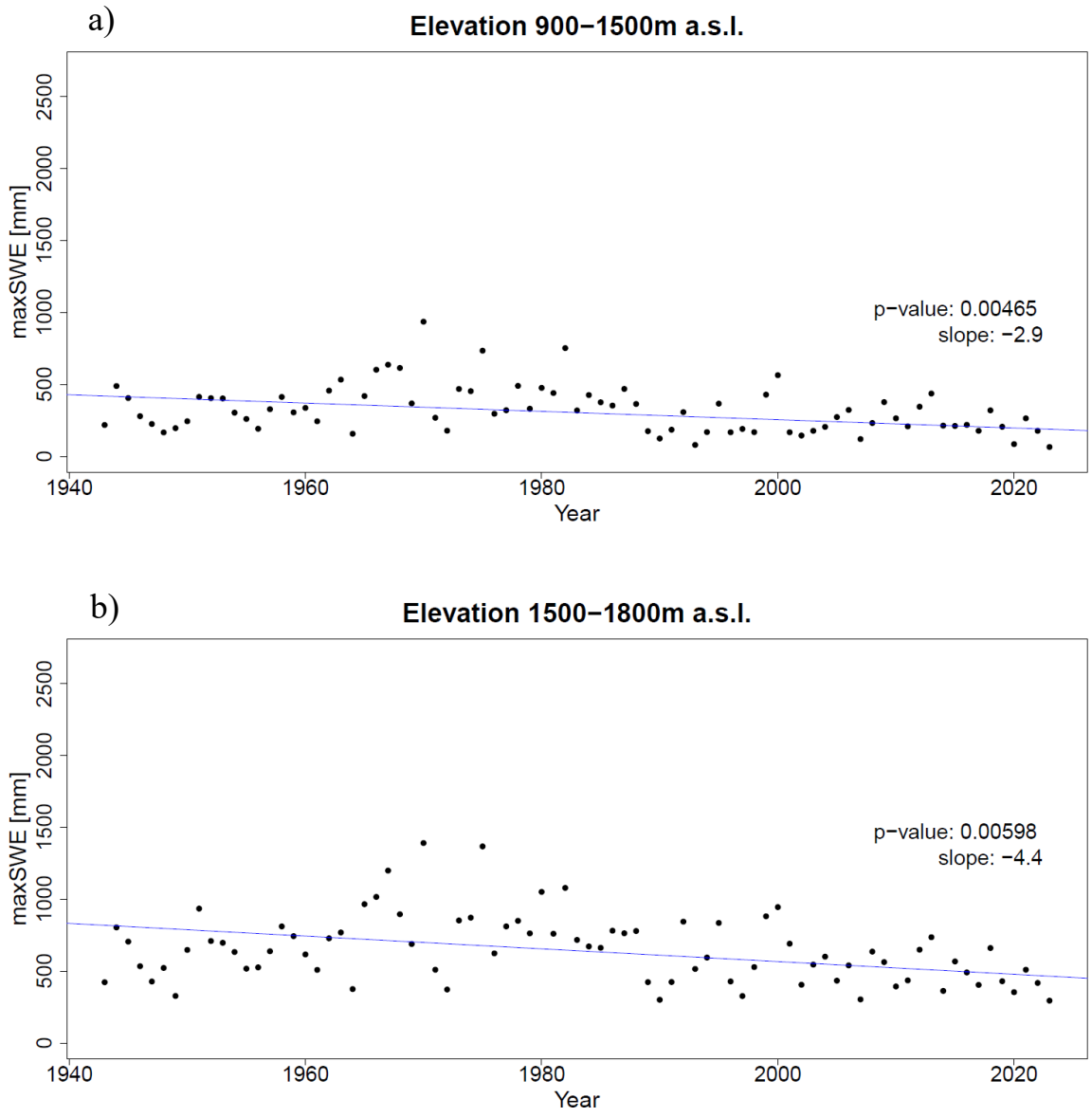

Figure 19: The simulated median maxSWE for measurement stations between 900-1500 m a.s.l. (a), and for measurement stations between 1500-1800 m a.s.l. (b) in black dots, and linear trend line (blue).

The statistical outcomes of the trend analysis for each group are detailed in Table 2. Across all group parameters, the trends are consistently negative and statistically significant. The most pronounced negative trend, with a slope of 4.4 mm per year, is observed in stations located between 1500 and 1800 m a.s.l., indicating a steeper decline in maxSWE at higher elevations. Conversely, the mildest negative trend, with a slope of 1.9 mm per year, is found in stations oriented towards the south (aspect S). All p-values for the trends are below 0.05, confirming the statistical significance of these negative trends and underscoring the robustness of the findings. The Theil-Sen slope values, being generally more negative for groups compared to individual stations, suggest that analyzing data in groups provides a clearer and more comprehensive understanding of the overall trends in maxSWE across the catchment area.

Table 2: Summary of statistical values of trend analysis for the groups elevation, aspect, and slope.

Group	Theil-Sen Slope	p-value MK-test
elevation 900-1500 m a.s.l.	-2.9	0.00465
elevation 1500-1800 m a.s.l.	-4.4	0.00598
aspect E	-3.1	0.00332
aspect N	-2.9	0.00378
aspect S	-1.9	0.0109
aspect W	-3.2	0.00042
slope 0-10°	-3.2	0.00332
slope 10-15°	-2.8	0.00341
slope 15-20°	-2.7	0.00199
slope 20-25°	-2.5	0.00135

5.4.3 Temporal Trends

The discussed trend plots focused on how the maxSWE changed over the entire period from 1943 to 2023. To give more detailed information about the development of the maxSWE and other parameters like trends in precipitation, temperature and snow cover throughout the years, the data is graphically presented in the following heatmaps. The heatmaps allow to show the intensity of changes across the different years. The start year (y-axis) and the end year (x-axis) define the periods over which changes are calculated, the respective square indicates by its color code the trend direction. The cells along the diagonal line represent changes over one year intervals. The heatmaps give a more detailed view of specific years or periods.

5.4.3.1 Meteorological changes 1943-2023

For precipitation, there is no clear trend in annual precipitation over the total time period, as indicated by the very light top right corner in Figure 20, left. Even though the trend over the total time period is slightly negative (1.9), it is not significant (p-value = 0.16). This also corresponds with the annual precipitation amounts throughout Switzerland where there are no statistically significant trends observed (Meteo Schweiz, 2024). Looking at 10-year time intervals, the colors are stronger, and therefore the changes are larger. The early periods, starting in the 1940s and 1960s, show more variability in precipitation changes. In more recent years, starting in the 1980s to 2000s there are more cells with lighter colors representing less variability. With several red clusters in the years until the 2000s, it looks like the trend was rather positive. Notable blue patches at the beginning of the 21st century suggest a shift in precipitation patterns.

An increase in average annual air temperature in the Wägital can be observed over the total study period, represented by the red coloring in the upper-right portion of the heatmap (Figure 20, right). Notable clusters of red were spotted in the 1940s, 1990s, and recent years, since ca. 2005. Notable clusters of

blue are visible in the 1960s and the late 1990s. The early periods until the 1960s show more variability with a mix of warming and cooling trends. From the 1980s onwards a clear trend of increasing temperatures is indicated. The results correspond to the findings by Begert & Frei (2018), who observed the temporal pattern in Switzerland from 1864 until 2016, with an apparent increase over time and relatively warm years in the 1940s.

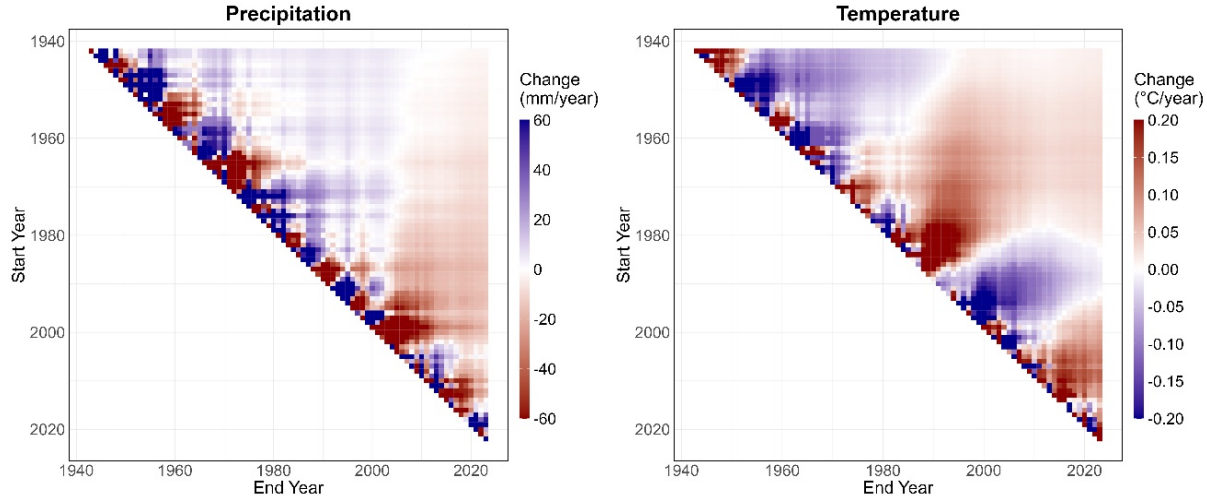

Figure 20: Changes in Precipitation (mm/year) and Temperature (°C/year) in the Wägital, shown for different start and end years of the observation period. For precipitation (left), blue indicates an increase and red a decrease in annual precipitation. For temperature (right) red indicates an increase and blue a decrease in annual temperature. The color intensity reflects the magnitude of the change.

After looking at the climatic changes in the Wägital, the next focus will be on the maxSWE and how it changed over time and space.

5.4.3.2 Changes in maxSWE

The following heatmaps represent the change of maxSWE, the color-coding is used to indicate the magnitude of change in mm/year, with blue representing an increase in SWE and orange representing a decrease.

Figure 21 shows the change in average annual maxSWE across the Wägtial. For that, the maxSWE of each station for each year was derived to calculate the average maxSWE of each year in the Wägital. It is noticeable that for shorter periods (years or decades), the variability is more extensive (indicated by the darker coloring) than when looking at longer periods. For the total observation period, it can be observed by the light orange color in the top right corner that there is a negative trend in the maxSWE, which is around 2.0 mm/year change. If the observation period is split up into two periods, 1943 to 1980 and from 1980 to 2023, a positive trend of 5.7 mm/year is observed in the first period, which is also indicated by the stronger blue tones until the 1980s, and a negative trend with a change of 4.6 mm/year is observed from 1980 until 2023. Most data sets that measured SWE start in the 1960s, and looking at the changes in the heatmap between the start year 1960 and the end year 2023, the triangle would mostly

be orange. In comparison to the total observation period the change from 1960 until 2023 shows, with 4.5 mm/year a stronger negative trend.

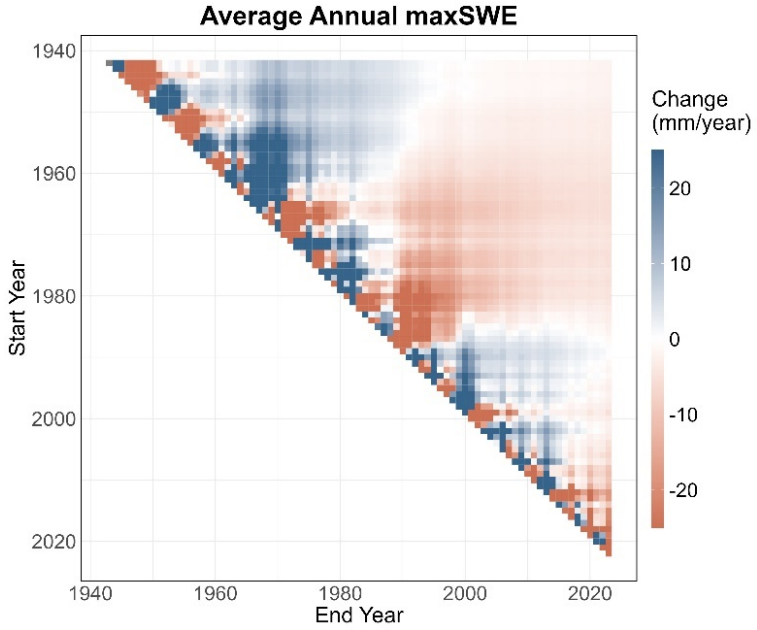

Figure 21: Change in Average Annual maxSWE (mm/year) for all measurement stations across the Wägital shown for different start and end years of the observation period. Blue indicating an increase and orange a decrease in average annual maxSWE. The color intensity reflects the magnitude of the change.

To provide a more comprehensive analysis of the variations in maxSWE throughout the Wägital, the alterations for the distinct groups are displayed, described and compared.

First, a look at the different elevation bands is taken in Figure 22. The maxSWE shows different trend patterns for the two elevation bands. However, all in all, a predominant trend towards a decrease in maxSWE over the total observation period is for both elevation bands recognizable. The overall lighter coloring for the lower elevation band suggests less change than for the higher elevation, which confirms the trend analysis in Chapter 5.4.2.

Focusing on temporal patterns, it is visible that during the period from 1940-1980, the patches of blue and orange both are stronger/darker than for the years 1980-2020, suggesting that the variability of the snowpack change was bigger in the first 40 years of the observation period. Furthermore, the trend until the 1980s suggests a positive trend for both elevation bands, which is slightly more pronounced for the higher elevation band. With end year later than 1980s the change is rather negative. In the 1990s a cold period with high snow years appears. For trend analyses starting in the 1990s until 2023, the change looks rather positive or close to 0 for the lower elevation band. For the higher elevation band, the trends until 2023 are still mostly negative.

Although the color scaling and the absolute trend analysis in Chapter 4.3.2 show that a decrease in maxSWE is greater at high altitudes (4.4 mm) than at low elevations (2.9 mm), it must be considered cautiously. The percentage decrease is smaller at high altitudes (0.71 %) than at low altitudes (0.96 %), which indicates that the impact of temperature and precipitation on the amount of snow at low elevations is greater than at high elevations.

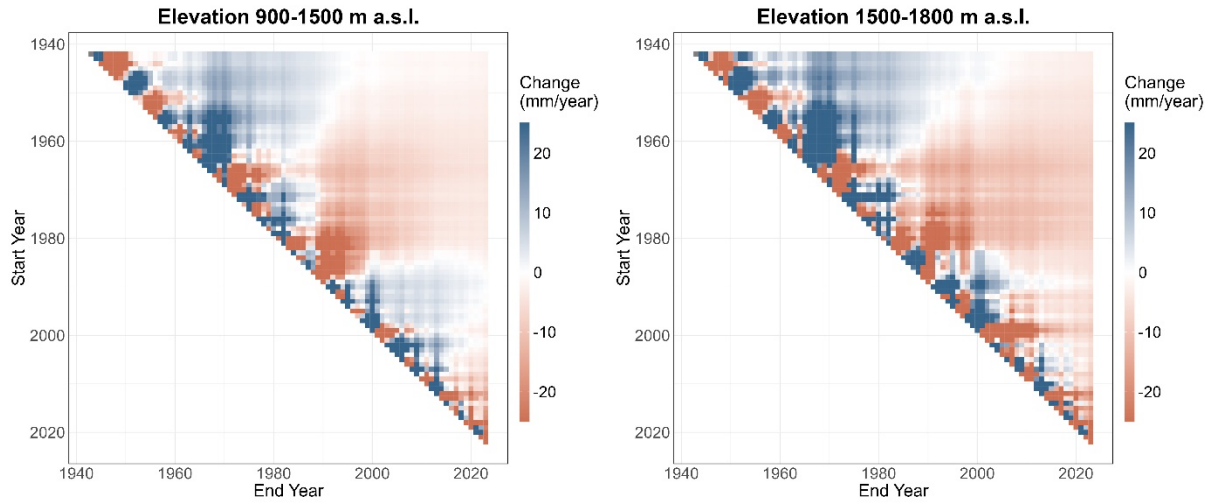

Figure 22: Change in maxSWE (mm/year) in the elevation bands 900-1500 m a.s.l. and 1500-1800 m a.s.l. shown for different start and end years of the observation period. Blue indicating an increase and orange a decrease in annual maxSWE. The color intensity reflects the magnitude of the change.

The maxSWE differentiated by aspect (Figure 23) shows a similar pattern for all aspects to the average annual maxSWE and the maxSWE looked at by elevation differences. The variability is more pronounced between the individual years and decadal changes compared to bigger time periods. However, in the second half of the observation period, the changes are less pronounced, with smaller color patches than in the first half. For all aspects, a positive trend until the 1980s is observable, but a predominant negative trend for all aspects over the total period is recognizable. The high snow years in the beginning of the 1970s and during the 1990s and their impact on the trend analysis are similar in all aspects.

Focusing on differences between the individual aspects, based on the very light color coding, Aspect S indicates the least strong changes, followed by Aspect W. For Aspect N and Aspect E, the heat maps look very similar, and no clear difference can be determined.

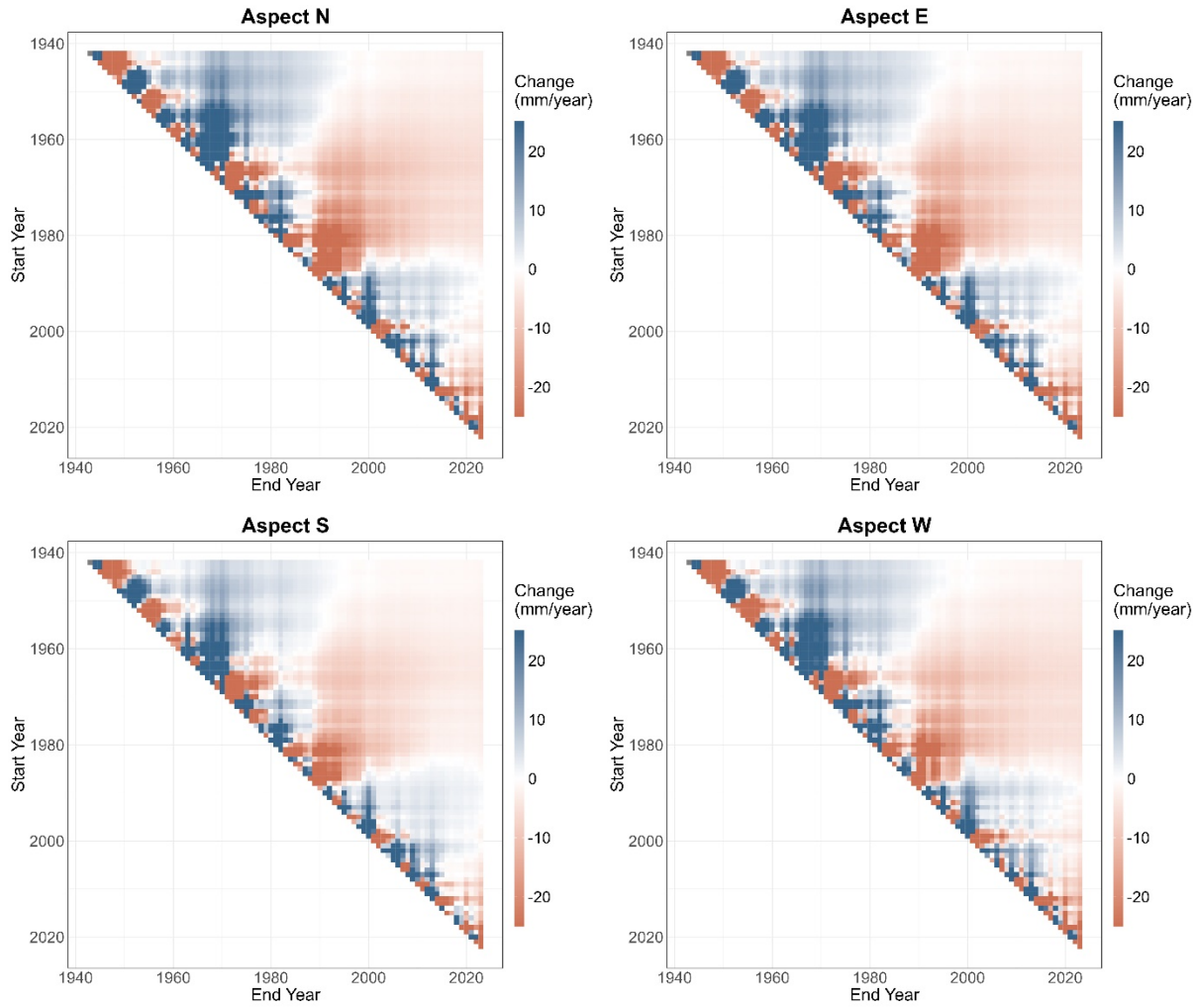

Figure 23: Change in maxSWE (mm/year) for the different aspects N, E, S, W shown for different start and end years of the observation period. Blue indicating an increase and orange a decrease in annual maxSWE. The color intensity reflects the magnitude of the change.

Regarding changes in maxSWE within different slopes (Figure 24), the patterns already look very similar to the heat maps that were discussed previously. Both displayed slope ranges show a general trend towards decreasing maxSWE over the observation period. Until the 1980s, an increase in maxSWE in flat and steep slopes is observed, followed by a decrease until the end of the observation period. Because of the similarity between the heatmaps of all slope ranges, the focus will be on the most gentle slope range (Slope 5-10°) and the steepest slope range (Slope 20-25°).

The gentle slope (Slope 5-10°) presents a slightly more distinct change than the steeper slopes (Slope 20-25°), indicated by the slightly stronger color coding. Especially until the 1970s, the trend looks more positive, indicating that the snow scarce winters in the 1940s have a bigger impact on gentle slopes than on steep slopes. The high snow years in the 1990s are pronounced for both slope ranges, and looking at trend analyses starting in 1990 there is almost no trend distinguishable until 2023.

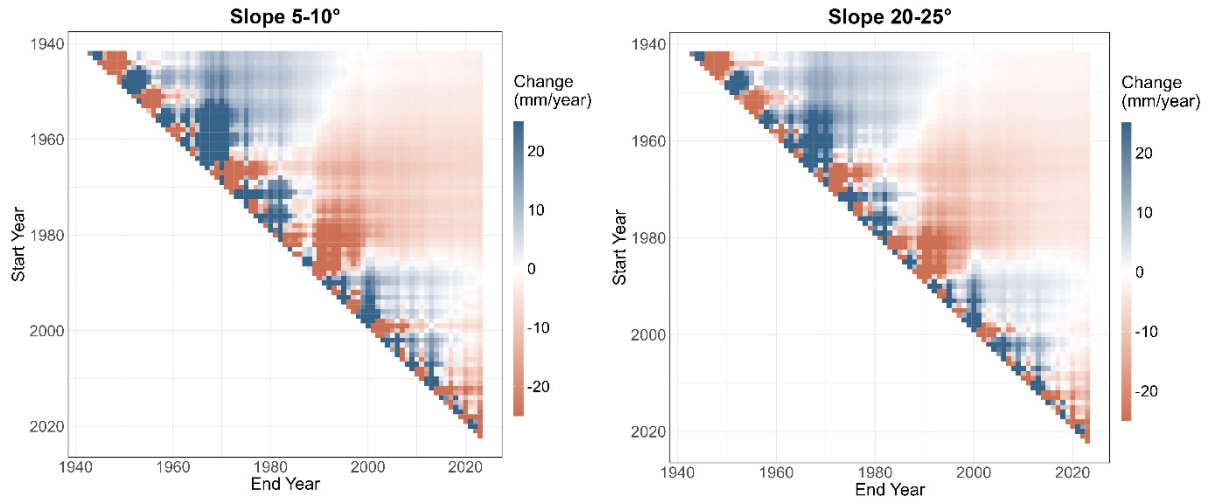

Figure 24: Change in maxSWE for measurement stations located on slopes 5-10° and slopes 20-25°, shown for different start and end years of the observation period. Blue indicating an increase and orange a decrease in annual maxSWE. The color intensity reflects the magnitude of the change.

It can be concluded that regardless of the spatial characteristics, all data plots concerning maxSWE exhibit a consistent pattern of increasing maxSWE until the 1980s, indicating low snow years in the 1940s. For the second half of the observation period, a decrease in maxSWE is evident. Moreover, it is noted that beginning the analysis in the 1960s yields a more negative change in maxSWE compared to starting in the 1940s. A cold period, characterized by high snow years in the 1990s, is visible across all plots; however, the trends for the most recent two decades indicate a negative change in maxSWE once again.

5.4.3.3 Changes in Snow Cover Days per year

For the examination of snow cover days, a threshold of 50 mm for a day to count as a snow cover day was established, ensuring that only days with significant snow accumulation are considered in the analysis. The 50 mm limit was derived from (Kelly, 2009; Kelly et al., 2003), who noted that the detection of shallow snow below 5 cm depths is unreliable. For each measurement station, the number of snow cover days was determined. To get an overview across the entire Wägital, the median number of snow cover days per year from all measurement stations was calculated for this analysis, presented in Figure 25. The violet colors indicate an increase in snow cover days in a year per year, and the orange colors indicate a decrease in snow cover days in a year per year.

The pattern of the change in snow cover days shows a very similar pattern to the changes in maxSWE. The variability between the individual years is strong regarding snow cover days, indicated by the dark colors (diagonal line in Figure 25). The variability lessens when looking at changes across longer periods. An increase in yearly snow cover days is observable from the 1940s until the 1980s. In the 1980s, there were several winters with low snow cover days, which indicates a turning point. After the 1980s, the change in snow cover days was negative. And for the total observation period, a general trend

towards decreasing days per year with a snow cover of more than 50 mm is displayed by the light orange color in the top right of the plot, suggesting that there are each year less snow covered days in the Wägital since the 1980s.

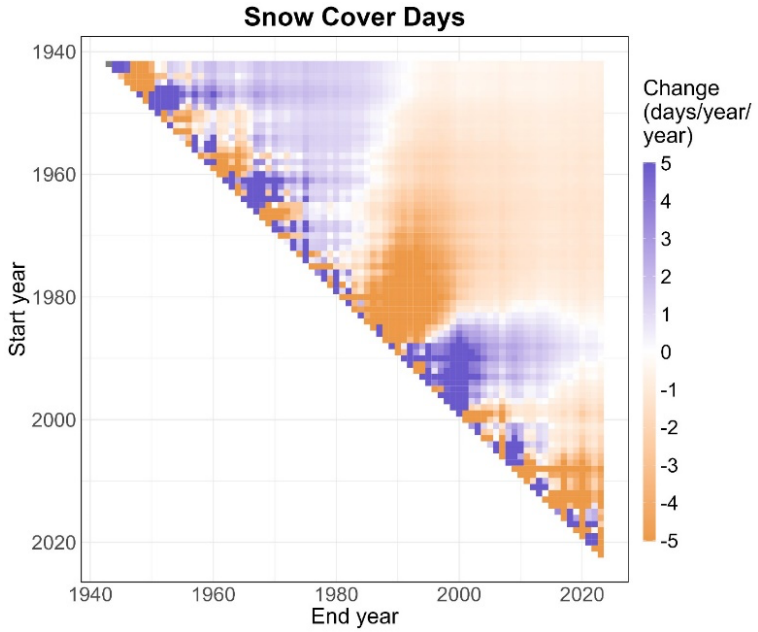

Figure 25: Changes in snow cover days (days/year/year) in the Wägital, shown for different start and end years of the observation period. Violet indicating an increase and orange a decrease in annual maxSWE. The color intensity reflects the magnitude of the change.

5.5 Meteorological Year Categories

In Figure 26, the distribution of maxSWE across different meteorological year categories and elevations is presented. The plot is divided into two panels, each representing the measurement stations located in the elevation zones 900-1500 m a.s.l. and 1500-1800 m a.s.l. Each panel contains boxplots for four meteorological year categories: cold and dry, cold and wet, warm and dry, and warm and wet. These boxplots depict the distribution of maxSWE in the respective year categories, showing the median, interquartile range, and potential outliers.

For the lower elevation zone (900-1500 m a.s.l.), the "warm and dry" category shows the lowest median maxSWE (around 200 mm) with very little variation, indicating minimal SWE in warm and dry years. The "cold and dry" category has a slightly higher median (around 250 mm) but with a wider variability. The "warm and wet" category has a median of around 300 mm with more variation. The "cold and wet" category has the highest median (around 425 mm) with some variation and a few outliers around 750 mm and 950 mm. Statistically, the difference between “cold and wet“ and “warm and dry” is highly significant ($p = 0.00004$), and the difference between “cold and wet” and “warm and wet” is also significant ($p = 0.004$). Comparison between the other categories is, however, not significant in the lower elevation zone.

The higher elevation zone (1500-1800 m a.s.l.) follows a similar pattern regarding median values. Most snow accumulates in "cold and wet" conditions and least in "warm and dry" years, this difference is also supported by the strong statistical significance ($p = 0.000003$). In "warm and wet" years, there is slightly more snow than in "cold and dry" years, however, statistical comparisons do not show significant differences.

Generally, higher elevations tend to have higher median maxSWE across all meteorological categories compared to the lower elevation zone. The variability is greater in the higher elevation zone for each meteorological category.

Overall, it is evident that maxSWE varies with different meteorological conditions and elevations. The variation across the different meteorological categories highlights the importance of considering both temperature and precipitation when assessing SWE.

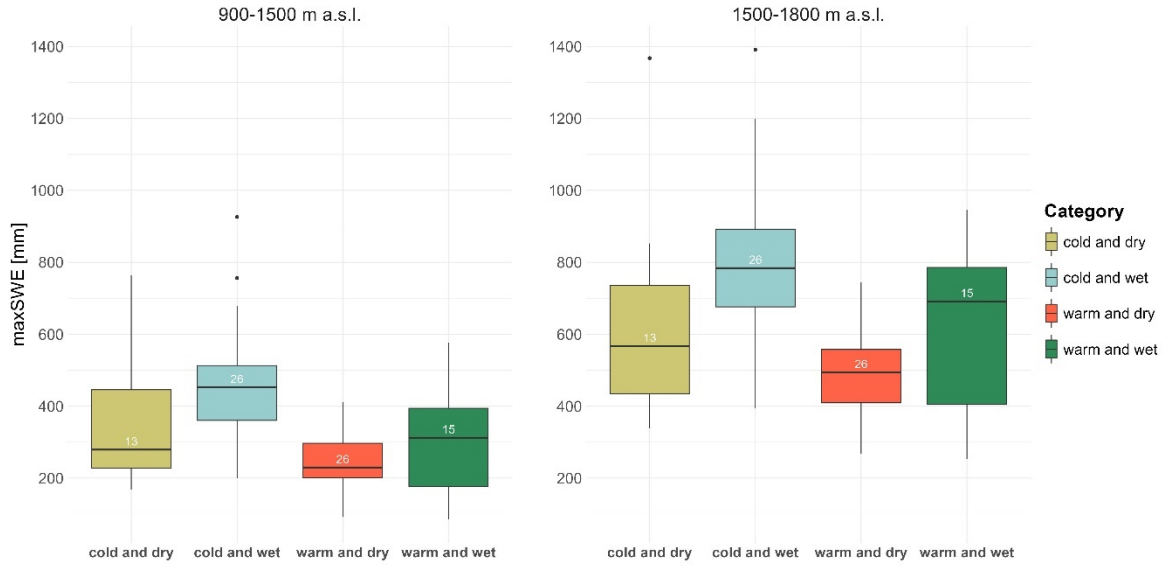

Figure 26: Boxplots of distribution of maxSWE in different meteorological years divided into two elevation bands. The number of years in each category is represented by the white numbers. Each box represents the interquartile range, the solid horizontal line the median, and the whiskers extend to the most extreme data points within 1.5 times the IQR from the first and third quartile. Data points outside this range are considered outliers and are shown as individual points.

6 Discussion

The SWE is a crucial measure for topics such as water management, agricultural planning, and climate policy. Historical SWE data provides valuable insights into climatic changes and acts as a base for various climate change scenarios. Numerous studies have analyzed SWE trends in Switzerland (Marty et al., 2023; Stähli & Gustafsson, 2006), as well as in other snow-covered regions like North and West America (Bohr & Aguado, 2001; Brown et al., 2019; Musselman et al., 2021) and High Mountain Asia (Smith & Bookhagen, 2018). The available data for these studies dates back to the mid-1950s at the latest. For the Wägital, SWE has been recorded on April 1st every year since 1943, making this dataset one of the longest-standing SWE datasets globally. However, since there is only one measurement per year, and April 1st may not always represent the date when maxSWE occurred, trend analyses based solely on this observational data could lead to misleading conclusions. It was, therefore, crucial to determine the maxSWE of each year by modeling daily SWE with a degree-day model and using the observed April 1st SWE to calibrate the model. The model output allowed to examine the behavior of maxSWE across different spatial features, analyze the trends dating back to the 1940s, and observe patterns of maxSWE according to meteorological year categories.

The results can be summarized as follows: The degree-day model developed to assess daily SWE in the Wägital demonstrates good performance overall, although there are some outliers for specific measurement stations. The model emphasizes the variability of maxSWE occurrence, showing that it can happen at various dates during the winter period, with the most dates of occurrence being before April 1st, however, during the observation period April 1st was the date where it most frequently occurred. Spatial analysis reveals that maxSWE increases with elevation, is lower on southern aspects, and tends to increase with decreasing slope gradients. Long-term trends in maxSWE are predominantly negative across all individual stations and group combinations. When focusing on shorter periods, similar trend patterns are observed for the groups. Trends from the 1940s to the 1980s are mostly positive, while trends from the 1980s until the 2020s are predominantly negative. Furthermore, trends starting in the 1960s until 2023 are more strongly negative than trend analyses starting in the 1940s. The snow scarce winters in the 1940s stand out, as well as the high snow years in the 1990s. The change in the amount of snow cover days in a year presents the same pattern as the maxSWE. Lastly, maxSWE varies with different meteorological conditions, with cold and wet years leading to high SWE years and warm and dry winters leading to snow scarce years, indicating the importance of considering temperature and precipitation when assessing SWE. The discussion will explore these findings now in greater detail.

6.1 Model Performance

Comparing the performance of the degree-day model constructed for this thesis to the degree-day model by Lopez et al. (2020) for the Allenbach catchment, also based on the HBV snow routine, the performance is slightly worse with model performance values of ~0.75 compared to ~0.90. Several factors can

contribute to this discrepancy. As input data, Lopez et al. (2020) used high-resolution gridded data, which provides a comprehensive spatial coverage of the entire catchment area. That allows to account for spatial variability in precipitation and temperature. The meteorological data used for this thesis might not capture the complete spatial variability across the catchment, leading to potential inaccuracies in the model outputs. Additionally, in the study by Lopez et al. (2020), the SWE data used for model calibration and validation consisted of 18 years of gridded daily SWE data based on observed snow data from 338 stations, which already included error correction methods which made the model calibration and validation especially robust.

Regarding potential pattern between the model bias and the spatial characteristics of the measurement stations, one observation was that four out of six stations at the extreme ends of bias (both <0.5 and >2) were associated with aspect W. Despite this, there are a total of 23 stations with aspect W, most of which showed a normal model performance, making it difficult to draw definitive conclusions from the aspect characteristic alone. An additional observation concerns stations located below 950 m a.s.l. Three out of five stations in this elevation range exhibited significant model bias. One hypothesis is that the model may struggle to accurately account for transitions between snow and rain events. As the zero-degree isotherm has risen significantly in the last 40 years (Scherrer et al., 2021), the model may be failing to fully capture this shift.

To further improve the degree-day model for the Wägital, more detailed input data should be used, and model calibration should be complemented by a thorough validation process. It was discussed that for the purposes of this thesis, it made sense to prioritize the use of as many observed data points as possible for calibration. However, if the model were to be applied to a different catchment or used for forecasting, validation would be essential to enhance robustness and reliability.

6.2 Model Significance

Marty et al. (2023) stated that trends on April 1st were similar to the maxSWE trends but with lower significance, and the variability for the individual years was higher for April 1st SWE than maxSWE. In a study regarding snowpack changes in three different American basins, the maxSWE values were greater than April 1st SWE for each year, highlighting the importance of daily data and especially using maxSWE instead of April 1st SWE for trend analyses (Harpold et al., 2012). As for the Wägital catchment, more than half of the maxSWE across all years and stations were measured before April 1^{st,} indicating that melting had already started on April 1st. This supports the hypothesis in research question (i) that April 1st SWE does not always represent the absolute peak in SWE, even though April 1st is still the date when maxSWE most frequently appeared. The trend analysis in this study, which identified significant trends in maxSWE, underscores the necessity of using maxSWE rather than April 1st SWE for accurate assessments and highlights the importance of implementing a degree-day model to determine

maxSWE. This is particularly evident when compared to the study by Noetzli & Rohrer (2014), where the analysis using April 1st SWE data from the Wägital did not reveal clear trends.

6.3 Spatial Distribution

The findings regarding the spatial distribution (research question ii) in elevation corroborate previous studies (Anderton et al., 2004; Pomeroy et al., 1998; Zhong et al., 2021), which highlight elevation as the dominant factor influencing snow cover properties. In the Wägital, it was observed that in the lower elevation band (900-1500 m a.s.l.), the median SWE was 302 mm with moderate variability. In the higher elevation band (1500-1800 m a.s.l.), the median SWE increased to 616 mm, indicating higher snow accumulation at greater altitudes. This pattern aligns with the findings of Grünewald et al. (2014) and Zhong et al. (2021), where snow depth also increased with elevation. The variability (IQR) in SWE was more prominent in the higher elevation band in the Wägital, suggesting a more heterogeneous snow distribution. This variability may be attributed to localized microclimatic conditions and topographical variations, as noted by Jost et al. (2007).

The highest median regarding the aspect was recorded on E facing slopes in the Wägital (365 mm), followed by north facing (337 mm) and west-facing slopes (319 mm). The smallest median SWE was observed on S facing slopes. This pattern supports the findings of Zhong et al. (2021) that leeward slopes, particularly those facing north, east, and southeast, tend to accumulate more snow due to wind patterns and reduced solar radiation. The larger IQR on aspect W indicates a greater variability in SWE, which could be due to the varying influence of wind and solar exposure.

Regarding the relationship between slope angle and SWE, the highest median SWE was found in flat terrain (0-10°) with 345 mm. The medians for slopes 10-15° and 15-20° were similar around 292-297 mm. A marked decrease in median SWE was noted for slopes of 20-25° (203 mm), suggesting that steeper slopes may lead to reducing SWE. This trend aligns with the findings by Zhong et al. (2021). The lower variability in flat terrain suggests a more uniform snow distribution, likely due to less influence from gravitational movement.

Similar to findings regarding the spatial variability and distribution of SWE in the Chinese Altai Mountains (Zhong et al., 2021), with the conclusions in British Columbia, Canada (Jost et al., 2007), and other parts of the Swiss Alps (Grünewald et al., 2014), the influence of elevation, slope, and aspect was observed in the Wägital. The fact that only statistically significant difference of maxSWE only showed in elevation, among the three spatial characteristics examined, elevation is the dominant factor in determining maxSWE at the measurement stations. However, the results do not consider the influence of vegetation cover, which Faria et al. (2002), Winkler et al. (2005), and Stähli et al. (2021) discussed.

6.4 Trends Analyses

The analysis revealed that all individual stations within the Wägital monitoring program exhibit statistically significant negative trends in maxSWE over the entire observation period (research question (iii)). The uniformity of these trends across diverse stations, regardless of altitude or other geographic factors, strongly indicates a widespread reduction in SWE in the region. This consistency is notable also when compared to other studies, such as the analysis of (Marty et al., 2023), who found a significant decrease of maxSWE for 40 % of stations across several different monitoring programs across Switzerland, as well as international studies such as those in North America (Musselman et al., 2021) and Canada (Brown et al., 2019).

When the stations were grouped by elevation, a more nuanced pattern emerged. Stations in the higher altitude band (1500-1800 m a.s.l.) exhibited a steeper negative trend compared to those at lower altitudes (900-1500 m a.s.l.). While this stronger trend at higher altitudes aligns with general findings from mountainous regions, such as High Mountain Asia (Smith & Bookhagen, 2018), their study reveals that the relationship between elevation and SWE trends is complex and varies significantly depending on the catchment and the elevation bands. For example, in some northern catchments of High Mountain Asia, such as the Syr Darya, strong positive SWE changes are observed in high-elevation winter months, while mid-elevation bands exhibit more pronounced negative trends in spring SWE. This pattern contrasts with the Ganges/Brahmaputra catchment, where the most negative SWE trends occur at the highest elevations due to increased temperatures in low-precipitation, high-altitude zones. This complexity suggests that while higher elevations in our study area may show a more rapid absolute decline in maxSWE, the specific patterns could vary depending on local climatic and topographic factors.

Moreover, while the absolute reduction in maxSWE at higher elevations in the Wägital region is larger, the percentage decrease compared to median maxSWE is lower than at lower altitudes. This implies that although high elevations experience greater snow accumulation and thus a larger absolute reduction, the relative impact is less severe. In contrast, lower elevations, which are more sensitive to temperature increases, could face more significant relative declines in SWE. These findings emphasize the importance of considering local and regional factors, such as elevation and exposure, in understanding snow decline trends.

In addition to elevation, trends regarding aspect and slope were also negative (research question (iii a.). Notably, stations with aspect S showed the least negative trend, likely due to increased solar radiation at these sites, which affects snow accumulation and melt patterns. This suggests that solar radiation plays a mitigating role in SWE decline. Meanwhile, trends in slope are relatively consistent ranging from -3.2 to -2.5 mm/year, indicating that the rate of maxSWE decline is not substantially different across slope ranges. This lack of variation suggests that slope may not be as strong a determinant of SWE trends in this region as elevation or aspect.

The long-term trends observed in the Wägital catchment, particularly the decreasing maxSWE, parallel findings in other mountainous regions worldwide (Brown et al., 2019; Smith & Bookhagen, 2018). However, it is noteworthy that in some regions, like the Arctic Circle, trends can be positive (Brown et al., 2019). The fact that all Wägital stations showed significant decreases emphasizes that this region is particularly vulnerable to reductions in snowpack.

The consistent and statistically significant decline in maxSWE across both individual stations and altitude groups has critical implications for the hydrological systems in the Wägital catchment. The decreasing snowpack could lead to reduced water availability during the melt season, impacting water resources, hydroelectric power generation, and potentially leading to earlier and more pronounced spring runoff.

Focusing on changes in maxSWE for different start and end years, specific patterns could be observed in the change of average maxSWE and maxSWE divided by group. First, the variability of maxSWE between the individual years is remarkable, when looking at changes in longer time periods, the variability becomes smaller. In winter, small-scale phenomena such as inversions and cold air lakes often determine local weather patterns in Switzerland (CH2018, 2018), which can lead to this yearly variability in SWE. Additionally, while no significant trend in precipitation was observed over the entire period, the variability in precipitation during shorter intervals could be influencing the year-to year variability in maxSWE. This suggests that while temperature is the dominant factor driving long-term trends, precipitation patterns play a role in short-term fluctuations. A noticeable shift from a positive trend in the earlier period (1943-1980) to a negative trend in maxSWE from 1980 onwards was revealed. These trend patterns indicate scarce snow winters in the 1940s which is consistent with the relatively warm temperatures and low precipitation years observed in the Wägital but also across Switzerland (Begert & Frei, 2018; Meteo Schweiz, 2024). The observed negative trends in maxSWE, particularly from the 1980s onwards, align with increasing air temperatures in the Wägital and in Switzerland (CH2018, 2018), emphasizing the influence of temperature on snowpack dynamics. The 1990s stand out as a period with high snow years, which temporarily disrupts the overall declining trend, except for trends in high elevations. This period is marked by cooler temperatures throughout the decade and higher precipitation in the beginning of the decade. It is, however, followed by a return to the negative trend in the 2000s. Trend analyses starting in the 1990s can, therefore, suggest an increase or no specific trend in maxSWE in Switzerland. If the trend analysis had started in the 1960s, the total trends would have been stronger negative than they are for the total observation period, which was indicated by the different color coding. The findings of this thesis visualized by the heatmaps highlight the significance of the start year and the length of the observation period in trend analysis, answering the research question (iii b.). The low snow years in the 1940s have a noticeable impact on the long-term trends, particularly in the

early part of the records. This suggests that the initial conditions of the dataset can significantly influence the interpretation of trends over time.

The consistency across spatial characteristics like elevation, aspect and slope with a unified pattern suggests that the observed trends are robust and reflect a broad-scale response of the snowpack to climatic changes rather than being heavily influenced by local topographic factors.

The stronger negative trends observed in recent decades could partly be explained by the snow-albedo feedback mechanism. The reduced snow cover days per year leads to lower surface reflectance and further warming. As the snow cover decreases, the ground absorbs more solar radiation, accelerating snowmelt and reducing maxSWE (Armstrong & Brown, 2008).

6.5 Meteorological Year Category

The results of the meteorological years category, which regards research question (iv), demonstrate that both temperature and precipitation are critical in determining SWE in the Wägital. Lower temperatures combined with higher precipitation lead to increased snow accumulation. The higher elevations were shown to be more conducive to snow accumulation, possibly due to cooler temperatures that prevent snowmelt and higher precipitation rates. The significant differences observed between the "cold and wet" and "warm and dry" categories highlight the substantial impact these conditions have on SWE. The variability was highest in the “cold and wet” category at higher elevations, indicated by the spread of maxSWE values, which could be a sign that other factors like wind patterns, snowpack density or local topography might also be influencing snow accumulation next to temperature and precipitation.

6.6 Limitations and Uncertainties

This thesis was initiated due to the limitation of having SWE data for only the April 1st of each year since 1943 in the Wägital catchment. This challenge was tackled by developing a degree-day model with daily precipitation and temperature data, which simulated SWE for each day of the observation period.

Results from modeling are inevitably subject to some uncertainty because models can only simulate actual conditions in a simplified form and do not represent the physical environment. One significant challenge in hydrological modeling is the uncertainty in input data (FOEN, 2018). In this thesis, the lack of continuous temperature measurements for the entire observation period in the Wägital region required the interpolation of data from the nearby Einsiedeln meteorological station. Daily precipitation and temperature data were used as inputs, but these daily averages do not account for temperature variations throughout the day. This limitation means that the model may not accurately capture the interactions between temperature and precipitation, potentially leading to discrepancies in snowmelt processes. For example, rapid daytime warming followed by freezing nighttime temperatures could create snowmelt dynamics that the model does not fully capture.

Additionally, the model assumes a fixed temperature threshold (TT) to distinguish between rain and snow, which might oversimplify the phase transition process. The use of a lapse rate to adjust temperature and precipitation data based on elevation could also lead to inaccuracies, as it fails to account for the unique spatial and natural variability of each measurement station. Furthermore, the TT, which also incorporates temperature compensation per altitude, might be overcorrected when combined with the lapse rate. The accuracy of the input data is crucial for reliable model outputs. This accounts also for the observed April 1st SWE data used for model calibration, where measurement errors or inconsistencies in the data collection could impact the accuracy of the results.

For each measurement station, the parameter set (TT, CFMAX, SFCF), which minimized the objective function, was extracted from the model. However, the concept of equifinality suggests that multiple parameter sets can produce similar performance during the calibration period but may behave differently outside these conditions (Hakala et al., 2019). This implies that the chosen parameter sets may not be the only optimal solutions, which could affect the robustness of the results. Moreover, the model calibration was not complemented by a robust validation phase, this might affect the reliability of the simulated maxSWE values. The validation would become particularly important when extending the model to future projections or applying it to other catchments.

Furthermore, this thesis does not account for the influence of vegetation cover, microtopography, microclimatic variability (such as wind exposure), or changes in land use. These factors could influence snow accumulation, the distribution of snow, and melting processes. The findings from the Wägital catchment may not be directly applicable to other regions with different climatic, topographic, or hydrological conditions. Additionally, the interpretation of trends, especially based on the color-coding in the heatmaps, may be subject to bias. While comparisons with international studies are provided, differences in data collection methods, and model types may limit the direct comparability of results.

6.7 Recommendations for Future Research

The limitations and uncertainties discussed in this thesis highlight several opportunities for future research to improve understanding and modeling of SWE dynamics.

Regarding the measurement monitoring in the Wägital, it is crucial to continue the program to see how the SWE evolves over time. Continuous collection of SWE data, along with detailed records of meteorological variables, will improve trend analyses and model accuracy. Expanding the network of observation locations in the Wägital would provide more detailed information about the spatial variability and heterogeneity of snow accumulation throughout the year. Instead of the timely extensive monitoring program, it could be considered to include remote sensing data which can provide high-resolution images that give valuable insights into snow cover and can help estimate the SWE (e.g. Steiner, 2019).

Additionally, Noetzli et al. (2019) explored the potential of drones to estimate snow reserves in the Wägital, which could be further elaborated.

As input factors for the model, future studies should aim to use high-resolution gridded meteorological data and integrate detailed spatial variability in temperature and precipitation. Additionally, incorporating parameters such as vegetation cover or land-use change could provide further insights into how these factors influence SWE trends. This would further help in understanding the impacts of human activities on snowpack dynamics. Further research using the same data set could explore how changes in maxSWE might affect downstream water availability, hydroelectric power generation, and agricultural planning.

To improve model robustness, future research with the same data set could include validation by splitting the observational data into different time periods. This would increase confidence in the simulation results. Considering the limitations of the degree-day model, it could be explored to use different modeling approaches, such as machine learning algorithms which could maybe handle the complexities and non-linearities in snowpack dynamics.

Instead of comparing the trends in SWE solely to local climatic changes, the research could be expanded to enhance the understanding of how local factors interact with global climate trends. Additionally, the model output could be used to explore questions about the duration of snow cover, and a closer look at the timing of maxSWE could be taken and how this has shifted throughout the years. The frequency and intensity of snow events could also be analyzed to gain deeper insights into changing snowpack dynamics.

While this thesis has provided valuable insights into SWE trends in the Wägital catchment, there remain numerous opportunities for future research to refine, validate, and expand upon these findings. By addressing the identified limitations and exploring new avenues for study, future research can contribute to a deeper understanding of snowpack dynamics and their implications for both local and global water resources.

7 Conclusions

This thesis has provided a comprehensive analysis of SWE trends in the Wägital catchment, utilizing one of the longest-standing SWE datasets known globally. By implementing a degree-day model to reconstruct daily SWE and determine maxSWE, this research has addressed the limitations of relying solely on April 1st measurements. The model results revealed that the April 1st measurement often does not represent the peak SWE, underscoring the importance of using maxSWE for more accurate trend analyses. The spatial analysis of maxSWE highlighted consistent patterns of snow accumulation, showing that SWE increases with elevation, is lowest on southern aspect, and decreases with steeper slopes. The temporal trends revealed a predominant decline in maxSWE across the catchment and the total time period. This trend is, however, not gradual, from the 1940s to the 1980s, trends are primarily positive, while trends observed from the 1980s onward are stronger negative. Depending on the year the trend analysis starts, the trends are revealed to be less or stronger negative. These findings provide a more nuanced understanding of snow dynamics in the Wägital catchment, they offer insights into both long-term trends and shorter-term fluctuations that are crucial for managing water resources in the region.

Moreover, the emphasis of the study on the spatial variability of SWE reinforces the complexity of snowpack behavior in mountainous regions, where elevation, aspect, and slope interact with meteorological conditions to influence snow accumulation and melt. The insights gained in this study improve the understanding of historical SWE trends and might enhance the ability to predict future changes in snowpack, which are important for water management, agricultural planning, and hydroelectric power generation.

Several limitations come with this study, including uncertainty in the input data, assumptions that had to be made to develop the degree-day model, and inherent uncertainties of the model itself. The degree-day approach, while effective for estimating snow accumulation and melt, simplifies complex processes. Other critical factors, such as variation in daily precipitation types, wind redistribution and vegetation cover, are not accounted for. These limitations leave room for future research on this topic.

By offering insights into long-term snowpack dynamics, this thesis adds valuable perspective to ongoing discussions on climate change. The insights gained in this thesis highlight the importance of historical data sets and the urgency of continued monitoring and research to be better equipped to mitigate and adapt to the evolving challenges posed by climate change.

Bibliography

Anderton, S. P., White, S. M., & Alvera, B. (2004). Evaluation of spatial variability in snow water equivalent for a high mountain catchment. *Hydrological Processes*, *18*(3), 435–453. https://doi.org/10.1002/HYP.1319

Armstrong, R. L., & Brown, R. (2008). *Snow and climate: physical processes, surface energy exchange and modeling* (R. L. Armstrong & E. Brun, Eds.). Cambridge University Press.

Arora, V. K., & Boer, G. J. (2001). Effects of simulated climate change on the hydrology of major river basins. *Journal of Geophysical Research: Atmospheres*, *106*(D4), 3335–3348. https://doi.org/10.1029/2000JD900620

Bader, V. H., Haefeli, R., Sucher, E., Neher, J., Eckei, O., Thams, C., & Niggli, P. (1939). Der Schnee und seine Metamorphose. In *Beitrage zur Geologie der Schweiz, Geotechnische Serie, Hydrologie* (Vol. 3). Kimmerly und Frey AG.

Begert, M., & Frei, C. (2018). Long-term area-mean temperature series for Switzerland—Combining homogenized station data and high resolution grid data. *International Journal of Climatology*, *38*(6), 2792–2807. https://doi.org/10.1002/JOC.5460

Berghuijs, W. R., Woods, R. A., Hutton, C. J., & Sivapalan, M. (2016). Dominant flood generating mechanisms across the United States. *Geophysical Research Letters*, *43*(9), 4382–4390. https://doi.org/10.1002/2016GL068070

Bergström, S. (1976). Development and Application of a Conceptual Runoff Model for Scandinavian Catchments. *Bulletin Series A*, *52*, Department of Water Resources Engineering, Lund Institute of Technology, University of Lund.

Beven, K. J. (2012). *Rainfall-runoff modelling : the primer* (2nd ed.). John Wiley & Sons.

Bohr, G. S., & Aguado, E. (2001). Use of April 1 SWE measurements as estimates of peak seasonal snowpack and total cold-season precipitation. *Water Resources Research*, *37*(1), 51–60. https://doi.org/10.1029/2000WR900256

Botteron, C., Dawes, N., Leclère, J., Skaloud, J., Weijs, S. V., & Farine, P. A. (2013). Soil moisture &snow properties determination with GNSS in alpine environments: Challenges, status, and perspectives. In *Remote Sensing* (Vol. 5, Issue 7, pp. 3516–3543). https://doi.org/10.3390/rs5073516

Brown, R. D., Fang, B., & Mudryk, L. (2019). Update of Canadian Historical Snow Survey Data and Analysis of Snow Water Equivalent Trends, 1967–2016. *Atmosphere - Ocean*, *57*(2), 149–156. https://doi.org/10.1080/07055900.2019.1598843/ASSET/F6036DB8-BCEF-455C-929A-2DBB7B41CA3F/ASSETS/IMAGES/TATO_A_1598843_F0006_OB.JPG

Cayan, D. (1996). Interannual Climate Variability and Snowpack in the Western United States. *Journal of Climate*, *9*(5), 928–948. https://doi.org/https://doi.org/10.1175/1520-0442(1996)009<0928:ICVASI>2.0.CO;2

CH2018. (2018). *CH2018-Climate Scenarios for Switzerland, Technical Report*. National Centre for Climate Services. Zurich.

Changnon, D., McKee, T. B., & Doesken, N. J. (1991). Hydroclimatic variability in the Rocky Mountains. *JAWRA Journal of the American Water Resources Association*, *27*(5), 733–743. https://doi.org/10.1111/J.1752-1688.1991.TB01471.X

Clark, M. P., Hendrikx, J., Slater, A. G., Kavetski, D., Anderson, B., Cullen, N. J., Kerr, T., Örn Hreinsson, E., & Woods, R. A. (2011). Representing spatial variability of snow water equivalent in hydrologic and land-surface models: A review. In *Water Resources Research* (Vol. 47, Issue 7). https://doi.org/10.1029/2011WR010745

Collins, E. H. (1934). Relationship of degree-days above freezing to runoff. *Eos, Transactions American Geophysical Union*, *15*(2), 624–629. https://doi.org/10.1029/TR015I002P00624-2

Croce, P., Formichi, P., Landi, F., Mercogliano, P., Bucchignani, E., Dosio, A., & Dimova, S. (2018). The snow load in Europe and the climate change. *Climate Risk Management*, *20*, 138–154. https://doi.org/10.1016/J.CRM.2018.03.001

Dai, A. (2008). Temperature and pressure dependence of the rain-snow phase transition over land and ocean. *Geophysical Research Letters*, *35*(12), 12802. https://doi.org/10.1029/2008GL033295

Dunn, O. J. (1964). Multiple Comparisons Using Rank Sums. *Technometrics*, *6*(3), 241–252. https://doi.org/10.1080/00401706.1964.10490181

Egli, L., Jonas, T., & Meister, R. (2009). Comparison of different automatic methods for estimating snow water equivalent. *Cold Regions Science and Technology*, *57*, 107–115. https://doi.org/10.1016/j.coldregions.2009.02.008

Faria, D. A., Pomeroy, J. W., & Essery, R. L. H. (2002). Effect of covariance between ablation and snow water equivalent on depletion of snow-covered area in a forest. *Hydrological Processes, 14*, 2683–2695. https://doi.org/10.1002/1099-1085(20001030)14:15

Fierz, C., Armstrong, R. L., Durand, Y., Etchevers, P., Greene, E., McClung, D. M., Nishimura, K., Satyawali, P. K., & Sokratov, S. A. (2009). The international classification for seasonal snow on the ground. *IHP-VII Technical Documents in Hydrology*, *83*(1).

FOEN: Federal Office of the Environment. (2021). Effects of climate change on Swiss water bodies. Hydrology, water ecology and water management. Environmental Studies, 2101, Berne.

Gemeinde Innerthal. (2024). *Geografische Lage Gemeinde Innerthal*. https://www.innerthal.ch/geschichte/gemeindestruktur (last access: 25.07.2024).

Girotto, M., Musselman, K. N., & Essery, R. L. H. (2020). Data Assimilation Improves Estimates of Climate-Sensitive Seasonal Snow. *Current Climate Change Reports*, *6*(3), 81–94. https://doi.org/10.1007/S40641-020-00159-7/FIGURES/2

Grünewald, T., Bühler, Y., & Lehning, M. (2014). Elevation dependency of mountain snow depth. *Cryosphere*, *8*(6), 2381–2394. https://doi.org/10.5194/TC-8-2381-2014

HADES: Hydrologischer Atlas der Schweiz. (2023). *Zusammenfassende Informationen zum Gebiet 154139*. https://hydromaps.ch/#de/12/47.0744/8.9212/bl_hds/154139 (last access: 25.07.2024)

Hakala, K., Addor, N., Teutschbein, C., Vis, M., Dakhlaoui, H., & Seibert, J. (2019). Hydrological Modeling of Climate Change Impacts. In *Encyclopedia of Water* (pp. 1–20). Wiley. https://doi.org/10.1002/9781119300762.wsts0062

Hantke, R., & Kuriger, E. (2003). Überblick über die Geologie des Kantons Schwyz und seine Nachbargebiete. *Geologie Und Geotope Im Kanton Schwyz, Berichte Der Schwyzerischen Naturforschenden Gesellschaft*, *14*, 9–34.

Harpold, A., Brooks, P., Rajagopal, S., Heidbuchel, I., Jardine, A., & Stielstra, C. (2012). Changes in snowpack accumulation and ablation in the intermountain west. *Water Resources Research*, *48*(11). https://doi.org/10.1029/2012WR011949

He, Z. H., Parajka, J., Tian, F. Q., & Blöschl, G. (2014). Estimating degree-day factors from MODIS for snowmelt runoff modeling. *Hydrology and Earth System Sciences*, *18*(12), 4773–4789. https://doi.org/10.5194/HESS-18-4773-2014

Hirabayashi, Y., Mahendran, R., Koirala, S., Konoshima, L., Yamazaki, D., Watanabe, S., Kim, H., & Kanae, S. (2013). Global flood risk under climate change. *Nature Climate Change 2013 3:9*, *3*(9), 816–821. https://doi.org/10.1038/nclimate1911

Jost, G., Weiler, M., Gluns, D. R., & Alila, Y. (2007). The influence of forest and topography on snow accumulation and melt at the watershed-scale. *Journal of Hydrology*, *347*(1–2), 101–115. https://doi.org/10.1016/j.jhydrol.2007.09.006

Kelly, R. (2009). The AMSR-E snow depth algorithm: Description and initial results. *Journal of Hte Remote Sensing Society of Japan*, *29*(1), 307–317.

Kelly, R. E., Chang, A. T., Tsang, L., & Foster, J. L. (2003). A prototype AMSR-E global snow area and snow depth algorithm. *IEEE Transactions on Geoscience and Remote Sensing*, *41*(2 PART 1), 230–242. https://doi.org/10.1109/TGRS.2003.809118

Kendall, M. G. (1955). Further Contributions to the Theory of Paired Comparisons. *Biometrics*, *11*(1), 43. https://doi.org/10.2307/3001479

Kokkonen Harri Koivusalo Tony Jakeman P Norton, T. J., Kokkonen, T., Koivusalo, H., Jakeman, A., & Norton, J. (2006). *Construction of a degree-day snow model in the light of the ten iterative steps in model development Construction of a Degree-Day Snow Model in the Light of the "Ten Iterative Steps in Model Development"* (Vol. 12). https://scholarsarchive.byu.edu/iemssconference/2006/all/73

Kruskal, W. H., & Wallis, W. A. (1952). Use of Ranks in One-Criterion Variance Analysis. *Journal of the American Statistical Association*, *47*(260), 583. https://doi.org/10.2307/2280779

Lopez, M. G., Vis, M., Jeníček, M., Griessinger, N., & Seibert, J. (2020). Complexity and performance of temperature-based snow routines for runoff modelling in mountainous areas in Central Europe. *Hydrology and Earth System Sciences Discussions*. https://doi.org/10.5194/HESS-2020-57

Magnusson, J., Gustafsson, D., Hüsler, F., & Jonas, T. (2014). Assimilation of point SWE data into a distributed snow cover model comparing two contrasting methods. *Water Resources Research*, *50*(10), 7816–7835. https://doi.org/10.1002/2014WR015302

Magnusson, J., Wever, N., Essery, R., Helbig, N., Winstral, A., & Jonas, T. (2015). Evaluating snow models with varying process representations for hydrological applications. *Water Resources Research*, *51*(4), 2707–2723. https://doi.org/10.1002/2014WR016498

Mann, H. B. (1945). Nonparametric Tests Against Trend. *Econometrica*, *13*(3), 245. https://doi.org/10.2307/1907187

Martinec, J. (1960). The degree-day factor for snowmelt runoff forecasting. *IUGG General Assembly of Helsinki, Vol. 51, IAHS Commisssion of Surface Waters, Helsinki, Finland*, 468–477.

Marty, C., Rohrer, M. B., Huss, M., & Stähli, M. (2023). Multi-decadal observations in the Alps reveal less and wetter snow, with increasing variability. *Frontiers in Earth Science*, *11*. https://doi.org/10.3389/feart.2023.1165861

Marty, C., Tilg, A. M., & Jonas, T. (2017). Recent Evidence of Large-Scale Receding Snow Water Equivalents in the European Alps. *Journal of Hydrometeorology*, *18*(4), 1021–1031. https://doi.org/10.1175/JHM-D-16-0188.1

Meteo Schweiz. (2024). *Changes in temperature, precipitation and sunshine*. Https://Www.Meteoswiss.Admin.Ch/Climate/Climate-Change/Changes-in-Temperature-Precipitation-and-Sunshine.Html. https://www.meteoswiss.admin.ch/climate/climate-change/changes-in-temperature-precipitation-and-sunshine.html

Musselman, K. N., Addor, N., Vano, J. A., & Molotch, N. P. (2021). Winter melt trends portend widespread declines in snow water resources. *Nature Climate Change*, *11*(5), 418–424. https://doi.org/10.1038/s41558-021-01014-9

Nijssen, B., O'donnell, G. M., Hamlet, A. F., & Lettenmaier, D. P. (2001). Hydrologic sensitivity of global rivers to climate change. *Climatic Change*, *50*(1–2), 143–175. https://doi.org/10.1023/A:1010616428763

Noetzli, C., Bühler, Y., Lorenzi, D., Stoffel, A., & Rohrer, M. (2019). Schneedecke als Wasserspeicher. Drohnen können helfen, die Abschätzungen der Schneereserven zu verbessern. *Wasser Energie Luft*, *111*(3), 153–157.

Noetzli, C., & Rohrer, M. (2014). Schneemessungen in alpinen Einzugsgebieten im Zeichen des Klimawandels. *Wasser Energie Luft*, *106*(4), 280–284.

Ohmura, A. (2001). Physical basis for the temperature-based melt-index method. *Journal of Applied Meteorology*, *40*(4), 753–761. https://doi.org/10.1175/1520-0450(2001)040<0753:PBFTTB>2.0.CO;2

Pagano, T., Garen, D., & Sorooshian, S. (2004). Evaluation of official western U.S. seasonal water supply outlooks, 1922-2002. *Journal of Hydrometeorology*, *5*(5), 896–909. https://doi.org/10.1175/1525-7541(2004)005<0896:EOOWUS>2.0.CO;2

Peters-Lidard, C. D., Hossain, F., Leung, L. R., McDowell, N., Rodell, M., Tapiador, F. J., Turk, F. J., & Wood, A. (2018). 100 Years of Progress in Hydrology. *Meteorological Monographs*, *59*(1), 25.1-25.51. https://doi.org/10.1175/AMSMONOGRAPHS-D-18-0019.1

Pielmeier, C., Zweifel, B., Techel, F., Marty, C., Grüter, S., & Stucki, T. (2024). *Schnee und Lawinen in den Schweizer Alpen* (Vol. 145). Swiss Federal Institute for Forest, Snow and Landscape Research, WSL. https://doi.org/10.55419/wsl:36046

Pomeroy, J. W., Gray, D. M., Shook, K. R., Toth, B., Essery, R. L. H., Pietroniro, A., & Hedstrom, N. (1998). An evaluation of snow accumulation and ablation processes for land surface modelling. *Hydrological Processes 12*, 2339–2367. https://doi.org/10.1002/(SICI)1099-1085(199812)12:15

R Core Team. (2023). *A language and environment for statistical computing.* R Foundation for Statistical Computing, Vienna, Austria. https://www.R-project.org/

Rohrer, M., Braun, L. N., & Lang, H. (1994). *Long-Term Records of Snow Cover Water Equivalent in the Swiss Alps 1. Analysis* (Vol. 25). http://iwaponline.com/hr/article-pdf/25/1-2/53/4335/53.pdf

Scherrer, S. C., Gubler, S., Wehrli, K., Fischer, A. M., & Kotlarski, S. (2021). The Swiss Alpine zero degree line: Methods, past evolution and sensitivities. *International Journal of Climatology*, *41*(15), 6785–6804. https://doi.org/10.1002/JOC.7228

Schmucki, E., Marty, C., Fierz, C., & Lehning, M. (2014). Evaluation of modelled snow depth and snow water equivalent at three contrasting sites in Switzerland using SNOWPACK simulations driven by different meteorological data input. *Cold Regions Science and Technology*, *99*, 27–37. https://doi.org/10.1016/J.COLDREGIONS.2013.12.004

Seibert, J., & Vis, M. J. P. (2012). Teaching hydrological modeling with a user-friendly catchment-runoff-model software package. *Hydrology and Earth System Sciences*, *16*(9), 3315–3325. https://doi.org/10.5194/hess-16-3315-2012

Sen, P. K. (1968). Estimates of the Regression Coefficient Based on Kendall's Tau. *Journal of the American Statistical Association*, *63*(324), 1379–1389. https://doi.org/10.1080/01621459.1968.10480934

Shapiro, S. S., & Wilk, M. B. (1965). An Analysis of Variance Test for Normality (Complete Samples). *Biometrika*, *52*(3/4), 591. https://doi.org/10.2307/2333709

Sicart, J. E., Hock, R., & Six, D. (2008). Glacier melt, air temperature, and energy balance in different climates: The Bolivian Tropics, the French Alps, and northern Sweden. *Journal of Geophysical Research Atmospheres*, *113*(24). https://doi.org/10.1029/2008JD010406

Sims, E. M., & Liu, G. (2015). A Parameterization of the Probability of Snow–Rain Transition. *Journal of Hydrometeorology*, *16*(4), 1466–1477. https://doi.org/10.1175/JHM-D-14-0211.1

Smith, T., & Bookhagen, B. (2018). Changes in seasonal snow water equivalent distribution in high mountain Asia (1987 to 2009). *Science Advances*, *4*(1). https://doi.org/10.1126/SCI-ADV.1701550/SUPPL_FILE/1701550_SM.PDF

Solomatine, D. P., & Wagener, T. (2011). Hydrological Modeling. *Treatise on Water Science*, 435–457.

Stahl, K., Hisdal, H., Hannaford, J., Tallaksen, L. M., Van Lanen, H. A. J., Sauquet, E., Demuth, S., Fendekova, M., & Ĵodar, J. (2010). Streamflow trends in Europe: Evidence from a dataset of near-natural catchments. *Hydrology and Earth System Sciences*, *14*(12), 2367–2382. https://doi.org/10.5194/HESS-14-2367-2010

Stähli, M., & Gustafsson, D. (2006). Long-term investigations of the snow cover in a subalpine semi-forested catchment. *Hydrological Processes*, *20*(2), 411–428. https://doi.org/10.1002/hyp.6058

Stähli, M., Seibert, J., Kirchner, J. W., von Freyberg, J., & van Meerveld, I. (2021). Hydrological trends and the evolution of catchment research in the Alptal valley, central Switzerland. *Hydrological Processes*, *35*(4). https://doi.org/10.1002/hyp.14113

Steiner, L. (2019). Snow Water Equivalent Observations Using Refracted GPS Signals. *ETH Library*. https://doi.org/10.3929/ethz-b-000345249

swisstopo: Federal Office of Topography. (2024a). *Koordinaten, Geo-Information und Services*. https://map.geo.admin.ch/#/map?lang=de&center=2660000,1190000&z=1&bgLayer=ch.swisstopo.pixelkarte-farbe&topic=swisstopo&layers=&catalogNodes=ech (last access: 28.08.2024)

swisstopo: Federal Office of Topography. (2024b). *The digital height model of Switzerland DHM25*. Topography - Geodata Distribution. https://www.swisstopo.admin.ch/en/height-model-dhm25 (last access: 29.08.2024)

Todd Walter, M., Brooks, E. S., McCool, D. K., King, L. G., Molnau, M., & Boll, J. (2005). Process-based snowmelt modeling: Does it require more input data than temperature-index modeling? *Journal of Hydrology*, *300*(1–4), 65–75. https://doi.org/10.1016/J.JHYDROL.2004.05.002

Valéry, A., Andréassian, V., & Perrin, C. (2014). "As simple as possible but not simpler": What is useful in a temperature-based snow-accounting routine? Part 1 - Comparison of six snow accounting routines on 380 catchments. *Journal of Hydrology*, *517*, 1166–1175. https://doi.org/10.1016/J.JHYDROL.2014.04.059

Viviroli, D., Dürr, H. H., Messerli, B., Meybeck, M., & Weingartner, R. (2007a). Mountains of the world, water towers for humanity: Typology, mapping, and global significance. *Water Resources Research*, *43*(7), 7447. https://doi.org/10.1029/2006WR005653

Viviroli, D., Gurtz, J., & Zappa, M. (2007b). *The Hydrological Modelling System PREVAH. Geographica Bernensia P40*. University of Berne.

Winkler, M., Schellander, H., & Gruber, S. (2021). Snow water equivalents exclusively from snow depths and their temporal changes: The 1SNOW model. *Hydrology and Earth System Sciences*, *25*(3), 1165–1187. https://doi.org/10.5194/HESS-25-1165-2021

Winkler, R. D., Spittlehouse, D. L., & Golding, D. L. (2005). Measured differences in snow accumulation and melt among clearcut, juvenile, and mature forests in southern British Columbia. *Hydrological Processes*, *19*(1), 51–62. https://doi.org/10.1002/HYP.5757

Wiscombe, W. J., & Warren, S. G. (1980). A Model for Spectral Albedo of Snow. I: Pure Snow. *Journal of the Atmospheric Sciences*, *37*, 2712–2733.

WSL: Eidg. Forschungsanstalt für Wald, S. und L. (2024). *Schneemonitoring*. https://www.slf.ch/de/schnee/schneemonitoring/ (last access: 21.08.2024)

Zhong, X., Zhang, T., Su, H., Xiao, X., Wang, S., Hu, Y., Wang, H., Zheng, L., Zhang, W., Xu, M., & Wang, J. (2021). Impacts of landscape and climatic factors on snow cover in the Altai Mountains, China. *Advances in Climate Change Research*, *12*(1), 95–107. https://www.sciencedirect.com/science/article/pii/S1674927821000228

Appendix

A1 Location Characteristics

T 1: Measurement Locations Characteristics

	Name	X coordinate	Y coordinate	Elevation [m a.s.l.]	Aspect	Slope [°]
1	Eggstofel	2710150	1217560	1325	S	8.9
2	Eggstofel-Boden	2709900	1217780	1330	N	4.7
3	Salzlecki	2708590	1216910	1440	N	4.7
4	Salzlecki-Bügel	2708860	1216340	1480	E	13.8
5	Heizlihöhe	2709290	1215880	1400	E	11.6
6	Heizlihöhe-Profil	2709340	1215700	1380	E	13.1
7	Heizlihöhe-Totalisator	2709700	1215520	1330	E	12
8	Tannstofel	2710100	1215650	1340	N	16.2
9	Mittl. Tannstofel	2710600	1216060	1250	N	6
10	Waldschneise	2710940	1216300	1220	N	8.6
11	Oberstock	2711470	1216500	1170	N	6.9
12	Stuckliwald	2713075	1218775	1190	N	8.9
13	Seeende_1	2711970	1213800	930	N	18.6
14	Aberenalp	2711530	1212507	1100	N	9.6
15	Rinderweid	2712424	1212950	1310	W	5.3
16	Lauibüel Hütte	2713060	1213430	1500	W	12.5
17	Lauibüel Totalisator W	2713019	1213595	1470	W	24.5
18	Lauibüel Totalisator S	2713122	1213507	1495	W	20.5
19	Löcherenwald	2713255	1213694	1560	W	13.9
20	Gängen	2713540	1213630	1600	W	8.6
21	Oberalp Hütten	2710845	1211270	1565	N	10.2
22	Oberalp Boden	2711675	1210975	1800	W	5
23	Schwarzenegg	2714500	1218050	1380	W	11.9
24	Schwarzenegg Hütten	2714320	1218080	1330	W	15.9
25	Schwarzenegg untere Hütten	2714200	1217900	1280	W	12.7
26	Masten	2714080	1217630	1210	S	13.1
27	Oberhalb Wald	2713950	1217550	1170	W	16.9
28	Unterhalb Wald	2713750	1217250	1090	S	16.2
29	Fällätschen	2713650	1217100	1030	W	14.7
30	Unterhalb Fällätschen	2713570	1217200	990	S	14.8
31	Hohfläschen_1	2714250	1215830	1480	W	19.5
32	Obere Hütten	2714330	1215650	1445	S	13.5
33	Unterhalb Hütten	2714220	1215670	1425	W	15.2
34	Oberhalb Naturfreundehaus Hütten	2714100	1215595	1390	W	11.8
35	Naturfreundehaus Hütten	2713985	1215570	1360	W	22.9
36	Unterhalb Naturfreundehaus Hütten	2713850	1215660	1320	W	24
37	Boden ob Gatter	2713650	1215640	1240	W	22.4
38	Aberligaden	2713400	1215390	1080	W	20
39	Ziggen	2713150	1215385	945	W	24.3
40	Unteralten	2713212	1216463	920	W	13.1

41	Seeende_2	2713195	1220219	1290	E	14.9
42	Rötstock	2708257	1218890	905	E	14.7
43	Rohr	2711949	1213958	1200	E	13.3
44	Hohfläschen_2	2710770	1217498	1510	W	15.6
45	Blattli	2714350	1215930	1510	W	12.6

A2 List of SSE and best parameter set

T 2: Results of the objective function (lowest SSE) and best-parameter sets (TT, CFMAX, SFCF). The parameters were selected from the defined parameter range, based on the minimization of the objective function.

	station	TT	CFMAX	SFCF	Lowest SSE
1	Eggstofel	0.9	3	0.6	1208783.5
2	Eggstofel-Boden	1.3	1	0.6	756495.0
3	Salzlecki	2	7.1	0.5	1182641.0
4	Salzlecki-Bügel	1.3	1	0.6	626356.8
5	Heizlihöhe	2	7.1	0.5	716864.2
6	Heizlihöhe-Profil	0.5	1.8	0.6	526140.4
7	Heizlihöhe-Totalisator	0.5	1.8	0.6	883529.7
8	Tannstofel	0.9	3	0.6	455687.8
9	Mittl. Tannstofel	1.3	1	0.6	555588.4
10	Waldschneise	1.3	1	0.6	407691.3
11	Oberstock	0.5	1.8	0.6	445506.0
12	Stuckliwald	0.9	3	0.6	634167.1
13	Seeende_1	1.1	1.3	0.8	444779.1
14	Aberenalp	2.5	4.1	0.8	918212.6
15	Rinderweid	0.5	1.8	0.6	986625.0
16	Lauibüel Hütte	0.9	3	0.6	736986.8
17	Lauibüel Totalisator W	0.9	3	0.6	982030.9
18	Lauibüel Totalisator S	-0.4	3	0.7	605506.9
19	Löcherenwald	0.5	1.8	0.6	932086.2
20	Gängen	0.5	1.8	0.6	988655.7
21	Oberalp Hütten	2.5	4.9	0.7	1164307.4
22	Oberalp Boden	1.7	8	0.9	1717548.8
23	Schwarzenegg	1	8.1	0.5	680382.5
24	Schwarzenegg Hütten	2.3	8.2	0.4	249409.8
25	Schwarzenegg untere Hütten	0.4	7.2	0.4	280648.4
26	Masten	0.9	4.4	0.5	228505.6
27	Oberhalb Wald	1.3	9.9	0.4	227366.7
28	Unterhalb Wald	-0.4	3	0.7	137680.3
29	Fällätschen	-0.4	3	0.7	113381.3
30	Unterhalb Fällätschen	-0.4	3	0.7	76302.5
31	Hohfläschen_1	0.1	8.7	0.6	736463.3
32	Obere Hütten	2.5	9.3	0.4	526552.1
33	Unterhalb Hütten	2	7.1	0.5	489496.6
34	Oberhalb Naturfreundehaus Hütten	1	8.1	0.5	452241.6
35	Naturfreundehaus Hütten	1	8.1	0.5	605003.5
36	Unterhalb Naturfreundehaus Hütten	2.3	8.2	0.4	374566.0
37	Boden ob Gatter	2.3	8.2	0.4	437498.7
38	Aberligaden	-0.4	3	0.7	175427.2
39	Ziggen	-0.4	3	0.7	89658.6
40	Unteralten	0.5	1.8	0.6	358440.6
41	Seeende_2	1.8	3	0.7	392831.3
42	Rötstock	0.9	4.4	0.5	323936.3
43	Rohr	0.9	3	0.6	719228.7
44	Hohfläschen_2	2	7.1	0.5	826297.5
45	Blattli	0.1	8.7	0.6	104635.5

A3 Model Performance

T 3: Linear Regression Results per measurement station.

	station	a	b	r2	bias
1	Eggstofel	1.00	-34.79	0.71	1.14
2	Eggstofel-Boden	0.93	38.60	0.73	1.28
3	Salzlecki	0.96	59.88	0.77	0.89
4	Salzlecki-Bügel	0.94	15.96	0.80	1.13
5	Heizlihöhe	0.89	104.70	0.80	0.84
6	Heizlihöhe-Profil	0.99	21.57	0.83	1.22
7	Heizlihöhe-Totalisator	0.93	30.38	0.73	0.99
8	Tannstofel	0.90	20.60	0.86	1.31
9	Mittl. Tannstofel	1.03	6.50	0.83	0.99
10	Waldschneise	0.92	36.74	0.83	1.24
11	Oberstock	0.95	18.81	0.81	0.98
12	Stuckliwald	0.78	125.45	0.71	0.67
13	Seeende_1	0.96	29.27	0.80	0.89
14	Aberenalp	0.92	168.00	0.77	0.63
15	Rinderweid	1.02	12.68	0.74	0.98
16	Lauibüel Hütte	0.89	18.50	0.80	1.14
17	Lauibüel Totalisator W	1.01	61.12	0.77	1.16
18	Lauibüel Totalisator S	0.81	150.64	0.83	1.12
19	Löcherenwald	1.09	-35.05	0.78	1.12
20	Gängen	1.07	-9.20	0.78	1.07
21	Oberalp Hütten	1.06	-58.36	0.78	1.69
22	Oberalp Boden	0.73	243.84	0.72	1.62
23	Schwarzenegg	1.04	109.40	0.74	1.06
24	Schwarzenegg Hütten	0.99	36.01	0.84	1.14
25	Schwarzenegg untere Hütten	1.08	91.56	0.67	0.74
26	Masten	0.84	32.54	0.79	1.41
27	Oberhalb Wald	0.97	72.85	0.58	0.65
28	Unterhalb Wald	0.69	9.61	0.74	1.71
29	Fällätschen	0.54	-2.71	0.64	2.46
30	Unterhalb Fällätschen	0.67	0.26	0.74	2.18
31	Hohfläschen_1	0.85	17.68	0.81	1.51
32	Obere Hütten	1.12	-20.47	0.81	1.32
33	Unterhalb Hütten	0.94	82.48	0.80	1.14
34	Oberhalb Naturfreundehaus Hütten	0.88	87.59	0.79	1.00
35	Naturfreundehaus Hütten	1.03	-151.03	0.71	2.22
36	Unterhalb Naturfreundehaus Hütten	1.02	41.89	0.65	1.33
37	Boden ob Gatter	0.88	25.61	0.71	1.08
38	Aberligaden	1.01	34.59	0.71	0.74
39	Ziggen	1.39	35.99	0.47	0.47
40	Unteralten	1.78	17.71	0.39	0.23
41	Seeende_2	0.94	68.51	0.83	0.90
42	Rötstock	0.95	-0.66	0.87	1.30
43	Rohr	1.05	90.76	0.53	0.39
44	Hohfläschen_2	0.79	-50.42	0.68	1.65
45	Blattli	1.14	-27.24	0.74	1.19

A4 Spatial Variation Compilations

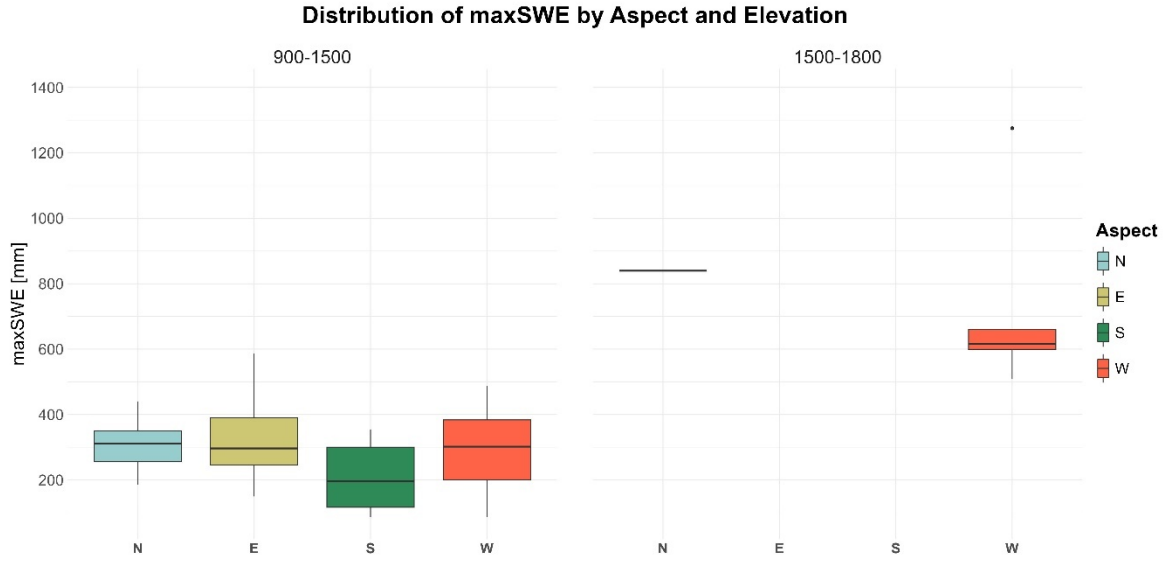

A 1: Boxplots of the maxSWE compiled for aspect and elevation, the left plot representing measurement stations in the lower elevation band (900-1500 m a.s.l.) and the right plot representing stations in the upper elevation zone (1500-1800 m a.s.l.). Each box represents the interquartile range, the solid horizontal line the median, and the whiskers extend to the most extreme data points within 1.5 times the IQR from the first and third quartile. Data points outside this range are considered outliers and are shown as individual points.

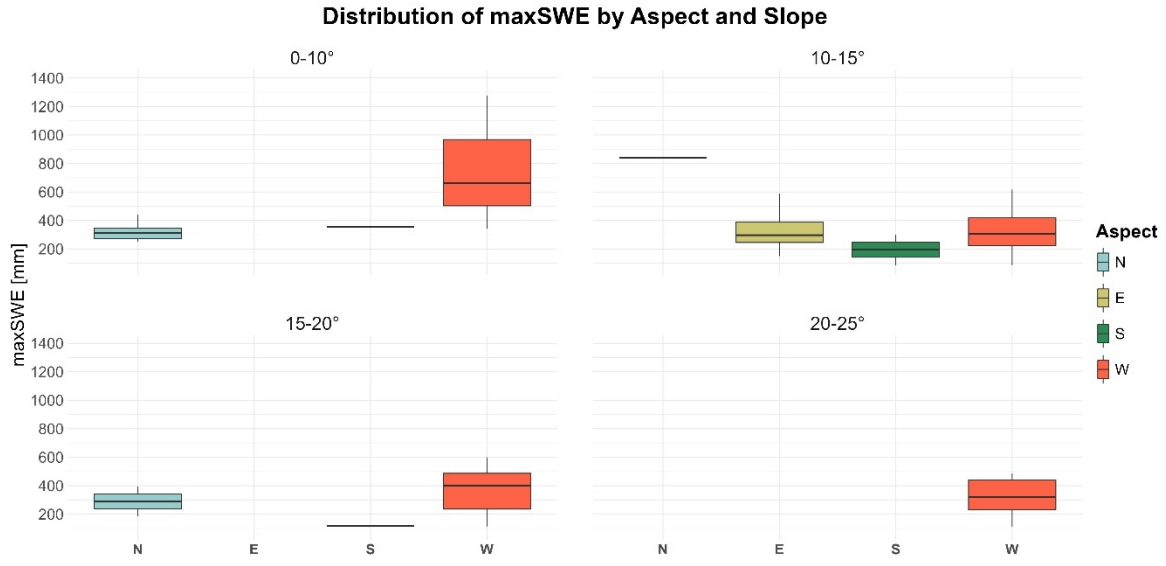

A 2: Boxplots of the maxSWE compiled for aspect and slope. Above each plot the representative slope range is marked. Each box represents the interquartile range, the solid horizontal line the median, and the whiskers extend to the most extreme data points within 1.5 times the IQR from the first and third quartile. Data points outside this range are considered outliers and are shown as individual points.

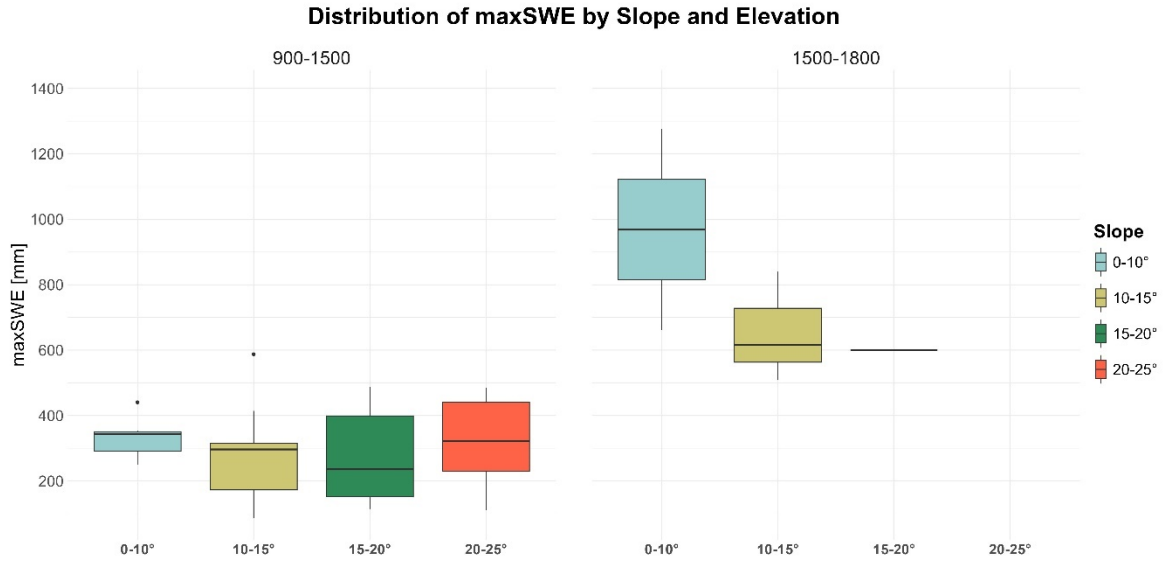

A 3: Boxplots of the maxSWE compiled for slope and elevation, the left plot representing measurement stations in the lower elevation band (900-1500 m a.s.l.) and the right plot representing stations in the upper elevation zone (1500-1800 m a.s.l.). Each box represents the interquartile range, the solid horizontal line the median, and the whiskers extend to the most extreme data points within 1.5 times the IQR from the first and third quartile. Data points outside this range are considered outliers and are shown as individual points.

A5 Results Trend Analysis individual Stations

T 4: Statistical results of the trend analysis for each individual measurement station. Including the Theil-Sen slope tau value and the MK-test p value regarding the statistical significance.

	Station	tau	p_value
1	Eggstofel	-0.191	0.011
2	Eggstofel-Boden	-0.181	0.016
3	Salzlecki	-0.164	0.029
4	Salzlecki-Bügel	-0.181	0.016
5	Heizlihöhe	-0.217	0.004
6	Heizlihöhe-Profil	-0.180	0.017
7	Heizlihöhe-Totalisator	-0.180	0.017
8	Tannstofel	-0.187	0.013
9	Mittl. Tannstofel	-0.181	0.016
10	Waldschneise	-0.181	0.016
11	Oberstock	-0.180	0.017
12	Stuckliwald	-0.192	0.011
13	Seeende_1	-0.183	0.015
14	Aberenalp	-0.106	0.161
15	Rinderweid	-0.180	0.017
16	Lauibüel Hütte	-0.191	0.011
17	Lauibüel Totalisator W	-0.187	0.013
18	Lauibüel Totalisator S	-0.186	0.013
19	Löcherenwald	-0.180	0.017
20	Gängen	-0.180	0.017
21	Oberalp Hütten	-0.170	0.024
22	Oberalp Boden	-0.184	0.015
23	Schwarzenegg	-0.214	0.004
24	Schwarzenegg Hütten	-0.187	0.013
25	Schwarzenegg untere Hütten	-0.176	0.019
26	Masten	-0.209	0.006
27	Oberhalb Wald	-0.206	0.006
28	Unterhalb Wald	-0.191	0.011
29	Fällätschen	-0.186	0.013
30	Unterhalb Fällätschen	-0.194	0.010
31	Hohfläschen_1	-0.199	0.008
32	Obere Hütten	-0.201	0.007
33	Unterhalb Hütten	-0.179	0.018
34	Oberhalb Naturfreundehaus Hütten	-0.214	0.004
35	Naturfreundehaus Hütten	-0.217	0.004
36	Unterhalb Naturfreundehaus Hütten	-0.182	0.016
37	Boden ob Gatter	-0.184	0.015
38	Aberligaden	-0.191	0.011
39	Ziggen	-0.191	0.011
40	Unteralten	-0.180	0.017
41	Seeende_2	-0.185	0.014
42	Rötstock	-0.188	0.013
43	Rohr	-0.192	0.011
44	Hohfläschen_2	-0.174	0.021
45	Blattli	-0.188	0.013

A6 Plots Trend Analysis Groups

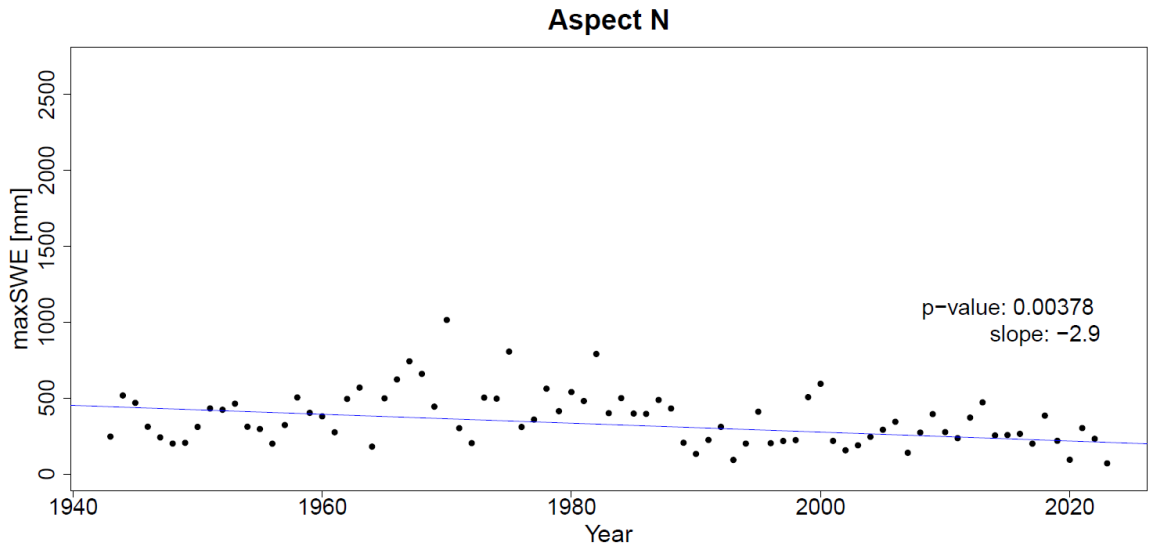

A 4: The simulated median maxSWE for measurement stations with aspect N in black dots, and linear trend line (blue).

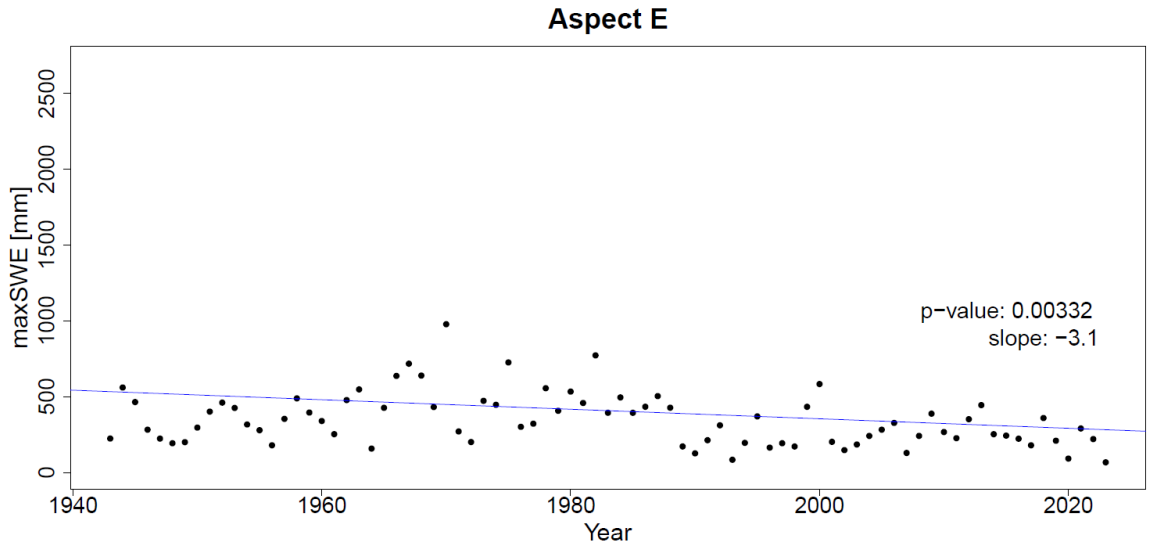

A 5: The simulated median maxSWE for measurement stations with aspect E in black dots, and linear trend line (blue).

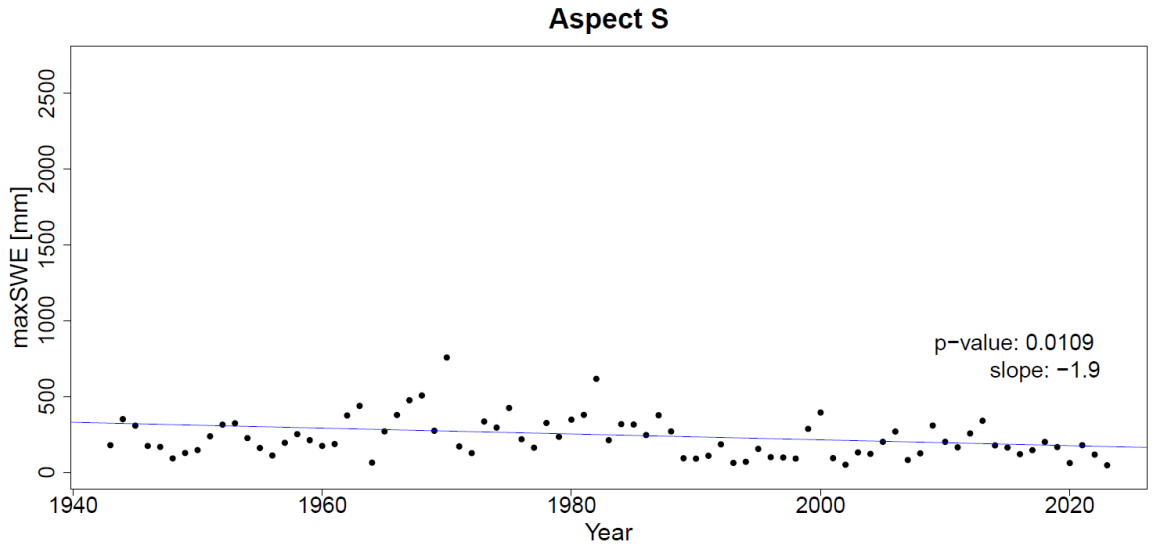

A 6: The simulated median maxSWE for measurement stations with aspect S in black dots, and linear trend line (blue).

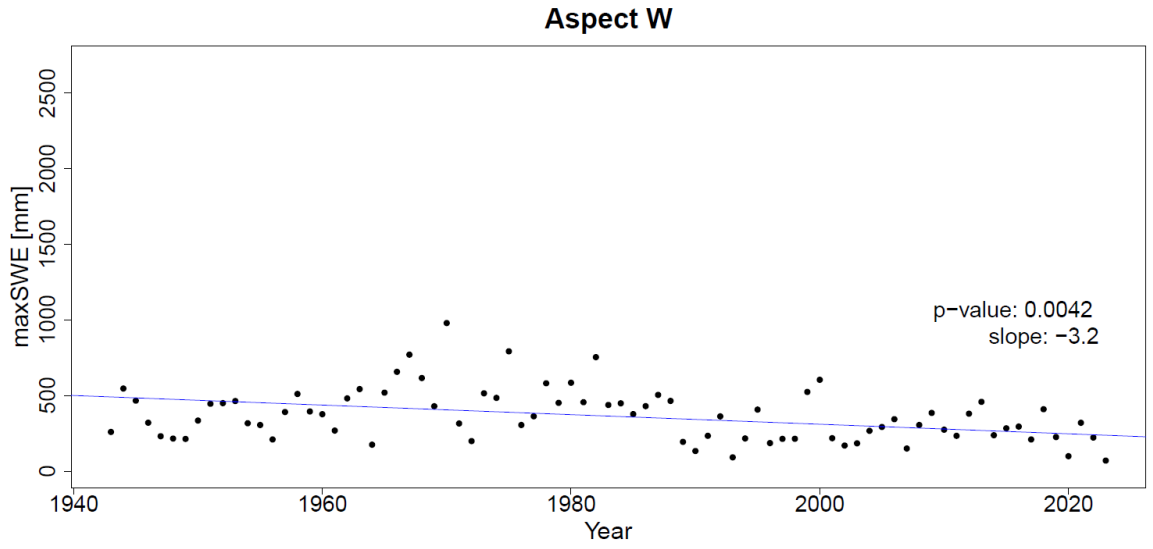

A 7: The simulated median maxSWE for measurement stations with aspect W in black dots, and linear trend line (blue).

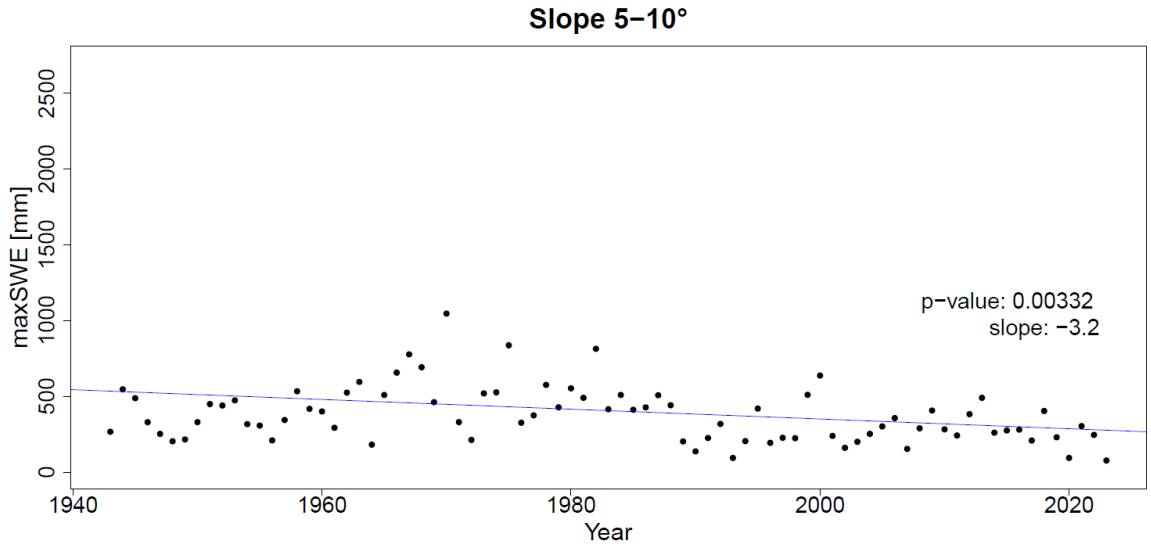

A 8: The simulated median maxSWE for measurement stations with slope 5-10° in black dots, and linear trend line (blue).

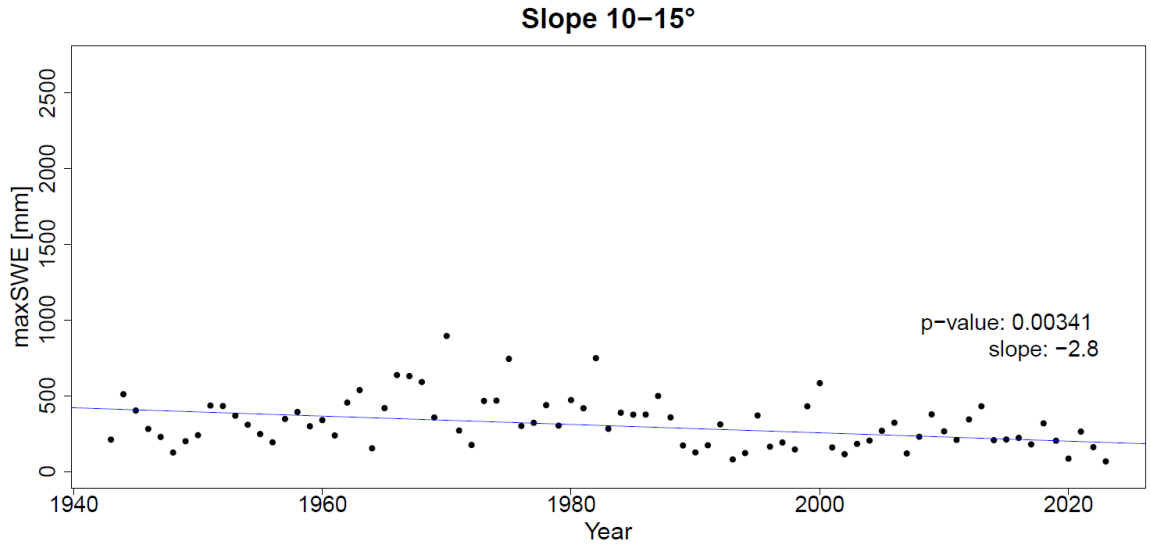

A 9: The simulated median maxSWE for measurement stations with slope 10-15° in black dots, and linear trend line (blue).

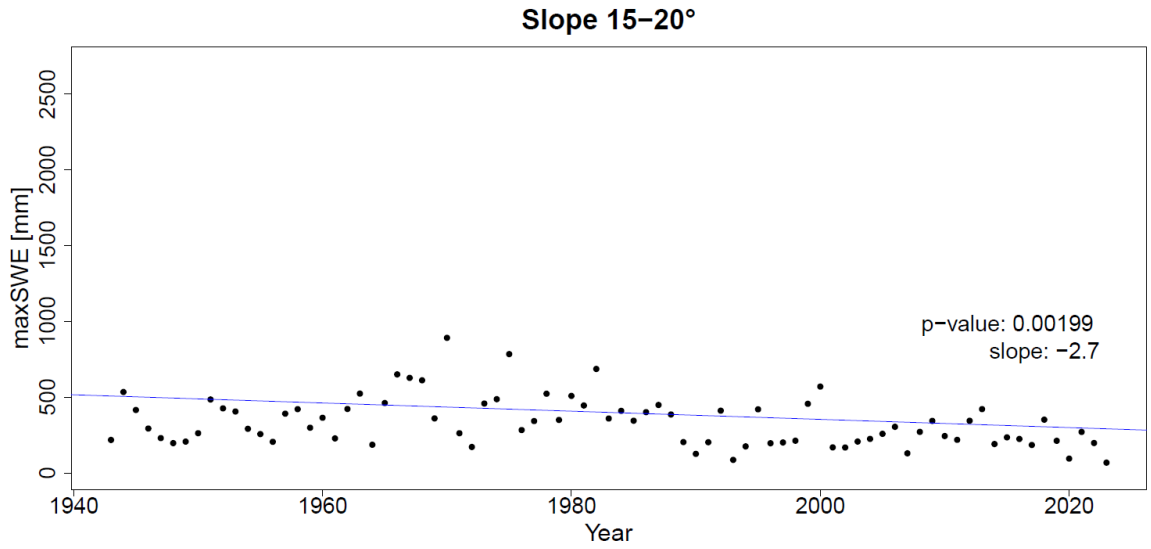

A 10: The simulated median maxSWE for measurement stations with slope 15-20° in black dots, and linear trend line (blue).

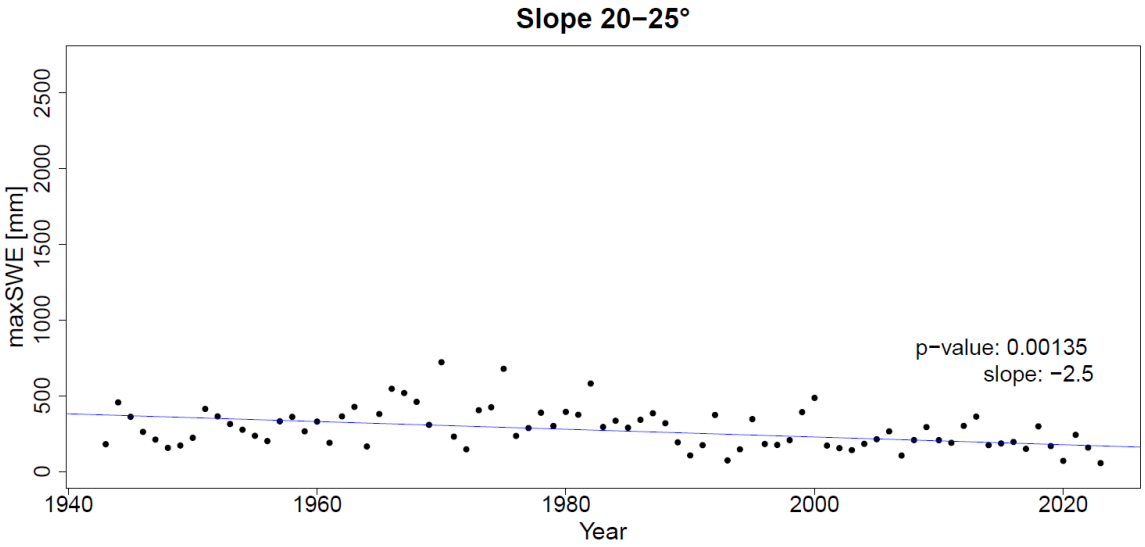

A 11: The simulated median maxSWE for measurement stations with slope 20-25° in black dots, and linear trend line (blue).

Personal Declaration

I hereby declare that the submitted thesis is the result of my own, independent work. All external sources are explicitly acknowledged in the thesis.

Date, Place

23. September 2024, Zürich

Signature